Applied Catalysis B: Environmental 325 (2023) 121733

Contents lists available at ScienceDirect

Applied Catalysis B: Environmental

journal homepage: www.elsevier.com/locate/apcatb

State-of-the-art and developmental trends in platinum group metal-free cathode catalyst for anion exchange membrane fuel cell (AEMFC)

Md. Mosaddek Hossen [a,*], Md. Shamim Hasan [a,1], Md. Riajul Islam Sardar [a,1], Jahid bin Haider [a], Mottakin [a], Kaido Tammeveski [b], Plamen Atanassov [c,*]

[a] Department of Applied Chemistry & Chemical Engineering, Bangabandhu Sheikh Mujibur Rahman Science and Technology University (BSMRSTU), Bangladesh
[b] Institute of Chemistry, University of Tartu, Estonia
[c] Department of Chemical and Biomolecular Engineering, University of California Irvine, CA, USA

ARTICLE INFO

Keywords:
Anion/ alkaline exchange membrane fuel cell
AEMFC
Oxygen reduction reaction
ORR
Hydrogen fuel cell
H_2/O_2
Non-platinum catalysts
PGM-free catalysts

ABSTRACT

AEMFC is becoming a prominent technology in portable energy sources. In an attempt to make it economical, non-platinum catalysts are necessary to recruit in the application. Numerous researches are accomplished on the development of platinum-free catalysts. This review summarizes the advancements in the synthesis of catalysts consisting of different components and structures. Rotating ring-disk electrode (RRDE) and fuel cell tests are commonly employed to evaluate the activity for oxygen reduction reaction (ORR) and performances of the catalysts. Here, along with the synthesis and characterization data, this information is assembled and analyzed correlating different factors. To the best of our knowledge, 13 among 203 catalysts have overcome the peak power density (PPD) threshold of 1000 $mW.cm^{-2}$, which belong to the four categories i.e. Metal-Nitrogen-Carbon (M-N-C), Bimetals-Nitrogen-Carbon (MM-N-C), Transition metal oxides (TMO), and non-metallic catalysts (NMC). The improvement in catalyst's porosity, surface area, conjugation of active sites, and thereby the synthesis procedures have a great effect on the ORR activity and fuel cell performance. In addition to catalyst properties, there are several other significant factors involved such as water management, properties of anion-exchange membrane (AEM) and anion-exchange ionomer (AEI), optimized operating conditions, etc. The previously low-performing catalysts with high ORR activity cannot be ignored from the top-tier catalysts, since enormous improvements are accomplished in membrane conductivity and water management recently.

1. Introduction

Modern human activities mostly rely on the energy supply around the world. Currently, almost the whole system including transport, communication, education, recreation, house appliances, researches, medical treatment, etc. primarily run on electricity. Since, the technology of the conversion of electrical energy into thermal, mechanical, light energy, etc., or vice versa is already established, electrical energy is becoming the common source of all sorts of energy. In the last centuries, the combustion of fossil fuels was vastly used as energy sources [1], but this has numerous adverse effects on the environment [2,3] and the greenhouse gases produced by combustion are primarily responsible for the global warming effect [4–7]. According to recent reports, fossil fuels i.e. oil, gas, and coal are still used to fulfill 84.3% of the total energy demand [8]. To save the climate, researchers from different disciplinary backgrounds are providing continuous efforts to attain efficient and abundant sources of green energy which could be benign to the environment [9–12]. For non-stationary vehicles, the hydrogen fuel cell can be a potential alternative to petroleum fuel as a portable energy source because of its high efficiency, vibration-free and quiet operation, environment friendliness, compact structure, and high specific energy storage density [13–16]. Combustion engines convert the chemical energy of petroleum fuel into thermal energy, which is finally transformed into mechanical energy to drive the vehicles. On the other side, the fuel cell converts the chemical energy of the fuel directly into electrical energy and the electrical energy then drives the motor and runs the vehicle. The fuel cells are of different types among which H_2/O_2 fed fuel cell is getting much attention because of its low-temperature operation and high energy density at low weight [17–20].

Among hydrogen fuel cells, proton exchange membrane fuel cell

* Corresponding authors.
E-mail addresses: mosaddek.saju@bsmrstu.edu.bd (Md.M. Hossen), plamen.atanassov@uci.edu (P. Atanassov).
[1] Contributed equally

https://doi.org/10.1016/j.apcatb.2022.121733
Received 13 December 2021; Received in revised form 15 June 2022; Accepted 10 July 2022
Available online 6 August 2022

(PEMFC) is substantially studied for decades and it showed better candidacy compared to alkaline exchange membrane fuel cell (AEMFC) [21,22]. Proton is more diffusive than OH^- ion, which provides an advantage to obtain higher ionic conductivity in PEMFC [23]. Nonetheless, PEMFC has durability issues due to its acidic conditions even for the noble metal-based catalysts [19,24–27]. On the other hand, AEMFC allows the use of inexpensive non-noble metals and non-metal catalysts in the alkaline environment [22,28–31]. It was found in a study that catalyst deactivation by H_2O_2 was more severe in acidic conditions than alkaline [32]. Also, unlike proton exchange membrane (PEM), AEM can be synthesized without incorporating any fluorinated compounds, which are expensive and toxic too [27]. ORR is more favorable with a faster electrochemical kinetics in alkaline than acidic conditions and thus the alkaline media allows one to use of lower catalyst loading [33–35]. Also, the alkaline environment is less corrosive [36,37], thereby creates an opportunity to apply a broad category of materials for flow field plates [38] and non-noble metals for electrocatalysts [39,40].

Till now, numerous researches have been carried out on the improvement of AEMFC performance [41] by optimizing the anode and cathode catalysts [42–50], membrane [51–54], ionomer [55–57], gas diffusion layer (GDL) [58,59], bipolar plates [60–62], operating conditions [63,64], water management [65,66], durability [67,68] etc. The ORR is a sluggish reaction and rate-limiting process in fuel cells and ORR at cathode shows a higher overpotential compared to HOR at anode [69–73], so the optimization of the cathode catalyst is one of the prime concerns. Since PtRu/C sets a benchmark as anode catalyst [74,75] and Pt/C as cathode catalyst for AEMFC by showing the highest performance [52,56,76–82] but being expensive and scarce [41,80,81], researchers are focused to obtain a similar or better functionality by using non-platinum catalysts and several studies proved it to be achievable [43–47,83–89].

In the exploration of inexpensive non-platinum catalysts, researchers synthesized hundreds of catalysts using different types of metal-containing or non-metallic starting compounds. This review paper is an attempt to summarize these efforts and compare the performances of different cathode catalysts applied in H_2/O_2 fed all-solid-state AEMFCs since 2006. U.S. Department of Energy (D.O.E.) set targets for polymer electrolyte membrane fuel cell (both AEMFCs and PEMFCs) in the year of 2020 such as cost at 14 $\$/kW_{net}$, durability after 5000 cycles with less than 10% drop in rated power after test at 80°C (or upto peak temperature), the current density of 300 $mA.cm^{-2}$ at 0.8 V, and rated power of 1000 $mW.cm^{-2}$ at 150 kPa_{abs} with maximum inlet RH of 40% respectively [90]. A new broad classification of the catalysts is presented in this article. The identification of the catalysts as per classification is important to compare their usefulness. Many catalysts which were explored only for the ORR activity test but not tested in a single cell AEMFC are excluded from this article's discussion. Also, several catalysts, which were studied for the ORR in different cells other than H_2/O_2 fed AEMFC are also ignored from the list. In this work, a list of 212 non-platinum catalysts from 159 articles is prepared. The statistical analysis of the information provides important aspects and guidelines for the future direction in the research. The findings from the previous researches are documented in different sections accordingly. The activities and performances of the catalysts depend on several factors such as porosity, surface area, nitrogen or heteroatom contents, transition metal content, different active sites, edge defects, ionomer content, catalyst loading, etc. as determined by the rotating (ring)-disk electrode method. In addition to these factors, the AEMFC performance is influenced by anion exchange membrane and ionomer, water management, catalyst-ionomer interactions, fuel cell operating conditions, etc. All these aspects are thoroughly discussed in this review article.

1.1. AEMFC mechanism

In hydrogen fuel cells, H_2 is supplied as a fuel and O_2 as an oxidant. Unlike PEMFC, OH^- ions are generated in AEMFC and an AEM is used to transport OH^- ions. Practically air may be used as a source of O_2, so purification is necessary since air may contain CO_2 and dust particles, since CO_2 may neutralize the electrolyte (OH^-), form weaker nucleophiles i.e. carbonates/ bicarbonates and thereby decrease the concentration of electrolyte, deactivate the membrane and degrade the cell performance [91–93]. However, solid alkaline-electrolyte membrane is somewhat advantageous compared to previously used electrolyte solution due to its CO_2 tolerance properties [19]. H_2 and O_2 are fed at the anode and cathode side, respectively. The schematic diagram of AEMFC is shown in Fig. 1. At the triple-phase boundaries, the electrochemical reactions occur. In the presence of water, O_2 at the cathode is reduced into OH^- ions which move through the membrane to the anode side and react with H_2 to produce H_2O. Water is consumed at the cathode and produced twice at the anode, so if water management is not maintained properly, the cathode may get dried and the anode may get flooded. During redox reaction, electrons that are produced on the anode side are collected by the current collectors and transferred to the cathode side through the external circuits. The membrane is selected as such that it specifically transports OH^- ion.

The ORR may follow two pathways as follows:

($4e^-$ pathway).

$$O_2 + 2\,H_2O + 4e^- \rightarrow 4\,OH^-;\ E^0 = +\,0.401\ V\ vs\ SHE \quad (1)$$

($2e^-$ pathway).

$$i)\ O_2 + H_2O + 2e^- \rightarrow HO_2^- + OH^-;\ E^0 = -\,0.065\ V\ vs\ SHE \quad (2)$$

$$ii)\ HO_2^- + H_2O + 2e^- \rightarrow 3OH^-;\ E^0 = +\,0.867\ V\ vs\ SHE \quad (3)$$

$$Or,\ 2HO_2^- \rightarrow 2OH^- + O_2 \quad (4)$$

Anode reaction is occurred as follows:

$$2\,H_2 + 4OH^- \rightarrow 4\,H_2O + 4e^-;\ E^0 = +0.8277\ V\ vs\ SHE \quad (5)$$

The overall reaction is -

$$O_2 + 2\,H_2 \rightarrow 2\,H_2O;\ E^0 = +1.229\ V \quad (6)$$

The peroxide produced during $2e^-$ pathway is detrimental to catalyst and membrane stability. The formation of peroxide also reduces the fuel cell efficiency. For this reason, $4e^-$ pathway is desired for ORR. The number of electrons transferred (n_{e^-}) and percentage yield of peroxide formation during the ORR process can be calculated from the RRDE data. Since ORR is a slow reaction because of its high bond energy, the search for suitable cathode catalysts gets much importance.

1.2. Half-Cell / RRDE/ RDE experiment

The electrocatalytic activity of the AEMFC cathode catalysts for ORR can be measured using a rotating ring-disk electrode (RRDE) or rotating disk electrode (RDE) setup. Both of these tests are important to comprehend the structure-activity relationship and limiting factors [73,77]. The techniques are widely used due to their several advantages such as standard protocol, a small amount of catalyst required for the test, a

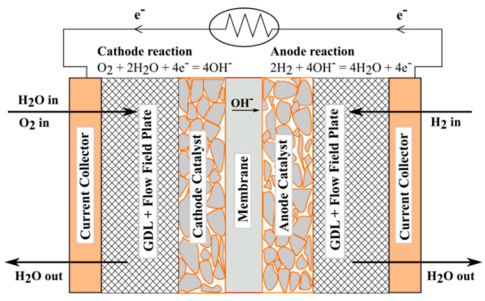

Fig. 1. Schematic diagram of an AEMFC showing its components.

well-established methodology available to obtain kinetic parameters etc. [94–97]. Nonetheless, the experimental conditions in RDE mismatch the practical environment of a fuel cell from several aspects such as thin layer of catalyst in RDE, rotation of working electrode, small area, current density at different range, glassy carbon disk used instead of gas diffusion layer, differences in gas flow pattern etc. [94]. Thereby, several other alternative approaches such as passive purge half-cells, forced or convective flow in half cells, half-cell combining flow field, conventional GDE or catalyst-coated membrane (CCM) etc. have been proposed [94,97–103]. These approaches are expected to better understand the activity, stability and GDE properties by covering the gap between RDE and MEA investigations. However, since RDE is still a most commonly used approach, this technique is shortly discussed below.

The difference between RDE and RRDE setup is a ring electrode generally made of platinum, which is present in RRDE, but absent in RDE. The setup consists of three electrodes including working, counter, and reference electrode. Both RRDE and RDE consist of a disk which works as a working electrode. The rotation speed of the working electrode can be controlled. Since the purpose of this experiment is to determine the ORR electrocatalytic activity of the catalysts in an alkaline medium, so oxygen saturation is required in the solution. Generally, 0.1 M or, 1 M KOH solution is used as the electrolyte to evaluate the ORR catalysts. The catalyst ink that is a mixture of catalyst, ionomer and solvents is deposited on the working electrode to achieve a desired catalyst loading.

The potentiostat connected to the half-cell setup collects data such as cyclic voltammetry (CV), linear sweep voltammetry (LSV), chronoamperometry etc. The data can be obtained at different rotation rates of the working electrode. Additionally, ring current data at different potentials can be collected from the RRDE experiment. The potential is measured with respect to the reference electrode and applied between the working electrode and the counter electrode. Different electrodes such as Ag/AgCl, Hg/HgO, saturated calomel electrode (SCE), etc. may be used as the reference electrodes. All the potentials measured using different reference electrodes can be converted into the reversible hydrogen electrode potentials (V vs RHE) using the following equations.

$$E_{(RHE)} = E_{(Ag/AgCl)} + 0.197 + 0.0592 \times pH \quad (7)$$

$$E_{(RHE)} = E_{(SCE)} + 0.241 + 0.0592 \times pH \quad (8)$$

$$E_{(RHE)} = E_{(Hg/HgO)} + 0.098 + 0.0592 \times pH \quad (9)$$

$$E_{(RHE)} = E_{(SHE)} + 0.0592 \times pH \quad (10)$$

From the LSV experiment, onset potential (E_{on}) at which the ORR polarization curve commences (typically estimated at the ORR current density of −0.1 mA cm^{-2}) and half-wave potential ($E_{1/2}$) at which disk current is half of the limiting current can be determined. The high values of E_{on} and $E_{1/2}$ indicate high electrocatalytic activity toward ORR for the catalysts. For oxygen reduction on non-precious metal electrocatalysts in O_2-saturated 0.1 M KOH solution the values of E_{on} and $E_{1/2}$ should be at least 1.0 V and 0.9 V vs. RHE, respectively, using a typical catalyst loading of 0.2 mg cm^{-2}.

From the RRDE experiment, ring current (i_r) and disk current (i_d) can be obtained. Using those data, the number of electrons transferred during the ORR (n_{e^-}) and $\%H_2O_2$ yield can be calculated as per the following equations.

$$\%H_2O_2 = 200 \times \frac{\frac{i_r}{N}}{i_d + \frac{i_r}{N}} \quad (11)$$

$$n_{e^-} = 4 \times \frac{i_d}{i_d + \frac{i_r}{N}} \quad (12)$$

where collection efficiency (N) is assumed as a constant value for a specific RRDE tip.

The percentage yield of peroxide formation should be as low as possible for excellent ORR electrocatalysts. The formation of peroxide is detrimental for fuel cell catalysts and membranes and it also decreases the fuel cell efficiency. For non-precious metal electrocatalysts the % H_2O_2 value should be lower than 5% in the potential range relevant for AEM fuel cells (between 0.5 and 0.8 V).

The number of transferred electrons (n_{e^-}) can also be calculated from the Koutecky-Levich (K-L) equation using disk current (i_d) only from RRDE or RDE experiment. The equation is given below.

$$\frac{1}{i} = \frac{1}{i_L} + \frac{1}{i_k} = \frac{1}{B\omega^{1/2}} + \frac{1}{i_k} \quad (13)$$

$$B = 0{\cdot}62 n_{e^-} F C_0 (D_0)^{2/3} \nu^{-1/6} \quad (14)$$

where i_k is the kinetic current density, i_L is the mass transport limited current density, F is the Faraday's constant, C_0 is the bulk concentration of O_2 in the electrolyte solution, D_0 is the diffusion coefficient of O_2 in the electrolyte solution, ω is the angular velocity of rotating disk, and ν is the kinematic viscosity of the electrolyte solution. A linear relationship is observed between the inverse current density and the inverse square root of the electrode rotation rate. The linearity of the K-L plot indicates the first-order reaction kinetics toward the concentration of O_2 [104]. If i^{-1} vs $\omega^{-1/2}$ are plotted, then n_{e^-} can be calculated from the slope of the straight line using the K-L equation and i_k can be obtained from the intercept. The ORR activity data determined from these experiments are listed in Tables 1 and 2. Tafel plot (η vs log $|i_k|$) is applied in studying the kinetics of the ORR. The Tafel slope value can be used to evaluate the mechanism of the ORR. However, different mathematical models have also been published to determine ORR kinetic parameters [105–107].

However, the half-cell data may not always be used as a predictor to compare fuel cell performances, since there is a discrepancy in current densities between RRDE and fuel cell test. Also, there are mass transfer limitations phenomenon present in fuel cells but absent in the RRDE test [108].

1.3. Single fuel cell test experiment

The prepared non-platinum cathode catalyst and commonly platinum as an anode catalyst are tested in a single fuel cell to observe the performance practically. The catalyst inks are prepared by mixing them with the ionomer and solvent, where ionomer acts as a binder for catalyst or support particles and transport ions, reactant gases and water molecules within the catalyst layer. The colloidal state of the ink is helpful for the formation of continuous ion transport channels that favors triple phase boundary and reduces the mass transfer resistances [109]. The solvent is used to dissolve ionomers and disperse the catalyst into the solution properly. It also helps to obtain porous structures by getting evaporated during synthesis. It was found that smaller pore size in catalyst layer was achieved by a solvent of higher boiling point, while low boiling point solvent may facilitate to obtain mesoporous structures [110]. The solvent should be volatile and possess a high dielectric constant [111]. Isopropyl alcohol and deionized water are commonly used as the solvent. Also, solvents of different dielectric constants were used in previous studies to achieve different pore structures and triple phase boundaries in catalyst layers [109]. The cathode and anode catalyst inks may be sprayed or cast on either side of the membrane as shown in Fig. 2. The membrane is then called the catalyst coated membrane (CCM). The inks, instead, may also be coated on the surface of the gas diffusion layer (GDL). The GDL is then called a gas diffusion electrode (GDE). The substrate temperature and time interval between deposition of layers have effects on the formation of mesoporous structures [110]. There are several catalyst depositing techniques available in the industries and laboratories. The combination of membrane, catalysts, and GDL is called membrane electrode assembly (MEA). MEA is then sandwiched between gasket, flow field plates, and current collectors. The full assembly of a single fuel cell is shown in Fig. 2.

Table 1
Data of specific surface area, ORR activity (from RRDE test) and fuel cell (H_2/O_2 fed AEMFC) performance for the non-platinum cathode catalysts (2018-Present).

Catalysts [Ref]	Specific Surface Area ($m^2.g^{-1}$)	RRDE Test Data				H_2/O_2 AEMFC Fuel Cell Test Data			
		Onset Potential, E_{on} (V vs RHE)	Half-wave Potential, $E_{1/2}$ (V vs RHE)	No. Of electrons Transferred (n_e)	Max % H_2O_2 Yield	Open Circuit Voltage, OCV (V vs RHE)	Peak Power Density, PPD ($mW.cm^{-2}$)	Specific PPD ($mW.mg^{-1}_{Pt}$ Or $mW.mg^{-1}_{PtRu}$)	Current Density, i at PPD ($mA.cm^{-2}$)
a) **Transition metal ceramics (Ceram)**									
H.A.Ni[169]	8.9	0.80	0.58	3.20	–	0.65	11.5	57.5	28
H.A.Co[169]	6.8	0.80	0.52	–	–	0.56	3.0	15.0	11
Co/SiOC[195]	–	0.87	0.77	3.7	–	1.00	54.0	270.0	100
a) **Metal-Carbon Derived Catalysts (MCC)**									
i) Metal-Carbon (MCC-M-C)									
Ag/C[156]	102.0	1.08	0.90	–		0.85	200.0	625.0	500
40 wt% Co@G/C_600[164]	–	0.89	0.79	3.6	–	0.92	412.0	1030.0	900
Ag/MWCNT[196]	170.4	–	–	–	–	0.91	356.5	1114.1	850
Ag/AC[196]	98.4	–	–	–	–	1.02	256.6	801.9	700
Ag/CB[196]	139.9	–	–	–	–	0.90	329.3	1029.1	950
Ag/C[197]	–	–	–	–	–	0.93	516	1563.6	900
Ag/C[198]	–	–	–	–	–	0.91	520	650	1340
Ag/C VGDE[199]	18.1	–	–	–	–	0.88	215	537.5	667
ii) Bimetals-Carbon (MCC-MM-C)									
Cr–Ni–V[166]	288.0	0.83	0.73	2.8	–	0.80	22.0	64.7	50
iii) Bimetals- Nitrogen-Carbon (MCC-MM-N-C)									
CoCu/PNC-900[158]	403.4	0.91	0.81	–	–	0.74	62.0	155.0	180
FeCoNC-at[30]	292.0	0.96	0.83	3.8–4.1	–	1.04	415.0	691.7	820
Fe-Co-N-C[200]	256.0	0.90	0.76	–	7	0.90	420.0	583.3	1150
CoFe-N-CDC/CNT[151]	399.0	0.96	0.83	3.50–3.75	24	0.90	1120.0	1600.0	2040
Fe/Co/IL-CNF-800b[201]	351	1.01	1.01	3.75–4.1	–	1.05	195	325	350
FeCoN-MWCNT[202]	–	0.93	0.86	3.8–4.06	–	0.98	692	988.57	1570
FeMnN-MWCNT[202]	–	0.93	0.85	3.85–3.9	–	0.95	582	831.43	1190
0.14Co0.01Fe—CB[203]	–	0.96	0.86	–	–	0.99	304	394.8	620
FeMn-N-MPC[204]	583	0.98	0.89	3.8–4.0	12	0.99	474	592.5	895
FeCu1.0NC[205]	910	1	0.92	3.94–3.97	4	1.01	294	420	850
Zn/FeSA-PC/950/NH3[206]	1260	1	0.88	4	0.9	0.91	352	586.67	710
FeSiNC_50a[207]	629.0	1.02	0.86	4	–	0.96	200.0	500.0	555
Metal Organic Framework Derived (MCC-MM-N-C-MOF)									
Fe–N–Co@C-800-AL[83]	449.0	0.91	0.80	3.98	1.3	0.90	137.1	171.4	260
NiCo/NCNT[85]	358.8	0.98	0.88	3.98	–	0.96	65.0	541.7	130
Zn-Co/N/C-IL20[171]	43.0	0.93	0.84	3.88	–	0.94	300.0	500.0	680
iv) Metal-Nitrogen-Carbon (MCC-M-N-C)									
Fe-N-C[208]	725.0	0.99	0.89	3.75–4.00	13.50	1.02	220.0	366.7	350
FePc-KCB[185]	1343.0	1.00	0.92	–	–	0.99	108.0	216.0	188
SiCDC/CNT(1:3)/CoPc[175]	335.0	0.91	0.81	4	–	0.94	473.0	675.7	1100
Co-N-CDC/CNT_mel[46]	276.0	0.95	0.82	3.5–3.8	20.00	0.96	577.0	961.7	1150
Fe-NMG[86]	520.5	0.96	0.83	–	13.00	1.05	218.0	1090.0	335
Fe-NMP[86]	565.8	0.97	0.84	–	22.00	1.05	110.0	550.0	222
Fe-MBZ[86]	560.0	0.85	0.74	–	9.00	0.95	90.0	450.0	223
m-FePhen-C[87]	1437.0	1.00	0.90	3.70–4.00	5.00	1.03	272.0	1360.0	590
Fe-EDTA-Graphene (EFGC)[172]	385.0	1.03	0.86	3.9–4.0	5	0.97	330.0	1100.0	810
Fe/N/CDC[209]	1035.0	0.96	0.77	4.7–4.8	–	1.01	80.0	173.5	165
Co/N/CDC[209]	–	0.96	0.80	4.0–4.2	–	1.01	78.0	169.2	130
Fe-PAN-A800[163]	81.0	0.98	0.80	4.0–4.3	–	1.04	257.0	428.3	550
Co-PAN-A1000[163]	326.0	0.91	0.82	3.9–4.1	–	0.99	267.0	445.0	500
Fe/IL-PAN-A1000[163]	202.0	0.95	0.74	3.8–4.2	–	1.03	289.0	481.7	600
Co/IL-PAN-A800[163]	126.0	0.92	0.79	4.0–4.3	–	1.00	213.0	355.0	370
Fe—Phen/CNT[155]	–	0.99	0.90	3.85–4.0	–	1.00	410.0	820.0	800
Fe-N-Gra[124]	426.0	0.94	0.77	4.0–4.6	–	1.06	243.0	405.0	575
TiCDC/CNT(1:3)/FePc[176]	572.0	0.93	0.77	3.69–3.75	–	1.00	182.0	227.5	490
SiCDC/CNT(1:3)/FePc[176]	357.0	0.87	0.74	4.1–4.6	–	1.00	164.0	205.0	485
pyrolysed KB/FePc[176]	–	0.94	0.76	–	–	1.00	186.0	232.5	450
FeNC-4000[84]	–	1.05	0.94	3.9	5	1.08	526.0	–	900
FeNCF w (8%ZnCl2 + SWCNH)[210]	719.0	1.01	0.93	3.86–3.99	6.5	0.98	125.0	–	260
Fe(1,10-phen)/KB[211]	–	0.97	0.86	3.97	–	1.00	197.0	1059.1	480

(*continued on next page*)

Table 1 (*continued*)

Catalysts [Ref]	Specific Surface Area ($m^2.g^{-1}$)	RRDE Test Data				H_2/O_2 AEMFC Fuel Cell Test Data			
		Onset Potential, E_{on} (V vs RHE)	Half-wave Potential, $E_{1/2}$ (V vs RHE)	No. Of electrons Transferred (n_e)	Max % H_2O_2 Yield	Open Circuit Voltage, OCV (V vs RHE)	Peak Power Density, PPD ($mW.cm^{-2}$)	Specific PPD ($mW.mg^{-1}_{Pt}$ Or $mW.mg^{-1}_{PtRu}$)	Current Density, i at PPD ($mA.cm^{-2}$)
Fe-HT-N-800[212]	410.0	0.99	0.83	4	–	1.00	270.0	539.9	610
Fe-N-comp-2[213]	440.0	0.99	0.89	4.00–4.20	–	0.97	120.0	260.9	210
Fe-N-comp-0.5[213]	349.0	0.93	0.82	4.30–4.40	–	0.88	160.0	347.8	330
Fe-N-CDC/CNT[151]	404.0	0.99	0.86	3.70–3.90	15.00	0.97	880.0	1257.1	1950
Co-N-CDC/CNT[151]	393.0	0.93	0.84	3.40–3.60	32.00	0.92	1060.0	1514.3	1940
HT800-FeP aerogel[214]	–	0.96	0.86	3.9	0.9	0.93	580	816.9	1570
Fe2 + @NCS-A[215]	70	0.94	0.79	3.87–3.98	13	0.96	108	154.29	235
CNT/PC (Fe−N/C)[216]	–	0.96	0.88	3.52	–	0.95	350	700	800
Fe-N-C[142]	1165	1.00	0.88	–	12.8	0.97	1800	3000	3800
Fe-N-C[198]	–	–	–	–	–	1.02	750	937.5	1750
CoNC1000A900[217]	393.94	0.93	0.77	3.94	–	0.86	374.3	–	940
SNW-Fe/N/C@ 800[218]	739	1.10	0.94	3.97–4.0	1.5	0.96	266	665	660
Co3N/C[219]	–	0.94	0.86	3.84–3.90	7.8	0.91	700	1750	1750
Fe-N-MPC[204]	584	0.99	0.89	3.8–4.0	12	0.96	473	591.25	890
Co–N–C-THF[220]	–	–	–	–	–	1	181.7	454.25	450
Biomass derived heteroatom doped Carbon (MCC-M-N-C-BM)									
Co2P-NBSP (NBSCP)[194]	571.8	0.96	0.84	3.4–3.8	–	1.00	172.2	925.8	415
Fe-LC-900[221]	746.0	0.96	0.82	3.6–3.9	–	0.92	50.0	62.5	115
PBC/900/M[222]	607	1.01	0.862	3.99–4	0.5	0.95	658	1096.6	1500
Metal Organic Framework Derived (MCC-M-N-C-MOF)									
Co@C-800-AL[83]	437.6	0.93	0.82	3.96	2.1	0.80	125.8	157.3	330
FeNx-CNTs[146]	1135.4	1.08	0.94	4	0.01	0.85	1150.0	3833.3	3100
Co/NCNT[85]	–	0.95	0.84	–	–	0.94	55.0	458.3	92
ZIF-CB-700[47]	264.8	0.96	0.80	3.85–3.96	7.00	0.92	122.3	–	280
$Fe_{0.5}$-NH_3[165]	–	1.00	0.83	–	19.50	1.00	1060.0	2355.6	2250
5 at% Co-NC[223]	436.7	0.98	0.90	–	–	1.00	271.0	677.5	640
PVP-ZIF-8 @CNT-900[224]	78.0	0.96	0.80	3.80–3.90	10.00	0.95	45.0	56.3	88
h_CoNC/CNT[225]	490.88	1	0.89	3.81–3.98	–	0.92	133	332.5	450
Fe-N-C Act[147]	1420.0	1.01	0.90	3.93–4.00	3.50	0.98	786.0	1965.0	1600
Rock derived Carbon (MCC-M-N-C-R)									
SHUb-Fe/N-A[226]	–	0.94	0.80	4.0–4.1	–	1.01	234.0	390.0	570
SHUb-Co/N-A[226]	–	0.93	0.80	3.7–3.9	–	0.98	232.0	386.7	650
Single Atom Catalyst (MCC-M-N-C-SAC)									
C@PVI-(DFTPP)Fe-800[173]	868.0	0.99	0.88	3.9–4.1	2.5	0.93	104.0	260.0	300
Fe3C-NP/FeNx@Gr-900[227]	235.3	0.95	0.90	3.9	5	0.88	367.0	917.5	900
Cu SAC[228]	–	0.97	0.81	3.60–4.00	0.0078	0.85	196.0	392.0	460
Fe-N-C[139]	550	0.97	0.85	3.91–4.0	4	0.9	2040	3416.7	4600
Co1/CNH 700[229]	–	0.96	0.833	3.91	5	0.97	472	1180	1080
Non-metals doped M-N-C (MCC-M-N-C-NM)									
Cu–N/B–C-800[230]	757.0	0.95	0.84	3.80–3.85	10	0.85	80.0	200.0	250
FeCNB-900[231]	784.0	1.02	0.86	3.86–3.98	5	0.94	172.0	430.0	500
NFC@Fe/Fe3C-9[188]	392.6	0.97	0.87	4.07	–	0.85	96.0	240.0	250
FeFPc@BP2000[232]	319.49	1.01	0.934	3.9	–	0.98	165	275	335
Fe−P − Phen/CNT[155]	–	0.99	0.91	–	–	1.00	570.0	1140.0	1150
FeCN-S-800[180]	102.3	0.91	0.76	3.99	0.37	0.79	125.0	625.0	350
PMCNT-900[178]	1645.0	1.06	0.78	3.98–4	1.5	0.92	65.0	325.0	115
Fe−S−Phen/CNT[155]	–	0.99	0.91	–	–	1.00	635.0	1270.0	1350
a) **Transition metal oxides (TMO)**									
i) Metal oxide-Carbon (TMO-MOx-C)									
α-MnO2/C (#6)[233]	–	0.83	0.67	–	–	0.91	45.2	226.0	75
ii) Metal oxide-Nitrogen-Carbon (TMO-MOx-N-C)									
N-C-CoOx[162]	–	0.89	0.82	3.93–3.98	3.00	0.89	1050.0	1500.0	2500
iii) Metal-Metal oxide-Nitrogen-Carbon (TMO-M-MOx-N-C)									
Cr/rGO-MnO[43]	379.0	1.05	0.89	3.98–3.99	2.50	1.05	309.0	–	630
FeN-SiCDC-0.5–400-wet-PVP[89]	865.0	1.01	0.83	–	–	1.05	356.0	445.0	830
Zeolitic Imidazolate Frameworks Derived (TMO-M-MOx-N-C-ZIF)									
α-Mn_2O_3/Fe0.5-NH3[165]	–	1.00	0.78	–	4.50	1.00	1000.0	2222.2	2333
iv) Perovskite Oxide-Nitrogen-Carbon (TMO-ABX_3-N-C)									
	30.0	0.86	–	–	–	0.94	76.0	380.0	190

(*continued on next page*)

Table 1 (*continued*)

Catalysts [Ref]	Specific Surface Area ($m^2.g^{-1}$)	RRDE Test Data				H_2/O_2 AEMFC Fuel Cell Test Data			
		Onset Potential, E_{on} (V vs RHE)	Half-wave Potential, $E_{1/2}$ (V vs RHE)	No. Of electrons Transferred (n_e)	Max % H_2O_2 Yield	Open Circuit Voltage, OCV (V vs RHE)	Peak Power Density, PPD ($mW.cm^{-2}$)	Specific PPD ($mW.mg^{-1}_{Pt}$ Or $mW.mg^{-1}_{PtRu}$)	Current Density, i at PPD ($mA.cm^{-2}$)
LaAl-CaMnO3/N/C [168]									
v) Spinel Oxide-Carbon (TMO-AB_2X_4-C)									
Co-Fe/VC[143]	–	0.78	0.71	4	10.00	0.90	1350.0	1928.6	3150
$MnCo_2O_4$/C[174]	–	0.95	0.84	–	–	0.92	1170.0	1950.0	2780
$CoMn_2O_4$/C[174]	–	0.95	0.86	–	–	0.95	1100.0	1833.3	2400
Mn-Co spinel (MCS) [177]	–	0.95	0.86	–	8	0.95	1100.0	2750.0	2500
a) **Support-free Metal (SFM)**									
i) Single Metal (SFM-M)									
V-AgNs[234]	60.6	1	0.79	3.94–3.98	3	0.77	115.6	92.48	400
a) **Non-metallic catalysts (NMC)**									
i) Fluorine-Carbon (NMC-F-C)									
F-MC (5: 1)— 950[186]	428.9	0.91	0.79	3.4–3.8	–	0.75	10.0	50.0	20
ii) Fluorine-Nitrogen- Biomass derived Carbon (NMC-F-N-C-BM)									
N-F co-doped coffee carbon (N-F/CC)[235]	975.1	0.82	0.68	3.98	1.5	0.59	8.3	16.6	57
N-F/PGPC[236]	974.0	0.92	0.87	3.90–3.98	3.9	0.70	22.0	44.0	67
iii) Fluorine-Nitrogen-Carbon (NMC-F-N-C)									
N-F/CTC[187]	950.0	0.97	0.86	4.1–4.7	1.5	0.75	14.0	28.0	53
N-F co-doped GNF (GNF-H/N-F)[237]	810.0	1.02	0.88	3.97	1.1	0.84	51.0	510.0	130
GNF-L/N-F[237]	750.0	0.98	0.88	3.82–3.89	2.6	0.67	32.0	320.0	65
GNF-A/N-F[237]	780.0	1.03	0.88	3.85–3.95	1.9	0.72	42.0	420.0	100
iv) Nitrogen-Carbon (NMC-N-C)									
PAN-A1000[163]	–	0.88	0.69	2.4–2.7		0.96	180.0	300.0	480
N-CDC/CNT_mel[238]	408.0	0.91	0.76	3.75–4.0	–	0.95	310.0	516.7	820
NHCS–W[126]	360.0	0.95	0.86	3.71–3.83	–	1.00	132.0	–	325
N/C[239]	1320	0.91	0.81	3.64	–	0.91	56	18.7	131
N-doped-C[154]	–	–	–	–	–	0.94	1140	1628.6	2330
N-GLC[240]	530	0.92	0.83	3.55–3.75	20	0.72	6	12	20
v) Conducting Polymers (NMC-PM)									
BBL[241]	–	0.97	0.97	2.4–2.7	90	0.69	0.0325	–	0.32
vi) Oxygen-Sulphur-Nitrogen-Carbon (NMC-O-S-N-C)									
MH-DCNT[157]	366.0	0.92	0.81	3.5	–	0.90	250.0	1250.0	545
vii) Sulphur-Nitrogen- Biomass derived Carbon (NMC-S-N-C-BM)									
S, N co-doped bamboo carbons (SNBC12) [242]	349.1	0.96	0.85	3.3–3.8	32	0.96	217.0	434.0	550

Bipolar plates or flow field plates may have serpentine channels to facilitate the inlet and outlet flow of the reactants and products. The gas and liquid molecules pass through the pores of the GDL which has a hydrophobic surface at one side to disengage water molecules. Rubbery gaskets are used to fit the MEA in a leakproof condition. Current collectors are placed at the ends. The reactant gases (H_2 and O_2) may be supplied at definite humidity and backpressures. The polarization curves and the corresponding data can be obtained from the assembly using a fuel cell test station. The single fuel cell test data from the previous studies are listed in Table 1 and Table 2. The effect of the humidity, back pressure, etc. on the fuel cell performance is discussed later.

The polarization curve for a single cell represents the output of voltage versus current density. Open-circuit voltage is generally lower than the overall cell potential at 1.2 V and the voltage gets reduced with the increase of the current density. Three types of voltage losses or overpotentials are identified i.e. activation loss, ohmic loss, and mass transport loss. The slowness of the reaction induces some voltage loss known as activation loss. Ohmic loss indicates the loss from the resistance to the flow of ions and electrons, whereas mass transport loss arises due to the depletion of the reactants at the surface of the catalysts at high current densities.

The AEMFC performance depends on the following factors: (1) the application of suitable AEM with good chemical stability, high conductivity and proper water transport properties, (2) water management in the catalyst layers and membrane, (3) highly active electrocatalysts with tuneable porosity, and (4) decreasing the influence of CO_2 [112]. This review article concentrates mainly on the development of ORR electrocatalysts, however, the other factors are also discussed with special consideration.

2. Brief analysis of previous studies

Carbon is generally used as a support material because of its good mechanical strength, chemical and mechanical stability, high electrical conductivity, and specific surface area [113]. It was found in a research by Jahnke et al. in 1976 that carbon support and thermal treatment improved the ORR activity of phthalocyanine [114]. Pristine carbon materials such as carbon nanotubes (CNTs), graphene etc. showed poor ORR activity [115–117]. Transition metals in carbon matrix enhances charge transfer and thereby improves ORR activity and stability [118–120]. Heteroatom doped carbon materials showed higher ORR activity than undoped carbon-based materials [121–123]. A study showed that after nitrogen doping, the catalyst particle sizes became smaller, but the surface area was reduced because of clogging [124]. Also, it was claimed in previous studies that the presence of oxygen in the catalyst reduces ORR activity due to lowered turnover frequency of

Table 2
Data of specific surface area, ORR activity (from RRDE test) and fuel cell (H_2/O_2 fed AEMFC) performance for the non-platinum cathode catalysts (2006–2017).

Catalysts [Ref]	Specific Surface Area ($m^2.g^{-1}$)	RRDE Test Data				H_2/O_2 AEMFC Fuel Cell Test Data			
		Onset Potential, E_{on} (V vs RHE)	Half-wave Potential, $E_{1/2}$ (V vs RHE)	No. Of electrons Transferred (n_{e^-})	Max % H_2O_2 Yield	Open Circuit Voltage, OCV (V vs RHE)	Peak Power Density, PPD ($mW.cm^{-2}$)	Specific PPD ($mW.mg^{-1}_{Pt}$ Or $mW.mg^{-1}_{PtRu}$)	Current Density, i at PPD ($mA.cm^{-2}$)
a) **Transition metal chalcogenides (Chalc)**									
Co9S8/G-500 (1:1) [243]	–	0.95	0.86	3.90–3.99	5.0	0.92	31.0	62.0	60.0
MoS2/G-500 (1:1) [244]	–	0.91	0.80	3.80	–	0.93	29.0	58.0	68.0
MnS/G (50%)[245]	–	0.83	0.71	3.8–3.9	4.9	0.75	12	24	26.0
a) **Metal-Carbon Derived Catalysts (MCC)**									
i) Metal-Carbon (MCC-M-C)									
Ag-GNS[246]	10.7	–	–	–	–	1.02	287.8	575.6	525.0
Ag/C[247]	–	0.94	0.73	3.94	–	0.98	190.0	950.0	420.0
40 wt% Ag/CNT[248]	55.4	0.90	0.81	3.6–4	–	1.18	26.1	52.2	60.0
Ag/C[249]	–	–	–	–	–	0.69	109.0	290.7	32.0
60% Ag/C[250]	88.8	0.86	0.75	4.00	–	0.93	10.0	52.6	38.0
Ag/C[251]	–	–	–	–	–	0.83	19.0	38.0	50.0
Co/XC-72[252]	–	0.91	0.81	3.50	–	0.87	129.0	129.0	310.0
Ag/C[253]	–	–	–	–	–	0.94	48.0	480.0	118.0
Ag/C[254]	5.1	–	–	–	–	1.02	208.0	416.0	450.0
Co-based/C (GP4-GPM)[255]	–	–	–	–	50.0	0.85	260.0	520.0	450.0
Hypermec 4020[256]	–	–	–	–	–	1.01	205.0	455.6	500.0
ii) Bimetals-Carbon (MCC-MM-C)									
CoFe/MNT[252]	–	0.94	0.85	3.20	–	–	180.0	180.0	–
CoFe/XC-72[252]	–	0.97	0.83	3.40	–	–	185.0	185.0	–
iii) Bimetals- Nitrogen-Carbon (MCC-MM-N-C)									
CoMn/pNGr(2:1)[257]	–	0.94	0.79	3.73–3.95	14.0	0.92	35.2	110.0	65.0
Fe/Co-NpGr[258]	170.0	0.93	0.84	3.99–4.10	–	0.85	35.0	43.8	60.0
CoFeN/C-HLH[259]	–	0.95	0.82	3.9–3.99	–	0.97	177.0	442.5	350.0
CoFeNx/C[260]	–	0.95	0.84	3.3–4.0	–	0.87	38.0	95.0	74.0
iv) Metal-Nitrogen-Carbon (MCC-M-N-C)									
Ag-NW[246]	5.1	0.92	0.78	3.7–3.95	–	1.01	164.4	328.8	325.0
Ag-NW/GNS[246]	–	–	–	–	–	1.01	194.5	389.0	425.0
CoNC-900[261]	364.0	0.94	0.81	3.8–3.9	10.0	0.92	60.0	75.0	135.0
40% CoPc/CB[262]	–	–	–	–	–	0.86	55.0	110.0	140.0
Fe-M-LA/C-700[263]	199.7	0.93	0.79	3.99–4.0	0.5	0.94	137.0	428.1	320.0
FeNCNH-900[264]	1315.0	0.88	0.72	3.8–4.05	–	0.83	35.0	–	83.0
FePc/MWCNT[265]	–	0.86	–	2.5–2.8	–	0.98	53.0	132.5	140.0
CoPc/MWCNT[265]	–	0.91	–	3.1–3.6	–	0.99	105.0	262.5	240.0
HNCS71[266]	–	0.97	0.82	3.88–3.95	6.0	0.96	68.0	136.0	150.0
CNT/PC (Fe)[267]	–	0.97	0.88	–	–	0.96	380.0	–	870.0
MnPc/C[268]	–	0.72	0.55	3.00	–	0.90	97.0	–	245.0
FePc/C[268]	–	0.87	0.70	3.80	–	0.83	87.0	–	200.0
CoPc/C[268]	–	0.79	0.70	1.90	–	0.87	105.0	–	230.0
NiPc/C[268]	–	0.69	0.59	1.70	–	0.90	88.0	–	225.0
BP-H-Fe-N[269]	1191.4	1.07	0.90	3.92–3.99	4.0	0.95	145.0	–	300.0
30 nm@Fe-N-C[270]	1192.0	0.92	0.84	3.76–3.98	–	0.90	100.0	200.0	218.0
Fe-NMCSs[271]	674.0	1.03	0.86	3.95–4.00	3.0	1.07	506.0	–	1000.0
Fe-pyPANI-K 700 °C [272]	569.5	0.91	0.77	–	–	0.98	157.0	314.0	405.0
Fe–N–C[133]	377.5	1.00	0.86	3.95–3.98	2.6	1.04	75.0	150.0	185.0
Co–N–C[133]	369.3	0.93	0.81	3.93–3.95	3.2	0.99	68.0	136.0	160.0
Fe-N-C (BIDC3)[273]	930.0	1.02	0.86	–	9.5	0.75	47.0	391.7	90.0
Co/N/MWCNT[274]	–	1.06	0.84	3.9–4.5	–	0.95	115.0	287.5	255.0
CoPc/MWCNT[274]	–	0.91	0.72	–	–	0.98	90.0	225.0	240.0
CoPc/C[275]	–	0.85	0.69	–	–	0.90	12.6	63.0	24.0
CuPc/C[275]	–	0.74	0.61	–	–	0.87	6.8	34.0	16.0
NiPc/C[275]	–	0.79	0.63	–	–	0.73	6.0	30.0	17.0
ZnPc/C[275]	–	0.75	0.61	–	–	0.73	6.1	30.5	18.0
FePc/C (600°C)[276]	585.0	0.95	0.88	4.00	1.1	0.88	123.0	307.5	270.0
Fe-Nx/C (BPox-NFe) [277]	1100.0	1.07	0.90	3.88–3.9	7.0	0.83	110.0	36.7	300.0
Fe-N-CC[278]	1590.0	0.94	0.83	3.8–3.98	2.5	0.96	120.0	1200.0	275.0
CS_FePc_450[279]	212.5	0.97	0.88	3.91	–	1.00	178.0	890.0	400.0
Cu-tri/C[280]	–	–	–	–	–	0.95	75.0	75.0	225.0
Fe/N/C (1000°C)[281]	478.3	1.02	0.93	3.89–3.99	5.3	0.92	485.0	1212.5	1100.0
CoPc/C[282]	–	0.85	0.73	1.96	–	0.61	8.6	17.2	30.0
Py-CoPc/C[282]	–	0.88	0.74	2.36	–	0.86	20.0	40.0	45.0
AP-CoPc/C[282]	–	0.91	0.75	2.40	–	0.87	21.7	43.4	45.0

(*continued on next page*)

Table 2 (*continued*)

Catalysts [Ref]	Specific Surface Area ($m^2.g^{-1}$)	RRDE Test Data				H_2/O_2 AEMFC Fuel Cell Test Data			
		Onset Potential, E_{on} (V vs RHE)	Half-wave Potential, $E_{1/2}$ (V vs RHE)	No. Of electrons Transferred (n_{e^-})	Max % H_2O_2 Yield	Open Circuit Voltage, OCV (V vs RHE)	Peak Power Density, PPD ($mW.cm^{-2}$)	Specific PPD ($mW.mg^{-1}_{Pt}$ Or $mW.mg^{-1}_{PtRu}$)	Current Density, i at PPD ($mA.cm^{-2}$)
MP-CoPc/C[282]	–	0.92	0.77	2.42	–	0.89	21.7	43.4	48.0
v) Non-metals doped M-N-C (MCC-M-N-C-NM)									
AT-Fe/N/C[283]	708.0	1.04	0.93	3.97	1.5	0.98	164.0	–	400.0
a) **Transition metal oxides (TMO)**									
i) Metal oxide-Carbon (TMO-MOx-C)									
MnOx/GC[284]	–	0.85	0.74	3.27–3.61	–	0.95	98.0	196.0	240.0
ii) Metal oxide-Nitrogen-Carbon (TMO-MOx-N-C)									
MnO/NG-900[285]	–	0.89	0.77	3.5–3.75	25.0	0.75	13.0	26.0	32.5
CoO-rGO(N)[286]	–	0.93	0.83	2.0–4.0	7.5	0.97	248.0	–	610.0
iii) Metal-Metal oxide -Carbon (TMO-M-MOx-C)									
Co-Fe3O4/C[287]	–	0.90	0.79	3.99–4.00	0.5	0.85	114.0	142.5	250.0
iv) Metal-Metal oxide-Nitrogen-Carbon (TMO-M-MOx-N-C)									
Fe-Fe2O3/NGr[288]	–	0.94	0.82	3.4–3.98	23.0	0.70	54.4	155.4	160.0
CoO@Co/N–C[289]	769.4	0.99	0.86	3.9–4.0	–	1.08	237.0	474.0	440.0
Co/CoO-NGA[290]	–	0.91	0.78	3.55–3.75	–	0.97	110.0	550.0	300.0
v) Perovskite Oxide-Carbon (TMO-ABX3-C)									
$La_{1-x}Sr_xMnO_3$/KB (20 wt%RM-LS 0.17 M/KB)[291]	–	0.87	0.75	3.92	–	0.96	130.0	282.6	300.0
La0.6Sr 0.4 MnO3 (LS 0.4 M/KB)[292]	20.0	0.88	0.77	–	–	1.00	92.0	–	330.0
vi) Hollandite Oxide (TMO-HDO)									
KMC0.12-HT[293]	79.7	0.90	0.60	3.7–3.82	–	0.95	49.0	–	140.0
a) **Non-Metallic catalysts (NMC)**									
i) Fluorine-Sulphur-Nitrogen-Carbon (NMC-F-S-N-C)									
CNT/HDC-1000[294]	–	0.92	0.82	3.85–3.97	–	0.85	270.0	–	600.0
F,N,S-rGO[295]	575.0	0.85	0.75	2.7–3.3	–	0.80	46.0	230.0	145.0
ii) Nitrogen-Carbon (NMC-N-C)									
N-CNT[296]	–	0.92	0.79	3.80	–	0.87	37.0	74.0	110.0
N/C (GU)[152]	118.0	0.90	0.75	3.41–3.55	26.7	0.59	403.0	671.7	1100.0
N/C (FU)[152]	824.0	0.90	0.76	3.7–3.8	13.2	0.95	703.0	1171.7	1400.0
g-CN-CNF-700[297]	–	0.82	0.69	3.35–3.46	–	0.88	171.0	342.0	350.0
NHC[298]	573.0	1.02	0.88	3.01–3.98		0.85	228.0	228.0	560.0
N-800[299]	1836.0	0.89	0.83	3.32–3.55	–	0.75	30.0	–	65.0
NCG-1000[300]	–	0.92	0.74	3.80	–	0.79	63.0	315.0	151.0
NCNTs (ED-CNT)[301]	–	0.98	0.66	–	–	1.07	25.5	56.7	52.0
1:5 NG-800 °C[302]	–	0.85	0.70	3.75–3.95	12.0	0.72	2.6	–	6.5
NpGr-72[303]	204.0	0.89	0.72	3.2–3.8	17.0	0.82	27.0	84.4	61.0
iii) Phosphorous- Nitrogen-Carbon (NMC-P-N-C)									
NPOMC-L2[304]	1100	0.93	0.83	3.50	–	0.88	89.0	890.0	200.0
iv) Sulphur-Nitrogen-Carbon (NMC-S-N-C)									
S-rGO[305]	–	0.74	0.62	2.0–2.5	–	0.78	2.4	7.9	9.5
N-S/Gr-1000[306]	–	0.92	0.79	3.50–3.90	25.0	0.91	19.8	39.6	45.0
N-S-MPC[307]	–	–	–	–	–	0.93	21.7	54.3	33.0

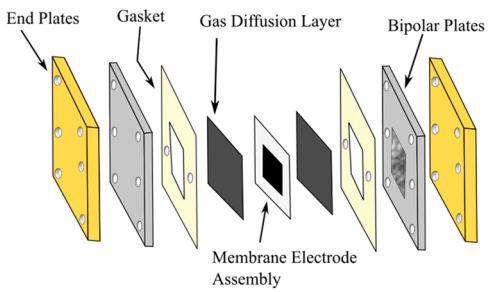

Fig. 2. Components for single fuel cell testing assembly.

Fe-N_x sites [124,125]. High graphitization is also important to achieve enhanced conductivity of carbon materials [126].

Nitrogen is a common element to be incorporated to the catalysts and different precursors are used as the nitrogen source. Li et al. stated three major groups of nitrogen precursors that were commonly used: (1) C≡N-based non-aromatic precursors, such as cyanamide, dicyandiamide, etc., (2) C-N-based nonaromatic amine precursors, such as ethylenediamine, etc. and (3) aromatic precursors, such as aniline, melamine, etc. [127].

Carbon-supported catalysts may show low performance because of the catalytic inertness of carbon. Support-free catalysts are expected to contain high active site density. Therefore, metal-organic frameworks (MOFs) containing the repeating units of metal centers coordinated to electron-donating organic ligands may serve as the support-free catalysts. MOF derived catalysts can be rationally designed to obtain uniformly distributed active sites, controlled microporosity and morphology [128]. Several MOF-based catalysts have already been studied using non-platinum metals [129]. An improvement in the ORR activity was observed after the replacement of carbon black support by the zeolitic imidazolate framework [130].

Pyrolysis is commonly used in the synthesis procedures of catalysts. It was claimed that pyrolysis enhanced the formation of the actives sites for ORR [131–133]. The pyrolysis temperature is still in dispute, but a range between 550 and 950°C is commonly used [132,134]. M-N_x

moieties were found to survive up to a critical temperature above which ORR activity extensively decreased [128,135–137]. The formation of pyridinic N and M-N_x sites dominates over 800ºC, although the decomposition of MN_4 macrocyclic compounds starts at 400ºC [132, 138].

Numerous studies were conducted using catalysts of different materials among which catalysts with outstanding performances and excellent outcomes have been described in this section. However, the classification based on the composition and statistical analysis are shown in the later sections.

Adabi et al. [139] used a commercial Fe–N–C cathode developed by Pajarito Powder and at the optimized conditions (backpressure at 200 kPa and cell temperature at 80ºC), they observed an excellent performance from the AEMFC that exceeded 2 W.cm^{-2} of peak power density. The optimization of dew points, cell temperature and backpressure is shown in Fig. 4. The catalyst was synthesized by VariPore method, which was the successor of the sacrificial support method developed by the Atanassov's research group at the University of New Mexico [86, 140,141]. The synthesis procedure is shown in Fig. 3. The fumed silica template was used as a sacrificial support and after the first pyrolysis, the silica particles were removed by HF to achieve highly porous structure. The catalyst was modified to increase its average pore size, level of graphitization and decrease the hydrophilicity. By optimizing catalyst structure, operating conditions and water management, the DOE target limits for the current density, durability, and anode PGM loading were achieved by their work. The current density of 100 mA.cm^{-2} was achieved at 0.9 V (*iR*-free) and a low platinum-group metal (PGM) loading of only 0.125 $mg_{PtRu}.cm^{-2}$ was applied to achieve such high performances. The fuel cell assembly also showed very stable performance upto 150 h in a durability test operating at at 600 mA.cm^{-2}.

In another study, Adabi et al. [142] synthesized highly stable Fe-N-C catalysts using ion precursors in anhydrous and hydrate forms. Catalysts derived from anhydrous iron precursor outperformed the counterpart and showed a peak power density (PPD) of 1.8 W.cm^{-2}.

In 2018, Hossen et al. [86] in Atanassov's research group at University of New Mexico, USA studied three iron-based catalysts (Fe-NMG, Fe-NMP, Fe-MBZ) comprising different sources of carbon and nitrogen (primarily glucoril, pipemedic acid and mebendazole) and correlated different catalytic sites with performance. Among them, Fe-NMG was observed to be better performing and it was claimed that the reason behind this was due to the presence of higher amount of surface oxides and pyridinic N and lower amount of graphitic carbon in Fe-NMG catalyst. From the observation as depicted in Fig. 5, surface oxides, Fe-N_x, pyridinic N were claimed to be the most active sites for ORR, although Fe-Nx were promoting the $2e^-$ pathway. On the other hand, the graphitic content and hydrogenated N showed negative effects on the ORR activity. The authors studied the effect of ionomer content on catalytic activities and noted 35 wt% to be the optimum ionomer-to-catalyst ratio. They suggested that ionic properties of the catalyst as well as fuel cell performance improved with the increase of the ionomer content up to a certain value beyond which ionomer instead might block the ORR active sites and thus decrease the performance.

Peng et al. [143] synthesized carbon black (VC) supported cobalt ferrite (CF) nanoparticles using the solvothermal method. The sample was heat-treated at moderate temperatures (130–150 °C). The metal particles were observed to be well distributed in the catalyst. XRD data suggested the increase of Co-Fe crystallinity due to the heat treatment. The characteristic peak of $CoFe_2O_4$ (spinel oxide) was well-matched with both CF and CF-VC as shown in Fig. 6.

EDS confirmed the proper distribution of ionomer in the catalyst. Although the ORR activity of the catalyst was relatively low (E_{on} = 0.78 V and $E_{1/2}$ = 0.71 V), the combination of the single AEMFC consisting of this cathode catalyst performed extraordinarily. Without applying any backpressure and using asymmetric humidification of the gases (RH_{anode} = 73%, $RH_{cathode}$ = 90%) at a flow rate of 1000 mL.min^{-1}, the single AEMFC at 65 °C showed the PPD of 1350 mW cm^{-2} using H_2/O_2 as the feed gases. As expected, comparatively lower performance was observed using CO_2 free air instead of O_2 as shown in Fig. 7. Pt-Ru/C

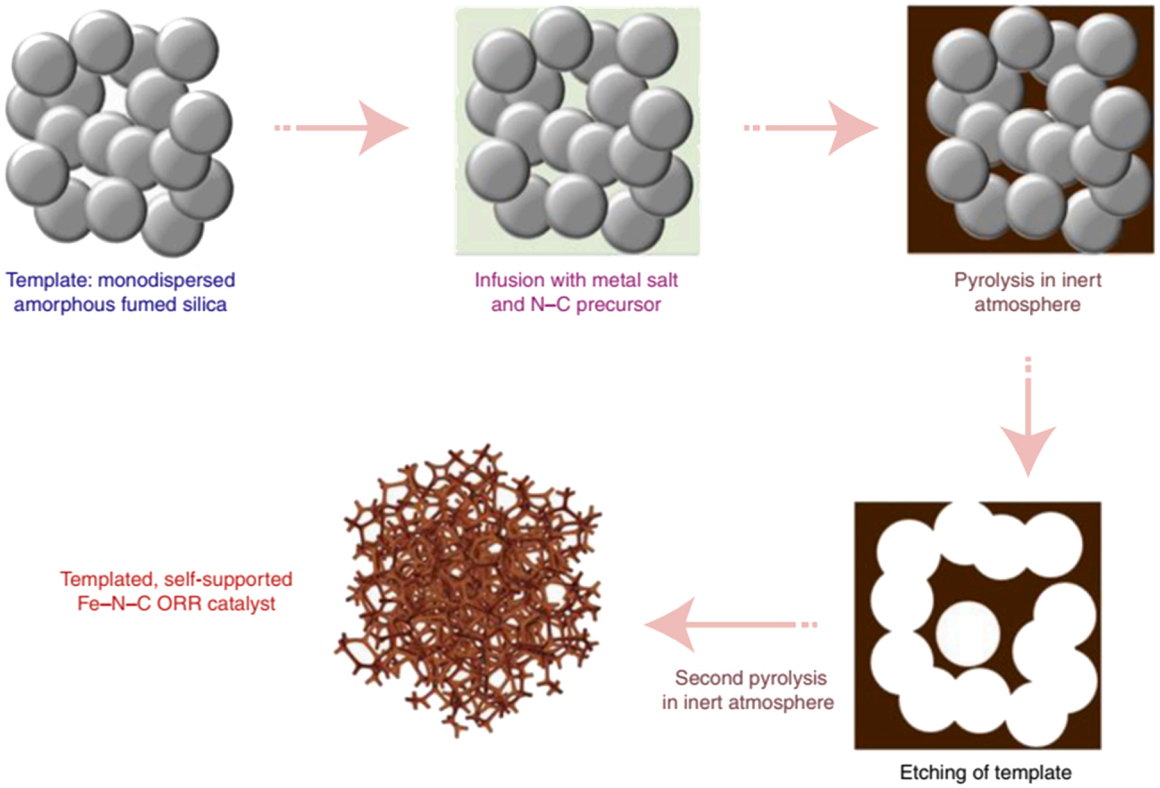

Fig. 3. synthesis pathway of Fe–N–C ORR catalyst.
Reprinted with permission from ref. [139]. Copyright 2021, Nature.

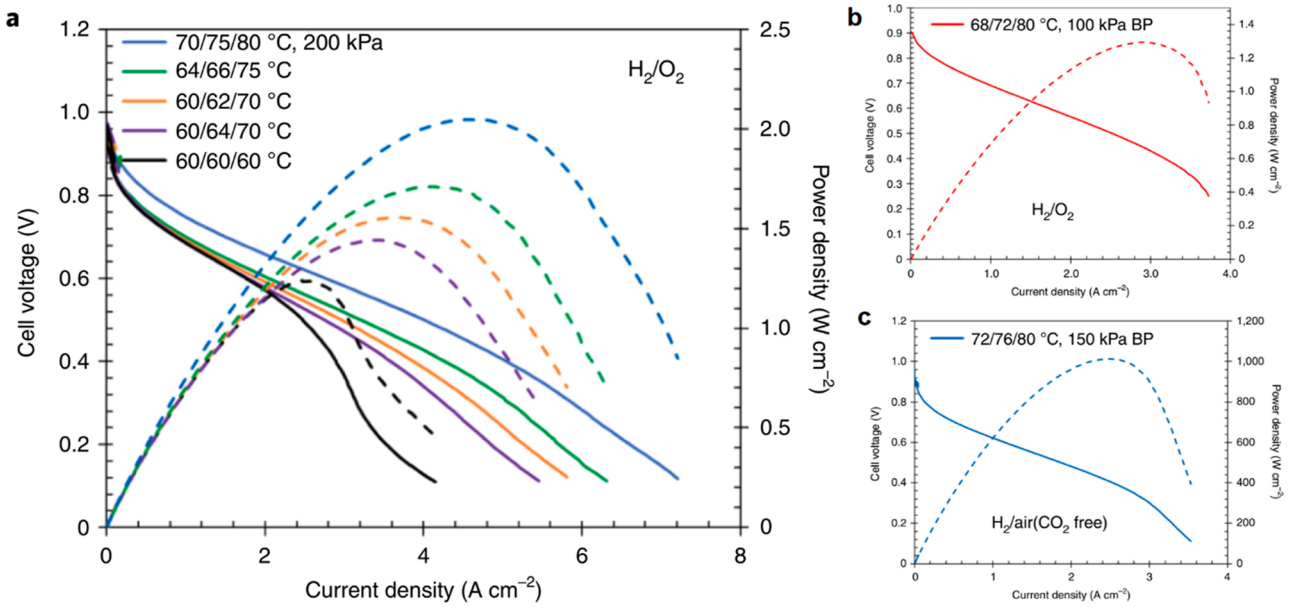

Fig. 4. Current density–cell voltage (solid) and current density–power density (dashed) curves for a) H_2/O_2 AEMFC with a cathode with 1 mg.cm^{-2} Fe–N–C, an anode with 0.6 mg.cm^{-2} PtRu and 1 L.min^{-1} gas flow, b) H_2/O_2 AEMFC with a cathode with 1 mg.cm^{-2} Fe–N–C and an anode with 0.125 mg.cm^{-2} PtRu with 0.1 MPa backpressurization of the 1 L.min^{-1} gas flow. c) H_2/air(CO_2-free) fuel cell with a cathode with 1 mg.cm^{-2} Fe–N–C and an anode with 0.6 mg cm^{-2} PtRu with 0.15 MPa backpressurization of the 1 L.min^{-1} gas flow. The anode dew point/cathode dew point /cell temperatures and pressurization state are given in the figure. Reprinted and adapted with permission from ref. [139]. Copyright 2021, Nature.

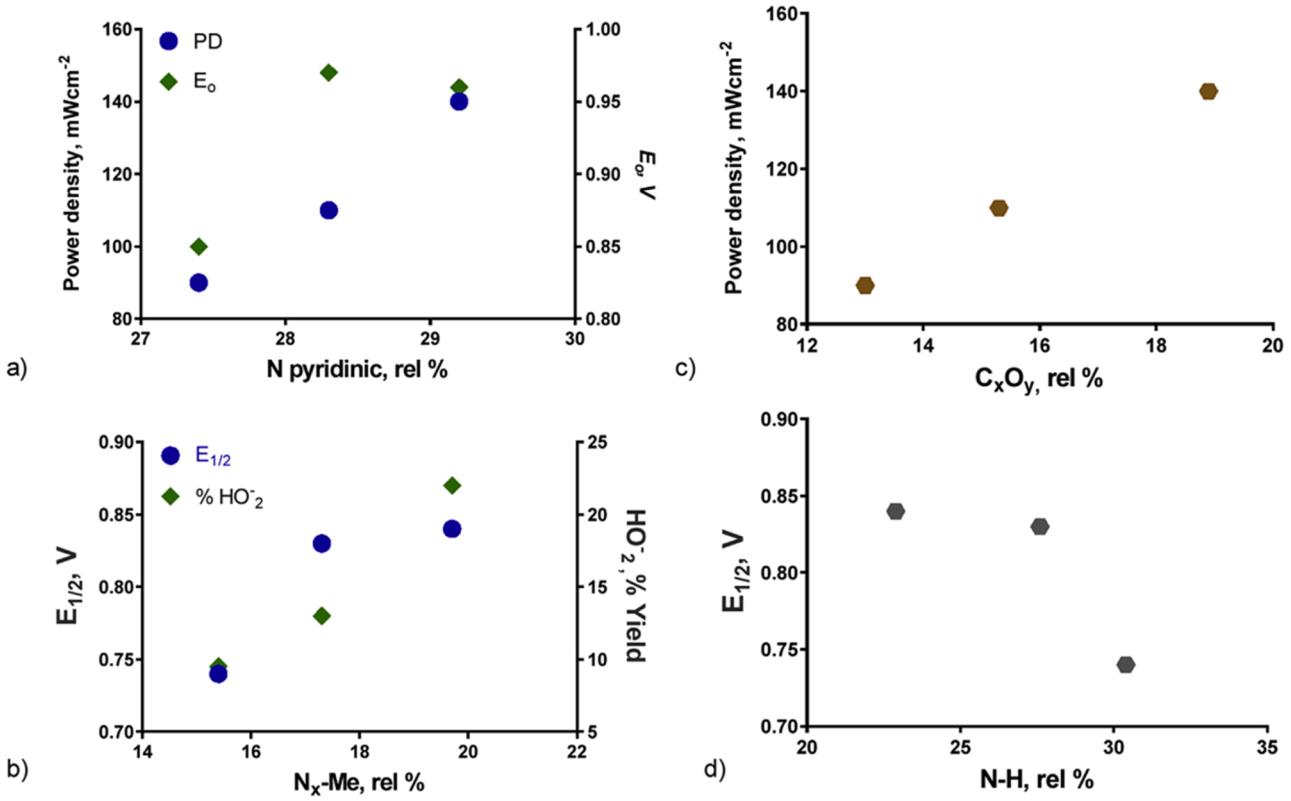

Fig. 5. Correlations of ORR activity and performances with different moieties and compositions. Reprinted and adapted with permission from ref. [86]. Copyright 2018, Elsevier.

anode, polyethylene-based radiation-grafted AEM, and ETFE-based ionomer were used for completing the single cell. The cathode and anode catalysts were incorporated with GDE and the loadings were 2.4 and 0.7 mg. cm^{-2} respectively.

Mun et al. [87] synthesized iron-based mesoporous catalyst using a co-polymer-assisted soft-template method. Fe-N and Fe-O sites were confirmed to be present in the catalyst and Fe-N bond was formed during the first heat-treatment. The I_D/I_G ratio from Raman spectroscopy

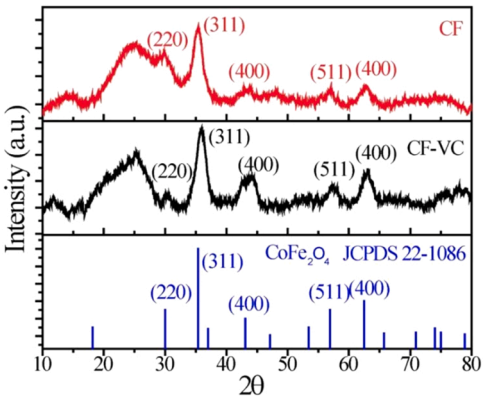

Fig. 6. XRD patterns for cobalt ferrite (CF) nanoparticles, the CF-VC composite catalyst, and CoFe2O4 (JCPDS 22–1086)
Reprinted with permission from ref. [143]. Copyright 2019, MDPI.

increased and size of the carbon crystallite decreased with the increase in pyrolysis temperature. It was previously claimed that the ORR activity of the Fe-N_x/C site increased by the decrease of the carbon crystallite size [144,145]. Also, Fe-Fe metallic bond which was absent at low pyrolysis conditions started to be observed at the catalyst thermally treated at 1000 °C, thus, Fe-N_x/C active sites were concluded to be stable up to 900 °C. They also observed that the voltage loss (below 0.7 V) became significant with the increase of catalyst loading due to the rise of ohmic and mass transfer loss at thicker catalyst layer. The optimized catalyst possessed high surface area, large pores, and large number of active sites due to mesoporous structure. Possessing comparable thickness and catalyst loading with respect to Pt/C catalyst, it exhibited high performance both in half-cell and single-cell systems.

He et al. [146] synthesized ZIF-based Fe-N-C catalyst using an effective polymer coating method, which was claimed to control nanostructure and active site density. A high specific surface area was achieved at 1135 $m^2.g^{-1}$. The coating of polypyrrole was claimed to have an impact on the increase of the surface area. It was suggested that the large delocalized π-electron system of polypyrrole enriched the carbon-carbon interaction between the polymer and Fe-ZIF, thereby restraining the agglomeration of Fe and the formation of CNT was facilitated. The synthesized highly graphitic multi-walled FeN_x-CNTs cathode catalyst showed an excellent performance of 1.15 $W.cm^{-2}$ in a single cell test as shown in Fig. 8.

Park et al. [147] introduced $ZnCl_2$ activation method to increase the surface area by mixing $ZnCl_2$ with ZIF-derived Fe-N-C catalyst and annealing at 800ºC in Ar atmosphere for 2 h. It was claimed that the carbonaceous structure was activated by $ZnCl_2$ by removing O_2 and decreasing total weight. The $ZnCl_2$ activation also induced higher Fe-N_x active site densities and thereby improved ORR activity comparing to the inactivated Fe-N-C catalyst as shown in Fig. 9a,b. A higher specific capacitance of activated Fe-N-C indicated the enhanced electrochemical surface area. Active site densities were determined by conducting a nitrite poisoning experiment and calculated by dividing the stripping charge by the specific resistance. It was found in a previous study that the use of a higher amount of Fe precursors with the intent to increase active sites may reduce ORR activity by enlarging the particle size [148]. On the other hand, $ZnCl_2$ activation improved surface area and active site densities without changing the single-atomic properties and pore structure of the catalysts. The single atomic Fe-sites were confirmed by the absence of metallic Fe-Fe configurations. The identical relaxation time constant of both activated and inactivated Fe-N-C catalysts revealed that the mass transport had a negligible effect on the improved ORR activity. The activated catalyst (Fe-N-C Act) presented the current density of 1076 mA cm^{-2} at 0.6 V and PPD of 786 mW cm^{-2} as shown in Fig. 9c.

Wang et al. [83] synthesized MOF derived Fe and Co based catalysts. The lack of Co−N_x and Fe−N_x moieties but the presence of Co−Co, Fe−Fe bond suggested that the ORR occurred at N-doped carbon sites wrapped with metal NPs. The enhanced ORR activity was a result of charge redistribution of the external carbon layers encapsulating the metal nanoparticles. Previous studies also support the ORR activity of

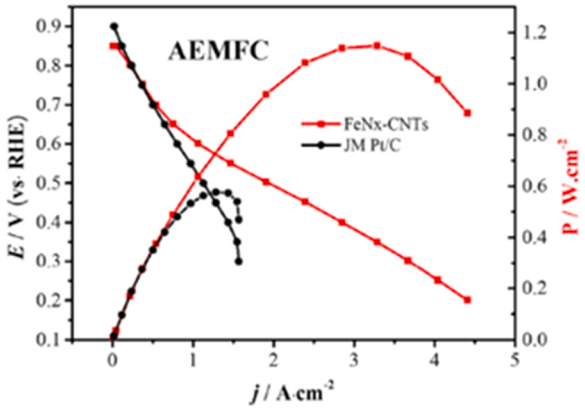

Fig. 8. Polarization curves and power densities of a single AEMFC fabricated with commercial PtRu/C as anode catalysts and FeNx-CNTs or commercial 60 wt% Pt/C as cathode catalysts (0.4 mg_{Pt} cm^{-2}).
Reprinted with permission from ref. [146]. Copyright 2019, Elsevier.

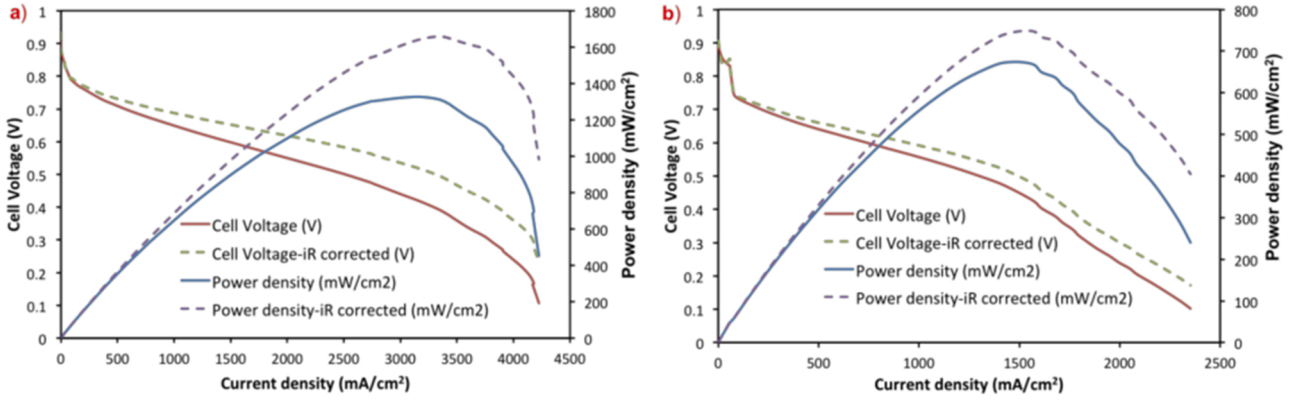

Fig. 7. Polarization curves and power density in two configurations operated at 70ºC. (a) H_2-O_2 gases fed at 1 L/min, RH_{anode}= 73%, $RH_{cathode}$= 90% without backpressure; (b) H_2-air (CO_2-free) at 1 L/min; anode: 0.7 mg_{PtRu} cm^{-2}, RH = 76%, 0.03Mpa backpressure; Cathode: 2.4 mg cm^{-2} CF-VC, RH = 93%, 0.1 MPa backpressure.
Reprinted with permission from ref. [143]. Copyright 2019, MDPI.

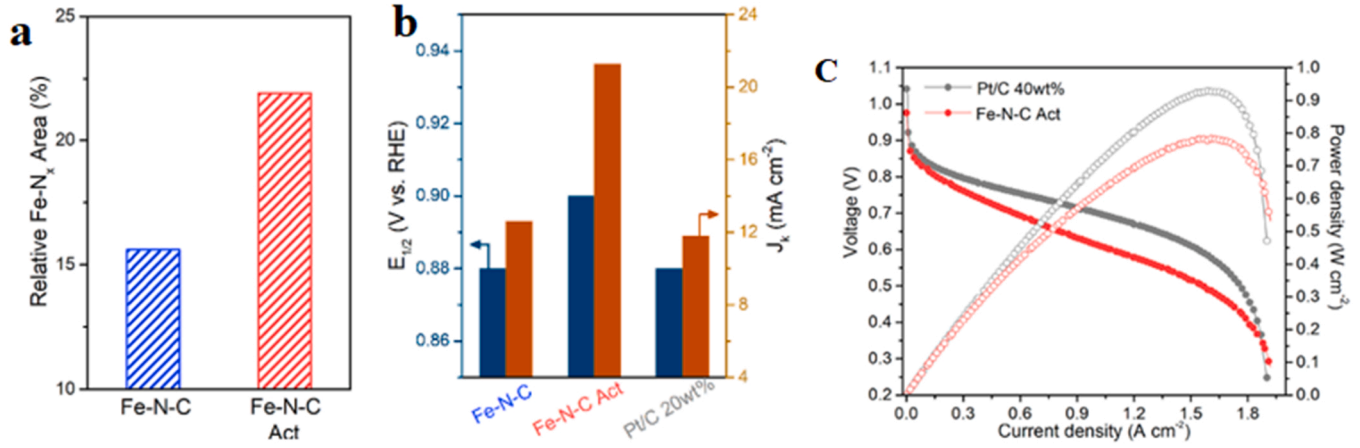

Fig. 9. a) Bar graph comparing relative Fe−N_x area in N 1 s spectra in XPS of Fe−N − C and Fe−N − C Act; b) The half-wave potential ($E_{1/2}$) and kinetic current density values (J_k) at 0.85 V vs RHE; c) polarization and power density curve for the AEMFC using 'Fe−N − C Act' as cathode and 'Pt/C 40 wt%' as anode. Reprinted (adapted) with permission from ref. [147]. Copyright (2021) American Chemical Society.

the nitrogen-doped carbon sites [149,150]. The carbon embedded structure showed higher stability by resisting the detachment of the active sites.

Khan et al. [43] synthesized Cr and Mn-based catalyst using the sol-gel method and achieved high specific surface area. Reduced graphene oxide, graphitic carbon, CrN phases were developed during the synthesis. The catalyst showed high catalytic activity by achieving PPD of 309 mW cm^{-2} and current density 610 mA.cm^{-2} in AEMFC test. The authors suggested that the sufficient metallic nature, high electron conductivity and high adsorption of O_2 molecules by the catalyst were primarily responsible for the high current density.

Lilloja et al. [151] prepared three catalysts Fe-N-CDC/CNT, Co-N-CDC/CNT, and CoFe-N-CDC/CNT using a simple high-temperature pyrolysis method. Carbide-derived carbon (CDC) materials are mainly microporous and possess high specific surface area (1363 $m^2.g^{-1}$). Micropores can be blocked by ionomer, therefore mesopores are necessary for uninterrupted mass transport [110]. To attain a dual characteristic of microporous and mesoporous structures, carbon nanotubes were used along with CDC. CNTs have high resistance to corrosion and electrical conductivity. The active site moieties i.e. pyridinic-N and M-N_x, can be identified from the XPS spectra as shown in Fig. 10. Due to belonging high number of active sites, Fe-N-CDC/CNT showed better ORR activity in terms of E_{on} and $E_{1/2}$. Nonetheless, CoFe-N-CDC/CNT showed the highest cell performance at 1120 mW.cm^{-2} as shown in Fig. 11 and high stability because of the synergistic effects of Fe-N_4 and Co-N_4 centers. The catalysts proved their high stability by showing a negligible decrease in $E_{1/2}$ after 10,000 cycles. In the chronoamperometry test, periodic spikes were observed due to the periodic drying in the cell which could have been improved by adequately humidifying the cell.

Lu et al. [152] synthesized two nitrogen-doped carbon-based catalysts, namely N/C(FU) and N/C(GU) from furfural/glucose, urea, and sulfuric acid-treated halloysite template. The sample was pyrolyzed at 1000 °C in N_2 atmosphere. The high specific surface area of 824 $m^2.g^{-1}$ was achieved for the furfural precursor. The presence of graphitic carbon was confirmed in the catalyst by XRD and Raman spectra. The

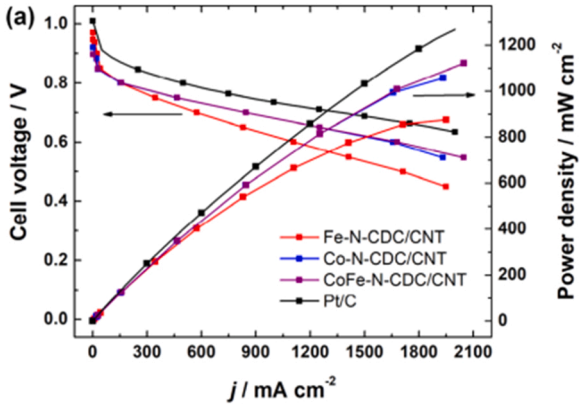

Fig. 11. Polarization and power density curves using various cathode catalysts shown in the legend.
Reprinted with permission from ref. [151]. Copyright 2021, ACS.

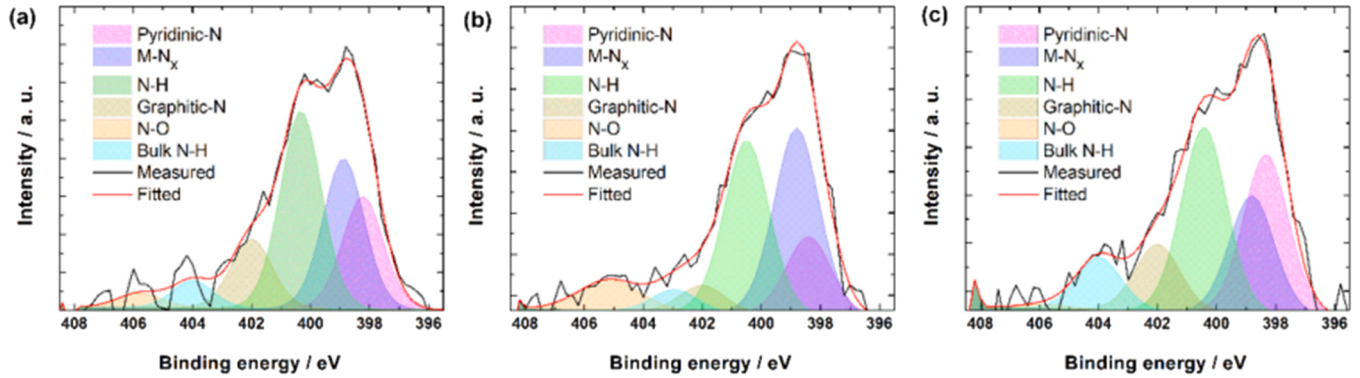

Fig. 10. N 1 s high-resolution XPS patterns for (a) Fe-N-CDC/CNT, (b) Co-N-CDC/CNT, and (c) CoFe-N-CDC/CNT.
Reprinted with permission from ref. [151]. Copyright 2021, ACS.

catalyst contained 5.2% nitrogen among which pyridinic-N 34.6%, graphitic-N 54%, pyrrolic-N 3.5% and pyridinic-N-oxide 6.5% were present. Since graphitic-N and pyridinic-N are the most active nitrogen species for ORR [153] and N/C(FU) contained a higher amount of both of them as shown in Fig. 12a, N/C(FU) performed better as a cathode catalyst. The N/C(FU) catalyst showed good ORR catalytic activity (E_{on} = 0.9 V, $E_{1/2}$ = 0.76 V) and single fuel cell performance (PPD = 703 mW.cm^{-2}). The polarization and power density curves are shown in Fig. 12b. The fuel cell test was conducted at 60 °C and H_2, O_2 gases were supplied at a flow rate of 1000 mL.min^{-1} with 83% relative humidity. The catalyst loadings were 0.80 $mg_{Pt\text{-}Ru}$.cm^{-2} at anode and 1.0 mg.cm^{-2} at cathode. ETFE-based membrane was used for MEA preparation. The authors suggested that the high performance was achieved because of its high surface area, pore volume, complex pore size distribution, and 1D rod-like morphology, where a large number of active species were accommodated in the surfaces, O_2 adsorption and diffusion were promoted by the pores, and electron transfer was enhanced by the rods.

Douglin et al. [154] recently synthesized critical raw material (CRM)-free nitrogen-doped carbon cathode catalyst and applied the AEMFC in high-temperature (HT) conditions (105 ºC). They reported an increase in current density, limiting current density and PPD with the shift of operating temperature from 80 ºC to 105 ºC. Radiation-grafted ETFE-based benzyltrimethylammonium (ETFE-BTMA) membrane and Fumion® polyaromate anion exchange ionomer functionalized with quaternary ammonium groups were used in MEA. A lower mean area-specific resistance (ASR) of the cell and an increased ionic conductivity were also observed at higher temperature. This HT-AEMFC with CRM-free cathode catalyst showed an excellent performance of PPD at 1.14 W.cm^{-2} and 81% retention of the catalyst layer capacitance was observed after 10 h. The effect of temperature on the performance is obvious in Fig. 13.

Woo et al. [155] synthesized iron and nitrogen co-doped carbon catalysts following silica coating-mediated synthetic strategy and using carbon nanotube, iron acetate and S or P containing organic precursors. The sample was heat-treated up to 900 °C. Both S and P containing catalysts showed high ORR electrocatalytic activity, but S-containing catalyst performed better in single AEMFC test than P-containing one. The maximum power density was observed at 635 mW.cm^{-2} for Fe-S-Phen-CNT catalyst. The polarization curves are shown in Fig. 14a,b. The single AEMFC test was performed at 80 °C where 100% humidified H_2 and O_2 were supplied at a flow rate of 400 and 1200 mL.min^{-1}. XRD, XPS, XANES, and EXAFS suggested the presence of higher density of Fe-N_x sites in the catalyst synthesized by silica-coating-mediated strategy and the catalyst also showed improved ORR activity than the uncoated one.

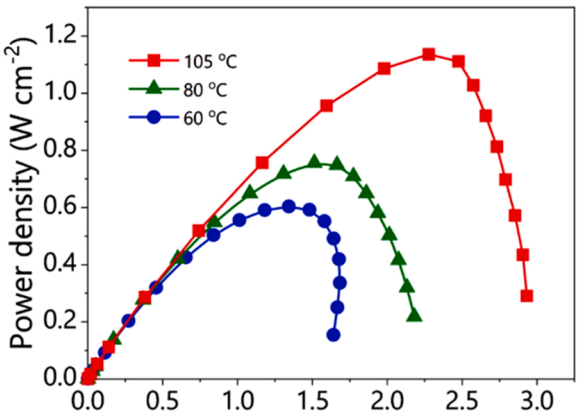

Fig. 13. Power density curve for AEMFC test data with H_2/O_2 gas flows of 1 L. min^{-1} under the following conditions: cell temperature of 105ºC with optimized dewpoints and 1.4 barg back-pressurization on both electrodes; 80ºC with optimized dewpoints and 1 barg back-pressurization on both electrodes; and 60ºC with optimized dewpoints and no back-pressurization.
Reprinted and adapted with permission from ref. [154]. Copyright 2021, Elsevier.

The wet impregnation method [156] improved the Ag dispersion on modified carbon black support (Ag/CB) and entrained oxygen functional groups (C═O). It was observed that Ag/CB catalyst showed PPD almost twice than Ag. Pham et al. [157] synthesized defect enriched multi-heteroatom doped carbon nanotube catalysts and it was observed that specific surface area and onset potential were increased with annealing temperatures. On the contrary, the defect density was not following linear relationship with annealing temperature, rather an optimum temperature at 800 °C was observed. It was also observed that lattice-defect density increases ORR kinetic current density and thus PPD. The authors suggested that lattice defects were enhanced by shortening the length of CNTs and creating vacancies via decomposition of doped F atoms.

Huang et al. [158] developed a novel synthesis method for MOF-based cobalt-copper catalyst. MOFs include metal ions linked with organic ligand, possess three-dimensional structure and high porosities [83,159–161]. The porous structure was achieved by decomposing Zn and incorporating a Cu-containing precursor. They showed that Zn/Co ratio in precursors influenced the catalyst's porous structure. The catalyst showed good electrocatalytic activity for ORR, but the performance

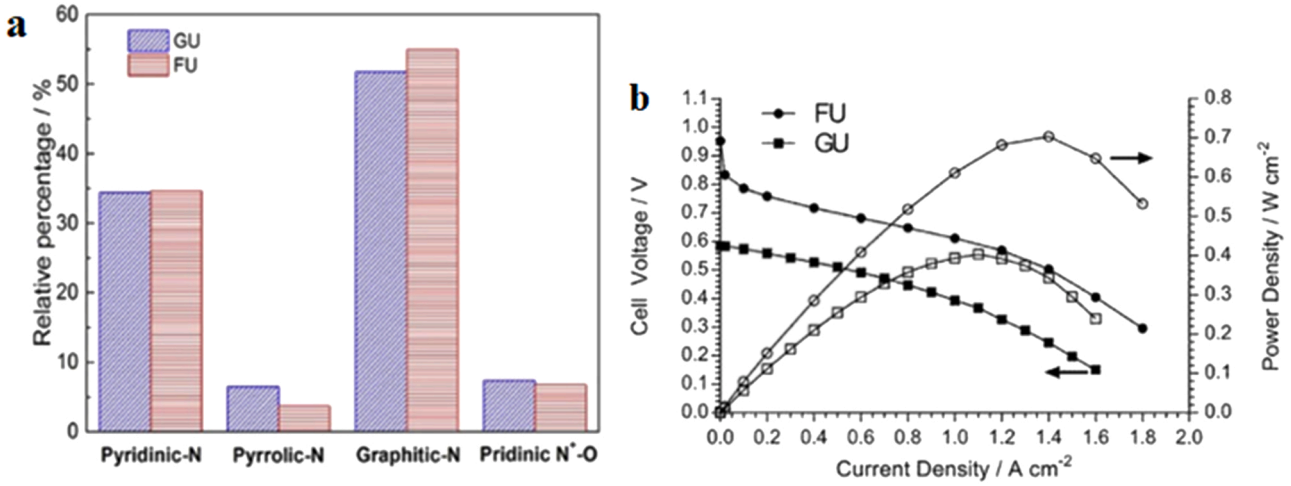

Fig. 12. a) Comparison of relative content of N species between N/C (FU) and N/C (GU) determined from XPS data; b) Polarization and power density curves. Reprinted and adapted with permission from ref. [152]. Copyright 2017, Elsevier.

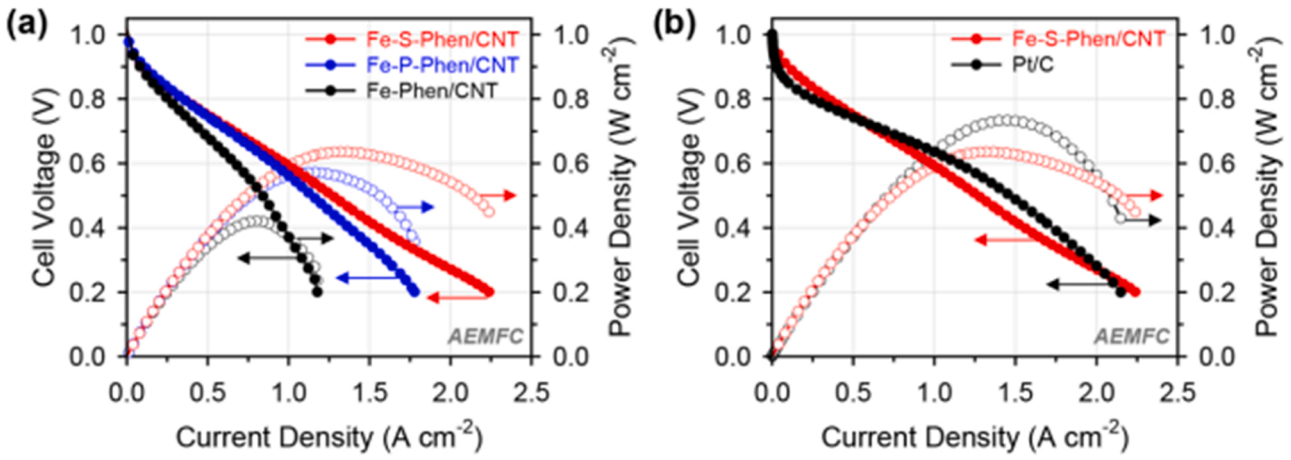

Fig. 14. Alkaline AEMFC performance of MEAs using (a) Fe−Phen/CNT, Fe−P − Phen/CNT, and Fe−S−Phen/CNT as cathode catalysts and (b) Fe−S−Phen/CNT and Pt/C as cathode catalysts.
Reprinted and adapted with permission from ref. [155]. Copyright 2018, ACS.

was relatively poor in the fuel cell test.

Peng et al. [162] synthesized highly active and stable nitrogen-doped carbon–CoO_x nanohybrids using NaCl, glucose, and EDTA precursors as a sacrificial template, carbon, and nitrogen sources, respectively. The precursor mixture was annealed at 700 °C under N_2 atmosphere. CoOx particles were coated with carbon nanosheets. The graphitic carbon was confirmed by XRD and the uniform distribution of Co, O, N, and C was noticed by EDS. The catalyst showed good ORR activity, stability, and performed highly in the single fuel cell. Using the low-density polyethylene (LDPE) with covalently-bound benzyltrimethyl-ammonium (BTMA) head-groups as a membrane and ETFE-BTMA as ionomer, the fuel cell test showed PPD of 1050 $mW.cm^{-2}$ at 65 °C and low backpressure. From the polarization curves shown in Fig. 15a,b, it is clear that H_2-O_2 fuel cells exhibited better performance than H_2-air (CO_2-free) fuel cells and a higher loading of anode catalyst showed higher performance. The catalyst loadings were 0.70 $mg_{Pt\text{-}Ru}.cm^{-2}$ at anode and 2.4 $mg.cm^{-2}$ at cathode. Despite the high fuel cell performance, the authors declared that water management was a limiting factor in the cell. They also studied morphology after the stability test and found that a small amount of CoOx was dissolved and redeposition of cobalt also happened thereafter.

Mooste et al. [163] synthesized polyacrylonitrile (PAN) derived carbon nanofiber (CNF) catalysts using the electrospinning technique combined with Fe or Co particles and also introduced ionic liquids (IL) in the synthesis. From their observation, PAN-derived CNF itself showed better performances than other combinations in single-cell tests, although a lower value of $E_{1/2}$ was observed. The effect of the ionic liquid on the performance was unclear as the incorporation of IL in Fe (Fe/IL-PAN) showed better performance than Fe-PAN, but Co/IL-PAN showed inferior performance comparing to Co-PAN. Also, both Fe/IL-PAN and Co/IL-PAN showed lower $E_{1/2}$ values than Fe-PAN and Co-PAN.

Sharma et al. [164] synthesized work function tailored 3D graphene shell encapsulated cobalt catalysts. The charge transfer from the core Co nanoparticles to the outer graphene shell occurred because of the strong interaction between d orbitals of cobalt and p_z orbitals of graphene. The work function of the n-type graphene shell was thus reduced. A lower work function value indicated a lower energetic barrier to donating electrons and therefore O_2 adsorption was facilitated. Although pristine graphene is not an ORR active material, the conjugation with cobalt in the core-shell structure enabled its ORR activity. The annealed catalysts comprised metallic Co encapsulated by graphene shell and were N-free, whereas the catalysts without annealing consisted of cobalt oxide particles with no or partial outer layer as shown in Fig. 16. The carbon shell

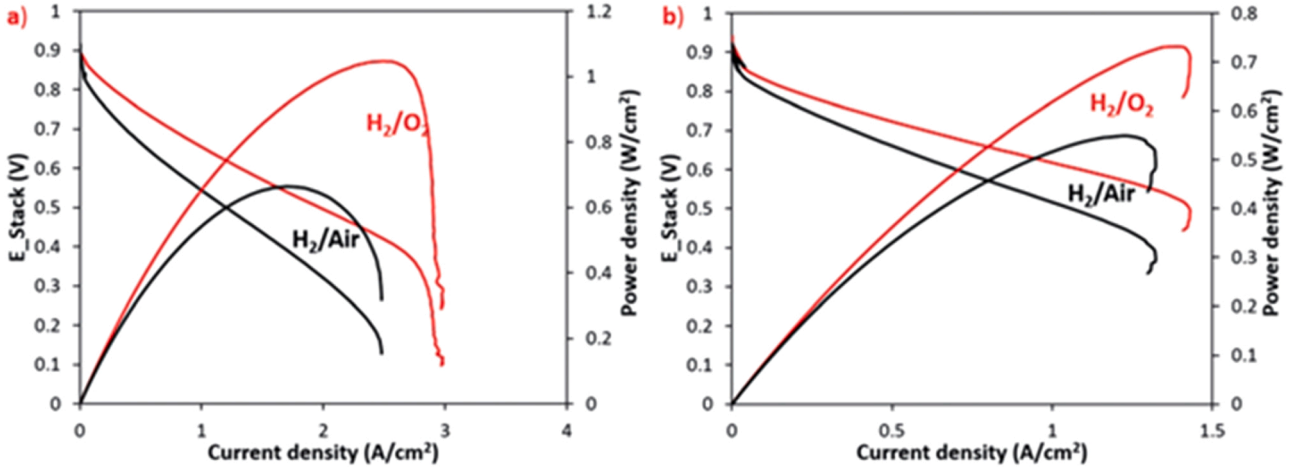

Fig. 15. Polarization curves and power density curves for H_2-O_2 and H_2-air (CO_2-free) fuel cells at different conditions, a) cathode: 2.4 mg cm^{-2} of N-C-CoOx, 0.08 MPa backpressure; anode: 0.70 mg cm^{-2} of PtRu, 0.12 MPa backpressure; T_{cell}= 65ºC (data presented without iR-correction); b) cathode: 2.4 mg cm^{-2} of N-C-CoOx, 0.09 MPa backpressure; anode: 0.10 mg cm^{-2} of PtRu, 0.1 MPa backpressure; T_{cell}= 65ºC (data presented without iR-correction).
Reprinted and adapted with permission from ref. [162]. Copyright 2019, Wiley.

acted as a protective layer against cobalt detachment, migration, and dissolution. With the increase of annealing temperature, the enhanced density and crystallinity of the graphene shell were observed and better durability was achieved. Very high ORR activity and single-cell performance were achieved using 40 wt% Co@G/C_600 catalyst. CN^- poisoning and CO stripping tests revealed a proper encapsulation of core Co nanoparticles by graphene shell and confirmed its reduced work function.

Santori et al. [165] synthesized FeNC and Mn-oxide (α-MnO_2, β-MnO_2, δ-MnO_2, α-Mn_2O_3)/FeNC cathode catalysts with the purpose to reduce the peroxide production. They studied the activity of the catalysts for the hydrogen peroxide reduction reaction (HPRR). It was found that the specific activity of α-Mn_2O_3 for the HPRR was higher than the other Mn-oxides as shown in Fig. 17a, although α-Mn_2O_3 had a lower BET surface area than the other MnO_x. The incorporation of MnO_x in FeNC proved less peroxide yield. Both FeNC and α-Mn_2O_3/FeNC showed good ORR catalytic activity in the RRDE test. In the single-cell test, both showed very high PPD of 1060 and 1000 mW.cm^{-2} respectively as shown in Fig. 17b,c. The author suggested optimizing the mass transfer for the catalyst to improve the performance to a higher level.

Faubert et al. [166] developed carbon supported chromium-nickel catalyst, which is thermally stable up to 120 °C by electrospinning fabrication method. Although, the catalyst had a high specific surface area (288 m^2 g^{-1}) and was intrinsically active in ORR, it showed very poor performance (PPD 22 mW cm^{-2}) in fuel cell test. Goenaga et al. [167] synthesized fifteen different catalysts with very high specific surface area containing Ag, Ni, Co, Cu, Fe and their combinations in the same procedures. All the catalysts showed good catalytic activity and stability for ORR, although the bi-metallic catalysts were observed to perform better. Co and AgCo showed relatively higher PPD than the other synthesized catalysts, whereas CoFe showed the highest ORR activity. It was also observed that the mechanically-pressed MEAs were better than the hot-pressed MEAs in the fuel cell test. The effect of AS4 ionomer loading and catalyst loading were studied in fuel cell test and it was observed that the variation in ionomer loading did not have any measurable effect, but the catalyst loading had.

Kim et al. [84] applied two-step heat-treatments in the synthesis of Fe-N-C cathode catalyst and studied the factors that control the incorporation of active sites i.e. Fe-N_x and Fe-C. For a constant loading of iron and nitrogen precursors, they varied the mass of carbon sources (Ketjen black-KB). The observation claimed that with the increase of carbon content, Fe-N_x site density was enriched, but Fe nanoparticles and the thickness of the carbon coating layer were reduced by some degrees. Variation in Fe particles is responsible for graphitizing carbon content to a different extent. The amount and size of Fe particles affect the carbon crystallite size and encapsulation of carbon layers. The carbon shell on the nanoparticles was claimed to resist agglomeration of the nanoparticles during synthesis. Pyrosynthesis method was stated to be important to stabilize Fe nanoparticles since the catalyst prepared without pyrosynthesis showed an agglomeration and inferior performance. The C K-edge NEXAFS spectra of FeNC-4000 showed an increased intensity of the peak at 285 eV as depicted in Fig. 18 and revealed an enhanced interaction between the thin carbon coating and the Fe nanoparticles.

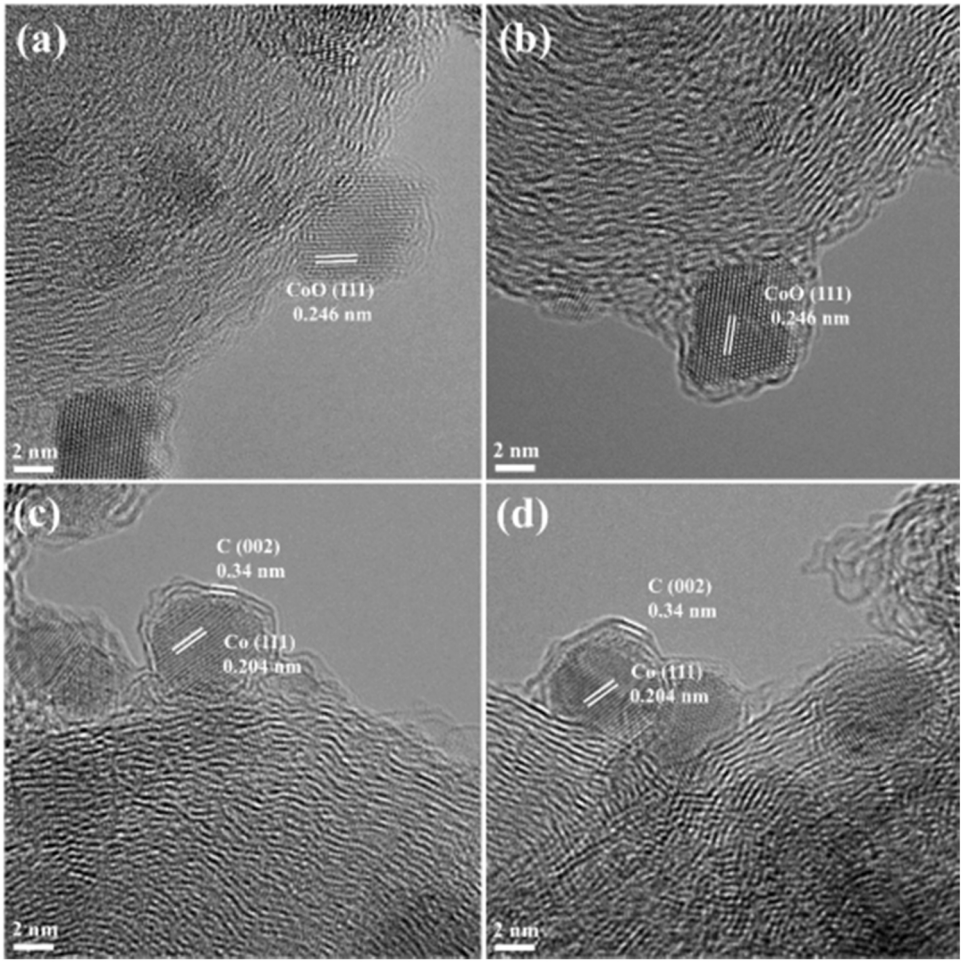

Fig. 16. HR-TEM images of the catalysts (a,b) without annealed (Co@G/C_ASP) and (c,d) annealed at 600ºC (Co@G/C_600). Reprinted with permission from ref. [164]. Copyright 2019, RSC.

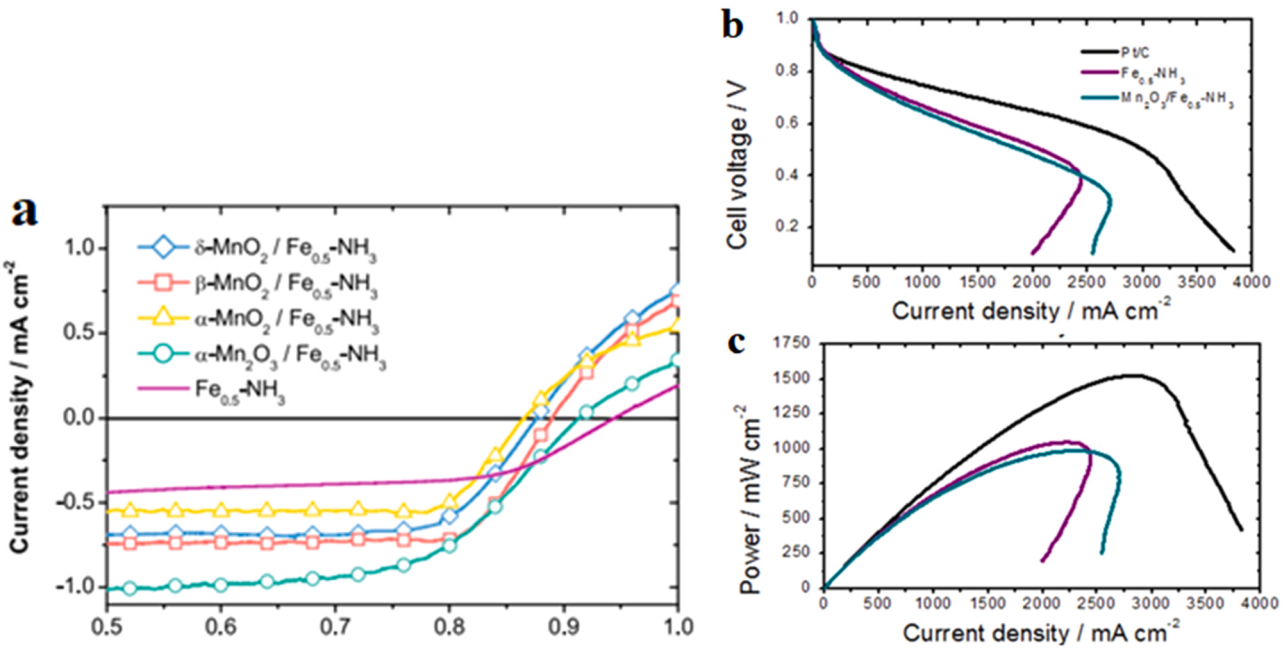

Fig. 17. a) Activity of different catalysts toward HPRR; b) Polarization curve; c) Power density curve.
Reprinted with permission from ref. [165]. Copyright 2020, ECS.

Dzara et al. [168] synthesized Ca, La, Al, Mn-based catalyst containing perovskite phases by aerogel method. They observed that the surface perovskite phases, which increased with the calcination temperature were responsible for the intrinsic electrocatalytic activity. The highest ORR mass activity was observed at the optimum calcination temperature of 800 °C. Also, the composition of perovskite oxide:carbon at 30:70 were the best performing. It was also confirmed that nitrogen-doped Vulcan carbon black (CB) performed better than non-doped Vulcan CB as a support. Moni et al. [169] suggested that electrical conductivity is an important factor for charge transport and thus affect the electrocatalytic activity toward ORR. Hanif et al. [85] synthesized Ni, Co based catalyst from zeolitic imidazolate frameworks where in situ carbon nanotube (CNT) was grown. The catalyst consisting high specific surface area showed very high intrinsic activity for ORR. Although the PPD observed was comparatively lower i.e. 65 mW cm^{-2}, it performed better than Pt/C catalyst in fuel cell test at the same conditions.

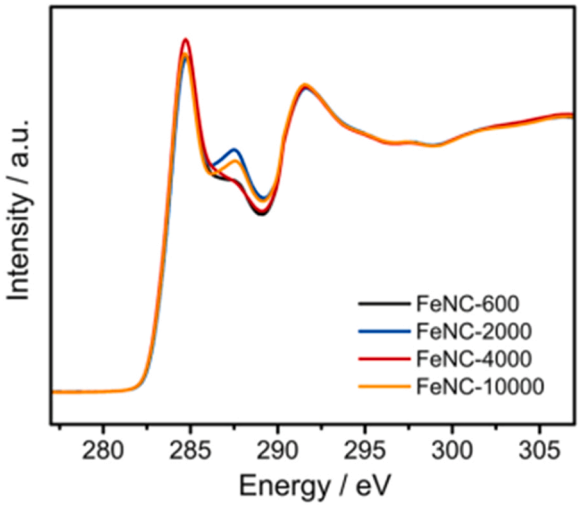

Fig. 18. C K-edge NEXAFS of the catalysts.
Reprinted with permission from ref. [84]. Copyright 2020, Elsevier.

Zhang et al. [47] synthesized cobalt-based catalyst using zeolitic imidazolate frameworks (ZIFs) and optimized the formation of triple phase boundary in the catalyst layer. The incorporation of carbon black in the catalyst increased the power density by fourth times since it improved the electrical properties of the catalyst. It was also indicated that pyridinic N and Co-N phases acted as the active sites for ORR [70]. The hierarchical porous structure and the smaller sizes of the metal particles enhanced the mass transfer and ORR activity as well. Since the thickness of the catalyst layer affects ion and electron transfer processes, and the effective area [170], thus the poor performance of ZIF-700 compared to ZIF-CB-700 was explained thereby.

Wang et al. [171] synthesized Zn, Co based MM-N-C catalysts and incorporated ionic liquid at different concentration. The catalyst itself had a very high specific surface area (649 $m^2 g^{-1}$) without the addition of ionic liquid. Although the ionic liquid decreased the specific surface area of catalyst, it helped by decreasing the charge transfer resistance. It was observed that 20 wt% ionic liquid showed the highest intrinsic activity and fuel cell performance (PPD = 300 mW cm^{-2}). They applied the catalyst for both PEMFC and AEMFC, and concluded that the ionic liquid modification was more effective in acid than alkaline environment.

Chang et al. [172] synthesized highly active, porous and stable iron based catalyst comprising EDTA complex supported on graphene. They claimed the synthesis procedure as a cheap and rapid. Compared to Pt/C, the catalyst showed higher intrinsic activity toward ORR, but the PPD value was lower (389 mW cm^{-2}). Zhao et al. [173] synthesized highly active iron-based single-atom catalyst embedded in nitrogen- and fluorine-doped porous carbon materials with five coordinated $Fe-N_5$ sites. It was observed that the pyrolysis temperature influenced the specific surface area, the fluorine content, and the graphitization of the catalyst. In contrast, it was noted that higher pyrolysis temperature could cause a decrease in nitrogen contents. The substitution of fluorine from a precursor compound was suggested to have a positive effect on the electrocatalytic activity for ORR.

Yang et al. [174] synthesized Ketjen black supported Co-Mn spinel oxide catalysts ($MnCo_2O_4$ and $CoMn_2O_4$) from metal precursors by co-ordination with ammonium hydroxide. Catalysts with both structures performed highly as cathode catalysts. It was claimed that the electronic conductivity of the catalyst was a result of the crystal defects and small particle sizes. The optimization of metal loading, catalyst loading and

operating conditions were accomplished and the optimized values were found at 80 wt%, 0.8 mg.cm^{-2}, 80ºC at 0.1 MPa respectively as depicted in Fig. 19.

Praats et al. [175] synthesized CDC and CNT supported cobalt-based catalyst using Co phthalocyanine as a precursor. CDC was derived from two sources (i.e. titanium carbide and silicon carbide), and among them silicon carbide derived CDC catalyst was found to be catalytically more active. XPS data revealed that Si-CDC derived catalyst contained higher atomic percentage of nitrogen species than Ti-CDC derived catalyst, specifically graphitic-N and pyridinic-N. Thus, graphitic-N and pyridinic-N moieties can be considered as catalytically active and important N species for ORR along with Co-N_x sites. Also, from the observation, catalysts containing lower CDC:CNT ratio (1:3) possessed higher ORR catalytic activity, so CNT can be concluded to have a great impact on the ORR process. The AEMFC performance of this catalyst (PPD = 473 mW cm^{-2}) was close to that of the formerly described catalyst that Lilloja et al. [46] synthesized.

In another study, Praats et al. [176] reported similar research using iron-based catalyst and employing Fe phthalocyanine as Fe and N precursor. The catalyst consisting of TiC derived carbon showed better ORR activity than the catalyst consisting of SiC derived carbon. Catalysts with higher loading of multi-walled CNT showed higher ORR activity.

Wang et al. [177] developed Mn-Co spinel (MCS) catalyst that reached 1.1 W.cm^{-2} and 2.5 A.cm^{-2} at 60 °C and 100% relative humidity as shown in Fig. 20b. Although the catalyst exhibited inferior ORR activity than Pt in RDE, it outperformed Pt in the single-cell test. The comparison in performances at different conditions is shown in Fig. 20a. It was revealed that O_2 bound to Mn and Co sites facilitated proton-coupled electron transfer processes. For these synergistic effects, AEMFC comprising the MCS cathode outperformed Pt even at low humidity. The spinel structure of the cathode catalyst was confirmed by synchrotron XRD, XANES, and HAADF-STEM.

Bhange et al. [178] synthesized iron based catalyst with both Fe-N_x and Fe-S_x active sites supported on the CNTs and in situ grown carbon nanosheet. The highest porosity was achieved at an optimum pyrolysis temperature. It was also observed that N, S, O, and Fe content decreased with the pyrolysis temperature. Also, graphitic N increased and pyridinic N, SO_x decreased with the pyrolysis temperature. The optimum pyrolysis temperature was found at 900 °C. CNT acted as spacers by preventing the aggregation of the carbon sheets. CNT was also confirmed to have impact on achieving high surface area. Fe-S_x engrafted carbon was reported to be active for ORR in acidic medium [179]. Nonetheless, they found high ORR activity of this catalyst in both acidic and basic conditions. The authors noted that less oxidized carbon indicated higher electrical conductivity of the catalyst. Although, this catalyst showed comparatively lower PPD than other high performing catalysts, it showed higher AEMFC performance and ORR activity compared to Pt/C cathode at the same conditions.

Huang et al. [180] synthesized carbon-supported iron containing Prussian blue-derived catalyst. The morphological dissimilarities were observed at different pyrolysis temperature. The catalyst synthesized at 800 °C confirmed the presence of Fe_3C and FeS structures, quaternary N, pyridinic N, and pyrrolic N. The studies confirmed that the presence of FeS particles could enhance electrical conductivity and ORR activity [181–183]. The optimized catalyst was found to contain higher amount of Fe-N_x phases. From literature, Fe-N_x phases were claimed to enhance the ORR activity [184]. The optimized catalyst showed 4e$^-$ transfer pathway for ORR, but the PPD was found at lower value compared to

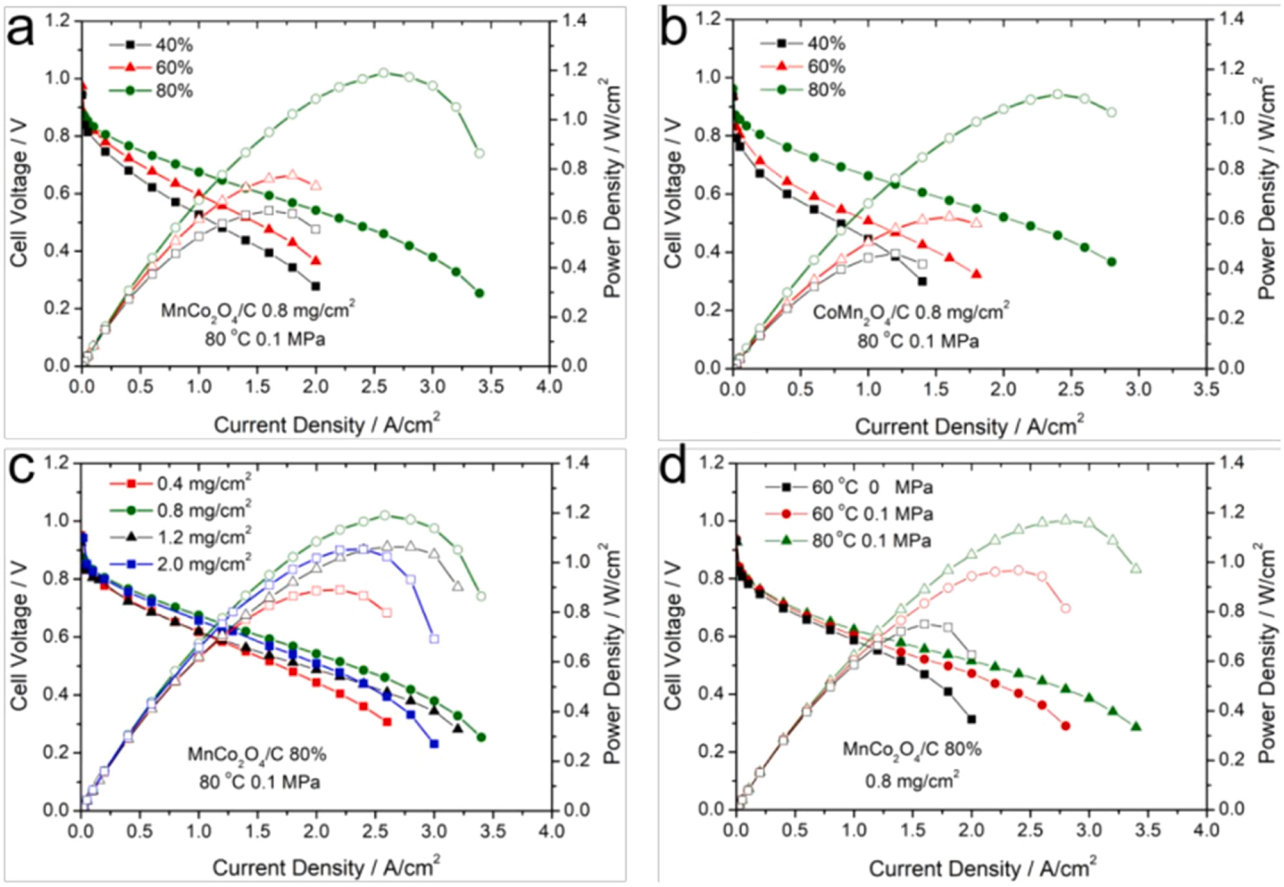

Fig. 19. Single-cell test result for a) different metal oxide loading of $MnCo_2O_4$/C at the cathode, b) different metal oxide loading of $CoMn_2O_4$/C at the cathode, c) different catalyst loading of $MnCo_2O_4$/C (80 wt%) at the cathode, d) different operating conditions of MnCo2O4/C (80 wt%, 0.8 mg.cm^{-2}).
Reprinted with permission from ref. [174]. Copyright 2019, ACS.

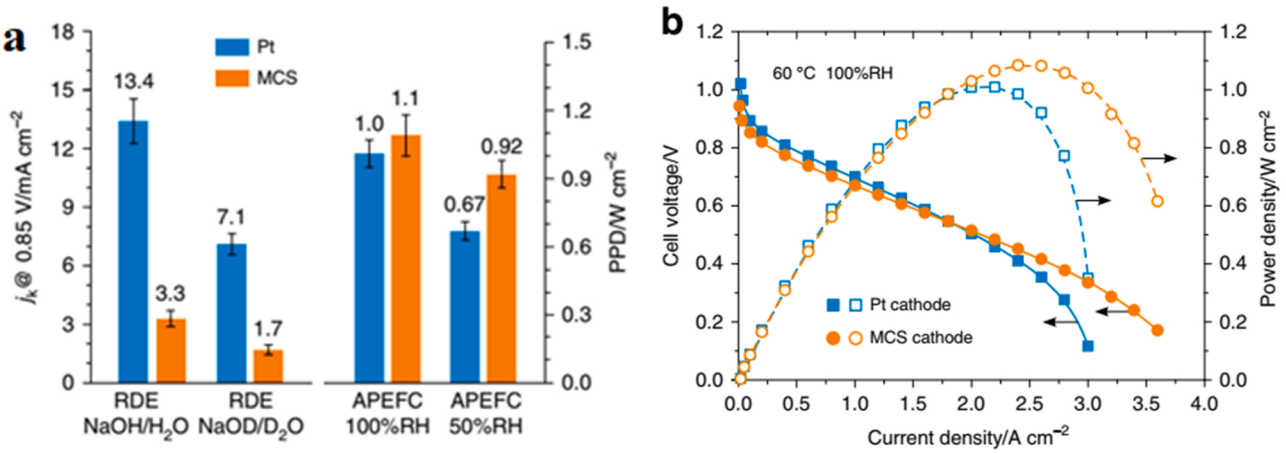

Fig. 20. a) Performance comparison: Kinetic current densities (jk) at 0.85 V, calculated from the RDE data recorded in 1 mol.L^{-1} NaOH/H_2O and 1 mol.L^{-1} NaOD/D_2O and the PPD resulting from APEFC tests; b) Polarization and power density curve.
Reprinted with permission from ref. [177] Copyright 2019, Nature.

other recently synthesized catalysts.

Yang et al. [185] performed a comparative study for different carbon supports applying to the same cathode catalyst (FePc). Seven different carbons i.e. Ketjenblack (KCB), Vulcan XC-72R (VC), multi-walled carbon nanotubes (MWCNT, Flotube 8–15 nm), MWCNT (Nikkiso 20 nm), single-walled carbon nanotubes (SWCNT, 3–5 nm), 3D mesoporous carbon-C450 (450 nm), 3D mesoporous carbon-C140 (140 nm) were studied and found that catalysts supported on KCB, SWNT, and 3D mesoporous carbons offered high specific surface area above 900 $m^2.g^{-1}$. They observed the order of the ORR activity based on $E_{1/2}$ as follows: FePc-KCB > FePc-Flotube > FePc-SWNT> FePc-C140 > FePc-VC > FePc-C450 > FePc-Nikkiso > Pt/C. The optimization of the cathode catalyst loading was conducted and loading at 1.0 mg.cm^{-2} performed higher than 2.0 and 3.0 mg.cm^{-2}.

Parthiban et al. [186] studied the effect of fluorine (F) on the mesoporous carbon (MC) and claimed that the doping of F atom increased the surface area, pore diameter, degree of graphitization and defective sites of the carbon matrix. The highly electronegative F atom polarized the adjacent carbon atoms, created ionic or semi-ionic C-F bonds and therefore, enhanced O_2 adsorption, weakened O-O bonding and facilitated ORR kinetics. The calcination temperature affected the formation of nanopores on the wall of mesopores and the production of the pure phase carbon. DFT calculations confirmed the 4e- pathway for ORR over F-MC catalyst. Another study claimed that semi-ionic C-F bonds are more ORR active than ionic C-F bonds, whereas covalent F is ORR inactive [187].

Lilloja et al. [46] synthesized highly active and stable cobalt-based catalyst using carbide-derived carbon and carbon nanotube composite as a support. The fuel cell test confirmed its high performance by showing the PPD value of 577 mW.cm^{-2} as presented in Fig. 21. The graphitic carbon phases, pyridinic N and Co-N_4 sites were present in the catalyst. The combination of highly porous structure, highly conductive CNTs, highly active Co nanoparticles, and the incorporation of N species confirmed its well performance in ORR catalyst. The membrane (HMT-PMBI) and ionomer used could have also impacted on its performance.

Ratso et al. [89] studied the effect of different synthesis parameters on the ORR activity of Fe-N-C catalyst. Prior to pyrolysis, the ball-milling was used to properly disperse the catalyst particles and reduce their sizes. It was observed that the low sizes of the ball at wet conditions using ethanol and surfactants was beneficial to achieve smaller particle sizes and high specific surface area. The rotation rate of the ball-milling was also optimized. Smaller sizes of the balls increased the nitrogen content and ethanol in wet ball-milling decreased the nitrogen content in the catalysts. The best-performing Fe-N-C catalyst achieved PPD of

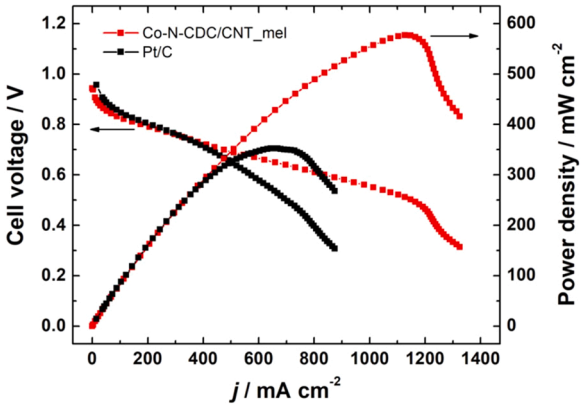

Fig. 21. Polarization and power density curve for H_2/O_2 AEMFC. Cathode catalyst: Co-N-CDC/CNT_mel or Pt/C, anode catalyst: Pt-Ru/C and AEM: HMT-PMBI. T = 60 °C.
Reprinted with permission from ref. [46] Copyright 2020, ACS.

356 mW cm^{-2} in an AEMFC. Karuppannan et al. [188] described an efficient, solvent-free, mechanochemical method for the synthesis of N, F doped carbon-encapsulated Fe/Fe_3C catalyst. From HRTEM, a 10 nm (approx.) thick carbon layer was observed around each Fe crystal. Fluorine doping occurred at close proximity of Fe clusters and nitrogen doping was performed uniformly. It was revealed that N, F doped carbon catalyst performed better than N doped carbon and the addition of Fe/Fe_3C (i.e. NFC@Fe/Fe_3C) surpassed both of them in performance. Similar results were observed from another study that N, F doped cotton-derived carbon showed better ORR activity than N doped and F doped catalysts [187].

Sibul et al. [124] synthesized Fe-N-C catalyst using graphene (Gra) or graphene oxide (GO) as the carbon support and compared their effects. It was observed that Fe-N-Gra showed better ORR activity than Fe-N-GO because of its higher surface area, combined micro and mesoporous structure, and higher active sites i.e. Fe-N_x/amines. It was also found that Fe-N-Gra comprised 2.5 times more iron than Fe-N-GO and half of the iron was confirmed as in the form of Fe-N_x active sites. Tong et al. [126] synthesized hollow and solid carbon spheres in aqueous (high dielectric constant) and ethanol (low dielectric constant) solution respectively from the ionic liquid 1-butyl-3-methylimidazolium chloride as a source of both carbon and nitrogen. It was observed that hollow carbon sphere catalyst showed better activity and stability than the solid carbon spheres.

Several researchers synthesized biomass derived carbons as the cathode catalyst, or as a support for the catalyst, but comparatively poor activities and performances were observed from their studies. It is also observed that electrocatalysts obtained from biomass suffer from reproducibility issues. Carbons derived from different biomass sources were found to be irregular porous structured with relatively wider pore sizes [187,189–191].

Ammonia heat treatment was used in several studies to synthesize active ORR catalysts. It was revealed that the etching effect of NH_3 helped to create micropores, thereby formed pathway from surface to mesopores [192,193]. A significant increase of specific surface area was achieved by the ammonia treatment [194].

The stability is a prime concern for AEMFC. The stability tests were performed in several studies. Sarapuu et al. suggested that the stability issue is related to membranes, operating conditions and the preparation of MEAs [77]. The synthesis procedures, characterization data, RRDE test conditions, and Single AEMFC test conditions for the cathode catalysts are listed in Table S1, Table S2, and Table S3 in the supplementary information.

2.1. Classification of catalysts

From the analysis of literature, the developed non-platinum cathode catalysts can be categorized in the following types.

i) Transition metal ceramics (Ceram)
   a. Metal Silicide-Carbon (M-Si-C)
   b. Metal Silicide-Nitrogen-Carbon (M-Si-N-C)
ii) Transition metal chalcogenides (Chalc)
   a. Metal-Sulphides-Carbon (M-S-C)
   b. Metal-Phosphorous-Sulfides-Carbon (M-P-S-C)
   c. Metal-Selenides (M-Se)
   d. Metal-Tellurides (M-Te)
iii) Transition Metal Catalysts supported on Carbon (MCC)
   a. Metal-Carbon (M-C)
   b. Bimetals-Carbon (MM-C)
   c. Bimetals -Nitrogen-Carbon (MM-N-C)

i. MOF Derived (MM-N-C-MOF)

1. ZIF Derived (MM-N-C-ZIF)

i. Single Atom Catalyst (MM-N-C-SAC)
   a. Metal-Nitrogen-Carbon (M-N-C)

i. Single Atom Catalyst (M-N-C-SAC)
ii. Metal Organic Framework (MOF) Derived (M-N-C-MOF)

1. Zeolitic Imidazolate Frameworks (ZIF) Derived (M-N-C-ZIF)

i. Biomass derived heteroatom doped Carbon (M-N-C-BM)
ii. Nitrogen-Rock derived Carbon (M-N-C-R)
   a. Non-metals doped M-N-C (M-N-C-NM)

   i. Sulphur doped (M-N-C-NM-S)
   ii. Phosphorous doped (M-N-C-NM-P)
   iii. Boron doped (M-N-C-NM-B)
   iv. Fluorine doped (M-N-C-NM-F)

i) Transition metal oxides (TMO)
   a. Metal oxide-Carbon (MOx-C)
   b. Metal oxide-Nitrogen-Carbon (MOx-N-C)
   c. Metal-Metal oxide -Carbon (M-MOx-C)
   d. Metal-Metal oxide-Nitrogen-Carbon (M-MOx-N-C)

i. MOF Derived (M-MOx-N-C-MOF)

1. ZIF Derived (M-MOx-N-C-ZIF)
   a. Perovskite Oxide-Carbon (ABX_3-C)
   b. Perovskite Oxide-Nitrogen-Carbon (ABX_3-N-C)
   c. Spinel Oxide-Carbon (AB_2X_4-C)
   d. Hollandite Oxide (HDO)

a) Support-free Metal (SFM)

a. Single Metal (M)
b. Bimetal (MM)

a) Non-Metallic catalysts (NMC)

a. Carbon / Carbon nanomaterials (C)
b. Fluorine-Carbon (F-C)
c. Fluorine-Nitrogen- Biomass derived Carbon (F-N-C-BM)
d. Fluorine-Nitrogen-Carbon (F-N-C)
e. Fluorine-Sulphur-Nitrogen-Carbon (F-S-N-C)
f. Nitrogen-Carbon (N-C)
g. Oxygen-Sulphur-Nitrogen-Carbon (O-S-N-C)
h. Biomass derived heteroatom doped Carbon (BC)
i. Phosphorous- Nitrogen-Carbon (P-N-C)
j. Sulphur-Nitrogen-Carbon (S-N-C)
k. Sulphur-Nitrogen- Biomass derived Carbon (S-N-C-BM)
l. Conducting Polymers (PM)

It is found that researchers are showing interests mostly in M-N-C and MM-N-C catalysts because of their better performance. Different metals such as Fe, Mn, Ag, Cu, Co, Ni, etc. were commonly used. Nitrogen doped carbon materials may be derived from different sources such as polymeric precursors, small organic molecules, and NH_3 or N_2 treatment. The other classes of catalysts are also showing competitive activity.

Several commercial catalysts from Acta S.p.A.-Hypermec (Italy), GPMaterials (France), Pajarito Powder, LLC (New Mexico, USA) were studied previously.

2.2. Catalysts' data

It is suggested to read the supporting information of this article where three more tables are provided. The synthesis procedures and the characterization data are included in Table S1 in lieu of analyzing the effect of different synthesis methods on the properties of the sample. Table S2 showed the RRDE experiment conditions, the data corresponding to the catalytic activities, and the stability data. The fuel cell test data and the operating conditions are listed in Table S3.

2.3. Previous data analysis

The cathode catalysts for H_2/O_2 fed AEMFC are listed in Table 1 and Table 2 by their categories. The tables include the test data of 203 catalysts from the selected 159 articles starting from 2006. There are several other catalysts whose single cell test data are unavailable and thus excluded from the tables. Categorizing the catalysts as shown earlier allows us to compare their performance and perceive the effects of different components and structures. Although some catalysts are difficult to specify into any single category, this is an attempt to classify all cathode catalysts into specific types. Immense variation in the cell performance was observed among the catalysts. The catalysts from the same metallic components also showed very different performance. The variation in the cell performances is a result of the dissimilarities in several factors such as synthesis methods, catalyst composition, ionomers, ink composition, precursors of the catalysts, catalyst supports, conjugation of active sites, test operating conditions, etc. Different synthesis methods offer variation in surface characteristics, and active sites and different materials have different intrinsic activities toward

ORR. The catalysts synthesized at recent times performed notably better than the catalysts synthesized decades ago mostly because of the improvement in AEMs and water management. Thus, the comparisons among the catalysts based on the cell performance may not always guide us to a concrete conclusion. For the effective comparison of any components in the catalysts, it is essential to set a standard for ink preparation, MEA configuration, test operating conditions, and other factors except the subject of the study. Researchers from numerous groups are working on every parameter till today and no standards are established yet. However, the comparison is demonstrated in this article acknowledging this limit.

All the catalysts are arranged in definite groups based on their composition. Among 203 catalysts, carbon-supported transition metal catalysts (MCC) were the most studied type. Around 69% of catalysts belong to this group. Transition metal ceramics (Ceram), chalcogenides (Chalc) and support-free single metal (SFM-M) are infrequently studied and are relatively poor performing as cathode catalysts. Non-metallic catalysts (NMC) and transition metal oxides (TMO) are adequately studied and appeared to be well-performing.

The percentage of catalysts from different groups is shown in Fig. 22. Among MCC, metal-nitrogen-carbon (M-N-C) catalysts were mostly studied. The research community showed much interest in M-N-C catalysts because of their well-recognized performance. This is also supported by Fig. 23a, b, where we can see that M-N-C catalysts showed the highest PPD and half-wave potential values comparing to other catalysts. From Fig. 23a, recent studies using Fe-N-C cathode catalyst showed an extraordinary performance of 2040 and 1800 mW.cm^{-2} as the best-performing cathode catalyst to date [139,142]. The nearest top performing catalyst is from TMO group, which showed PPD at 1350 mW.cm^{-2} [143]. Also, it can be concluded that nitrogen coordination in M-N-C and MM-N-C catalysts showed better activity towards ORR than M-C and MM-C catalysts. It is also supported by literature that metal-nitrogen centers are catalytically active for ORR [46,86,165]. Although, MM-C performed inferior, however, we cannot conclude any point since only a few examples cannot be enough, but the statistical data can be helpful to identify the potential of the electrocatalytic activity toward ORR.

It is observed that more than 74% of the catalysts showed PPD below 300 mW.cm^{-2} and 59% of the catalysts below 200 mW.cm^{-2}. Thus, it is clear that very few catalysts performed as expected in this area. From Fig. 24c, only 29 among 203 catalysts showed PPD value over 500 mW.cm^{-2} and 13 catalysts over 1000 mW.cm^{-2}. It can be seen from Fig. 23a that MM-N-C, M-N-C, NMC and TMO catalysts have already overtaken the 1000 mW.cm^{-2} limit. All types of catalysts showed good activity toward ORR as shown in Fig. 23b. All of them except transition metal ceramics exhibited $E_{1/2}$ value over 0.8 V within their range.

Onset potential (E_{on}) and half-wave potential ($E_{1/2}$) are measured from RDE or RRDE experiment. E_{on} or $E_{1/2}$ value for ORR for a specific catalyst is generally constant but may vary with the change of catalyst loading on disk, disk rotation rate, etc. For this reason, E_{on} and $E_{1/2}$ values at a rotation rate of 1600 rpm, or closer to this value are noted in Table 1 and Table 2. It can be seen from the histograms in Fig. 24a that almost a normal distribution is observed for onset potential with the highest frequency at the range between 0.90 and 0.95 V vs RHE and a left-skewed distribution as shown in Fig. 24b was noticed for the half-wave potential histogram with the highest frequency at 0.80–0.85 V vs RHE. The cathode catalysts having the E_{on} and $E_{1/2}$ values greater than 0.9 V and 0.8 V, respectively, may be considered as highly ORR active. A higher E_{on} and $E_{1/2}$ values can imply better activity toward ORR. Although approximately 60% of the cathode catalysts showed $E_{1/2}$ value over 0.8 V indicating high ORR activity, the single-cell test comprising the cathodes did not exhibit that much performance as depicted in Fig. 26a, which indicates that there are other significant factors involved in AEMFC performance apart from the activity of cathode catalyst itself. Water management, ionomer, and membrane properties have significant effects on the AEMFC performance what will be discussed in a later section.

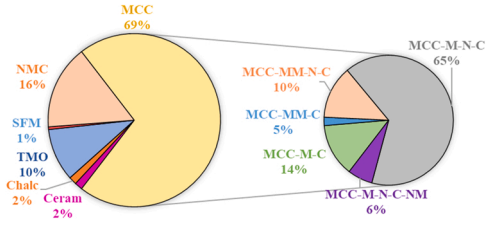

Fig. 22. Pie chart showing the percentage of 189 cathode catalysts in their corresponding groups.

As we know from thermodynamics, the standard potential of the cell is calculated from Gibbs free energy, which can be found using enthalpy and entropy data. Both enthalpy and entropy depend on temperature. Since AEMFC is operated mostly at a narrow range between 60 and 80°C, the standard potential for H_2, O_2 redox reaction should be within the limit between 1.15 and 1.18 V. The open-circuit potential can be derived from standard potential using the Nernst equation where the value depends on partial pressure or activities.

With the variation of the pressure and temperature, the open-circuit potential may differ from any set value. A high value of open-circuit potential may be achieved at a set condition, but it is required to optimize the operating conditions to obtain a high cell performance. From Fig. 24d, 77% of the catalysts showed open-circuit voltage (OCV) between 0.85 and 1.05 V. Only 22.9% of the catalysts crossed the limit of 1.0 V for OCV. Surprisingly one catalyst showed a high OCV value near to the standard potential [248].

Fig. 23a shows the maximum performances achieved in each category, but no quantitative information can be extracted. Therefore, Fig. 25 is presented which may help to comprehend how different types of catalysts performed quantitatively at different ranges. M-N-C has a good set of examples to prove its potentiality. Although MM-C, MM-N-C, and NMC have shown high performances, only trifle examples are ahead of us. Transition metal oxides (TMO), on the other hand, performed over 1000 mW.cm^{-2} by a good number, but to our knowledge, only ca. 20 catalysts are studied so far. Non-metallic catalysts (NMC) and the integration of nonmetals into M-N-C (M-N-C-NM) have exposed their potentiality as cathode catalysts by offering trivial instances of performances over 500 mW.cm^{-2}.

Numerous researches are being carried out to obtain highly active cathode catalysts, but in practical applications, the AEMFCs containing the highly active catalysts do not always show high performances. Therefore, no direct correlation can be established between PPD and $E_{1/2}$ from the statistical data as shown in Fig. 26a. It is observed that highly active catalysts even showed variation by a factor of 10 in their PPD values. This indicates that the overall ORR electrocatalytic activity is not a solely important factor that affects the AEMFC performance. The cell performances also depend on the AEM and AEI, water management in cells, preparation of MEAs, mass-transfer conditions, operating conditions of the cells (temperature, RH, gas flow rates), etc.

Specific surface area (SSA) is not always a good parameter to identify the activity and performances of ORR electrocatalysts. The ORR activity is determined by the intrinsic activity of active sites and by the number density of active sites. However, not all ORR-active sites are accessible to O_2 molecules, especially in the case of microporous catalysts. Therefore, the turn-over frequency (TOF) value may be considered as the best descriptor for the intrinsic electrocatalytic activity. Unfortunately, the TOF value has been determined only in a few articles. Usually, we do not know exactly which ones are the ORR-active sites and what is the number density of these active sites. Therefore, it would be virtually impossible to make proper correlations between the PPD values and ORR kinetics descriptors.

However, catalysts consisting of high surface area and porosity may have their active sites more accessible to reactants [147,308,309].

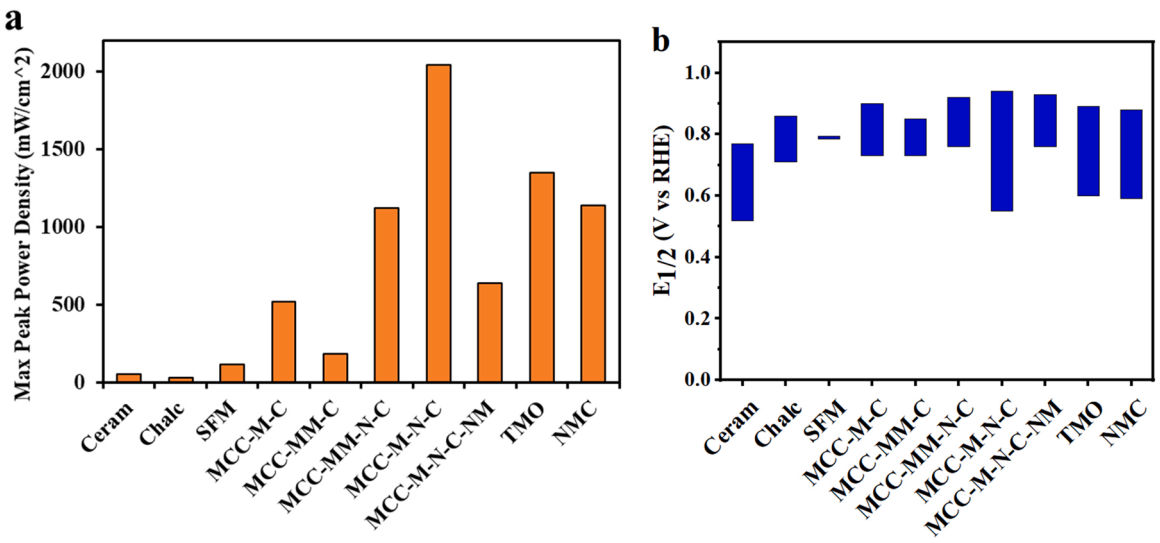

Fig. 23. a) Maximum PPD achieved from each category; b) The range of half-wave potential achieved from each category.

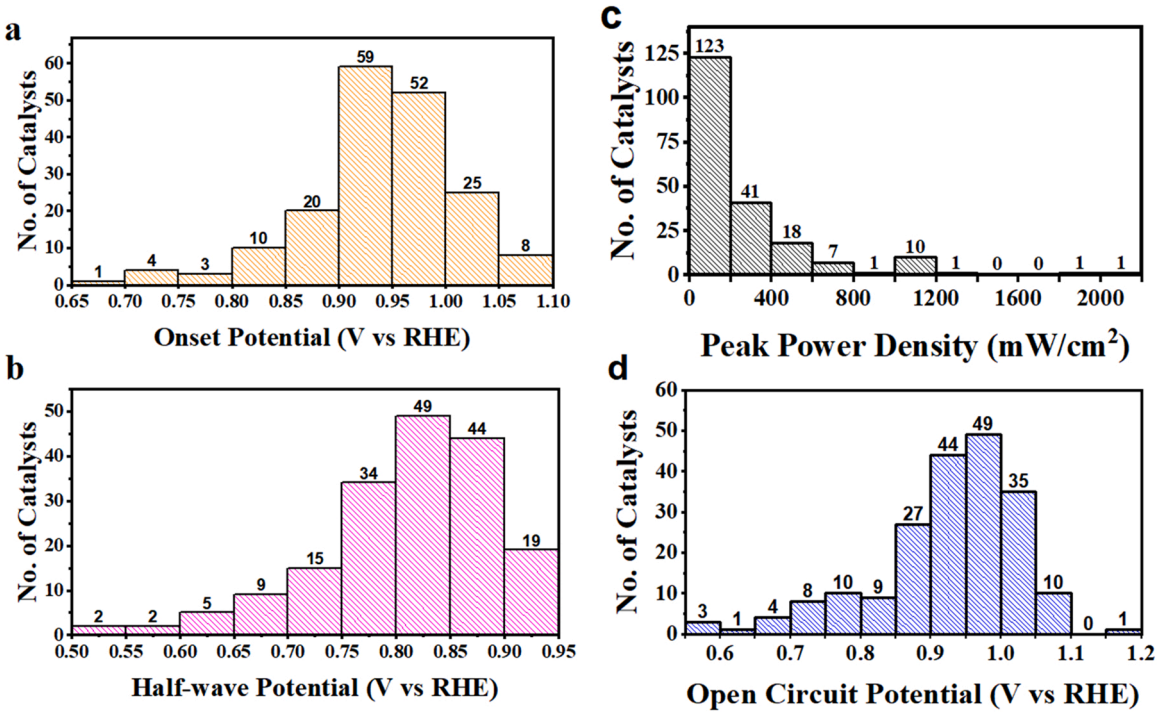

Fig. 24. Histogram of a) onset potential (E_{on}), b) Half-wave Potential ($E_{1/2}$); c) PPD, and d) open circuit potential for the catalysts available with the corresponding data.

Water transport and management are also convenient for porous catalysts with high SSA. The ORR activity and fuel cell performance are thus expected to improve with the increase of SSA, if only the ORR active site components, the density of active sites, testing conditions, and other important parameters may remain identical. Since different types of catalysts comprise different active sites, the SSA is not a good parameter to be correlated with PPD for catalysts from different groups and materials. Thus, Fig. 26b is not appropriate to find any specific relation between cell performance and SSA, and a very random behavior is observed.

All catalysts were not characterized by their surface area, so based on the available data, three distinct regions are indicated in Fig. 26b. In region-I, several catalysts i.e. Zn-Co/N/C, N/C, Fe-N/C, Fe-Co-N/C, Co-N/C, Fe-Mn/N/C, etc. showed high performance with low SSA [30,44,46,151,175,200,204,222,281], and in region-II, few catalysts i.e. N/C, Fe-N/C, Cu-N/C, etc. exhibited low performance at their high SSA [185,187,209,235,236,264,269,270,273,277,278,299,304,310]. Interestingly, similar elements or components are present in the catalysts from both regions. Catalysts in region-I can be assumed to be highly active with their low surface area and thus have the scope to perform better by modifying the structures during their synthesis to achieve higher surface area. On the other hand, catalysts in region-II may not have any chance to perform better by modifying their morphology, rather the conjugation of the active sites should be dealt with during synthesis. Catalysts such as N/C, Fe-N/C, etc. in region-III [142,146,147,152] represented a harmony between PPD and SSA by showing high performances with a large surface area. Some other catalysts having low SSA also showed moderate peak power densities [152,156,163,171,196,200,227,246,

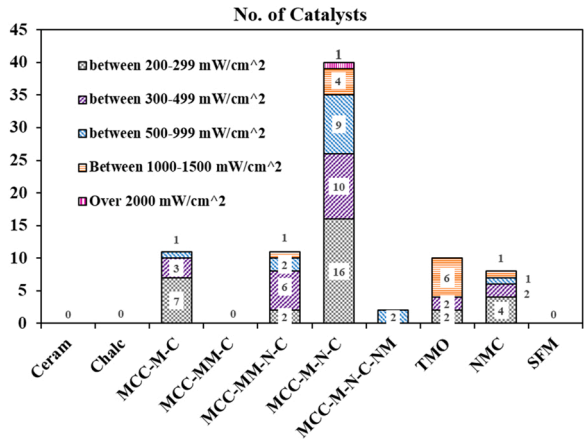

Fig. 25. No. of catalysts performed in a definite range of peak power densities for each type of catalyst group.

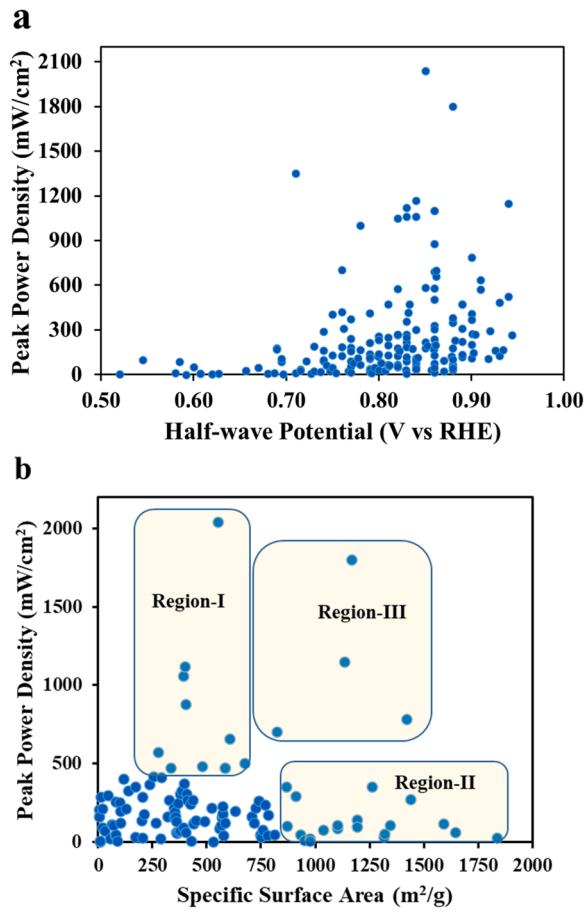

Fig. 26. a) Correlation between PPD and half-wave potential; b) Graphical representation correlating PPD and SSA ($m^2\ g^{-1}$).

254,311]. Their performances are also further expected to improve by enhancing the surface area, although it cannot be simply stated without further studies.

The polarization curves of 13 catalysts that showed performances over 1000 $mW.cm^{-2}$ in their single-cell tests are shown in Fig. 27. The catalysts i.e. Fe-N-C [139], Fe-N-C [142], Co-Fe/VC [143], N-doped-C [154], $CoMn_2O_4$/C [174], $MnCo_2O_4$/C [174], $Fe_{0.5}$-NH_3 [165], α-Mn_2O_3/Fe0.5-NH3 [165], Mn-Co spinel (MCS) [177], N-C-CoOx [162], FeNx-CNTs [146], Co-N-CDC/CNT [151], and CoFe-N-CDC/CNT [151] exhibited top-notch performances so far. All these MEAs also presented high current density output. A maximum current density of 7240 $mA.cm^{-2}$ was observed for Fe-N-C [139]. A high value of current density indicates a high conversion rate of the reactants which might be attained by reducing mass and electron transfer resistances, enhancing mass transport with the porous structure of the catalysts, and supplying a high flow rate of the reactants, etc. At these high current densities, some degree of water flooding may occur, but the excess water may also help to supply water at the cathode and maintain membrane humidification [312].

The fuel cell test data (PPD, Specific PPD, Current density at PPD) of the top-performing 29 catalysts are shown in Fig. 28. Specific PPD, here in this article, is defined by the maximum power achieved in a single cell per unit mass of Pt or Pt-Ru used at the anode. High specific PPD indicates a high performance using less amount of platinum. A similar trend of PPD, Specific PPD, and Current density at PPD (i_{PPD}) is observed. These catalysts include only a few metal elements i.e. Co, Fe, Mn, Ag. Surprisingly, a non-metal catalyst, N/C(FU) was placed on the list by performing over 700 $mW.cm^{-2}$.

3. Effect of different parameters on the activity and performances

3.1. Effect of catalyst conditions

Catalyst layers provide an active surface area and channels for catalyzing redox reactions and transporting reactants and products of the reactions. The ORR and HOR reactions occur at the triple-phase boundaries inside the catalyst layers where the liquid and gaseous reactants come in contact with the solid catalysts and ionomer/membrane [31,313]. Variation in nitrogen/carbon precursors, transitional metals, and thermal treatment conditions may have effects on the formation of nanostructures and performances [314]. One study claimed that the bimetallic catalysts exhibited better ORR activity than the single metal catalyst [315].

The doping of carbon materials with nitrogen [121,316,317], phosphorus [318–321], boron [319,322–328], sulfur [329–334] showed better ORR activities. It was revealed that the doping with heteroatoms of high electronegativity differences (N, F, P, B, etc.) interrupts the electro-neutrality of the carbon matrix by altering the electronic charge densities, spin densities, causes charge polarization [121,187,270, 335–343] and increases ORR activity thereby [121–123]. Also, carbon matrix after being doped with sulfur which has similar electronegativity to carbon atoms also showed better ORR activity [344].

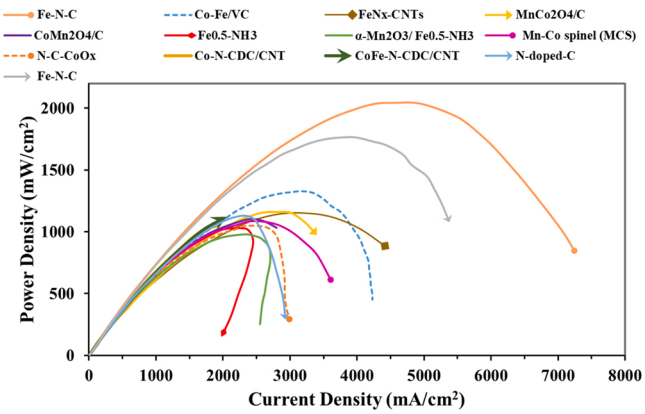

Fig. 27. Power density curves of the top performing catalysts i.e. Fe-N-C [139], Fe-N-C [142], Co-Fe/VC [143], N-doped-C [154], $CoMn_2O_4$/C [174], $MnCo_2O_4$/C [174], $Fe_{0.5}$-NH_3 [165], α-Mn_2O_3/Fe0.5-NH3 [165], Mn-Co spinel (MCS) [177], N-C-CoOx [162], FeNx-CNTs [146], Co-N-CDC/CNT [151], and CoFe-N-CDC/CNT [151] which showed PPD over 1000 $mW.cm^{-2}$.

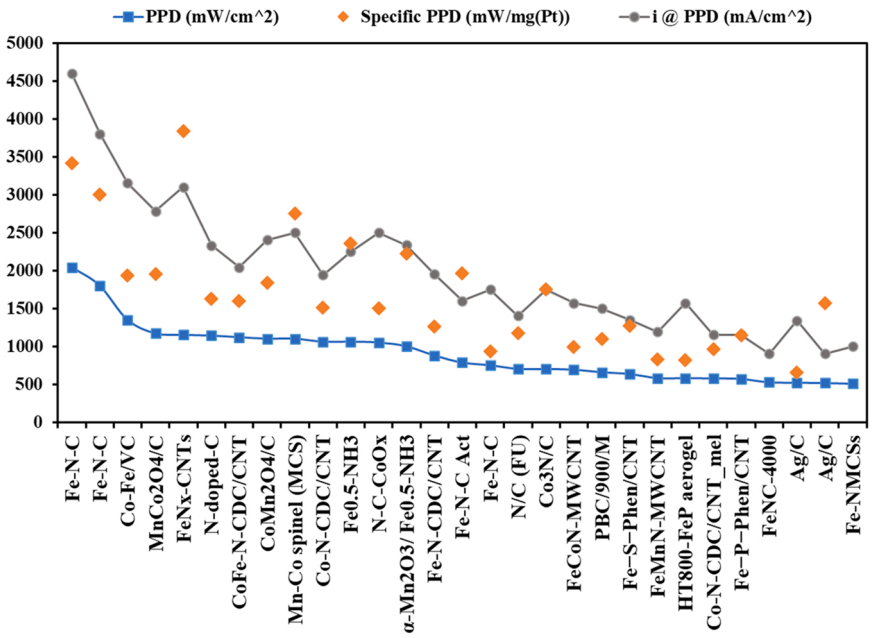

Fig. 28. PPD, Specific PPD, and current density (i @ PPD) data for top-performing catalysts.

Multi-heteroatom doped nanocarbons showed better activity than single or dual doped catalyst [326,328,329,345–350]. The N, F doping in carbon matrices were claimed to create edge defect sites, in other words, enhanced the degree of disorder and thereby created the active catalytic sites for ORR [187]. Several factors such as SSA, ratio of N/O, porous structure, edge and topological defects etc. affect the ORR performances [351–355]. Typically, a higher nitrogen content also indicates higher ORR activity [192,356,357]. Total nitrogen content and proportions of different nitrogen moieties except for oxidized-N in the catalyst affect the activity toward ORR [83,358]. In contrast, a study claimed that total N content is not important for ORR process [359]. The catalyst with highest total nitrogen contents showed better ORR activity than the catalyst consisted of more pyridinic N with less total nitrogen content [124]. Also, an opposite scenario of better performance with less total nitrogen content, but with higher pyridinic N and graphitic N contents were observed [360,361]. Similarly, another study suggested that ORR activity depends on pyridinic-N and quaternary-N, rather than total N content [362].

Pyridinic N and pyrrolic N indicate those N atoms which are bonded in six and five-membered heterocyclic aromatic rings respectively [266, 363]. Also, graphitic N represent those N atoms which are bonded to three C atoms in a graphene plane and oxidized N indicate them which are incorporated to one O atom and two C atoms [363]. Generally, pyridinic-N and M-N_x are considered to be the most active sites for ORR in alkaline media [126,266,364–371]. However, it was also suggested that graphitic N, rather than pyridinic N, significantly influence the ORR activity [297,372]. It was also claimed that Fe nanoparticles embedded in CN_x graphitic plane were the active sites rather than FeN_4 [373], whereas CN_x itself also showed inferior ORR activity compared to MN_x sites [374,375]. Pyridinic N facilitates O_2 adsorption by exerting a conjugation effect on its lone pair of electrons and π system [263,359, 376–378]. Pyridinic N increases $\pi\pi$ states density near Fermi level, modifies carbon band structure, and reduces the work function [359, 379,380], whereas graphitic N induces higher positive spins and charge densities to the neighboring carbons [381]. Thus, both pyridinic and graphitic N improve the ORR activity.

It was previously claimed that Fe-N_x [365,382,383], pyridinic-N [384,385] stimulates $4e^-$ reaction pathway, whereas graphitic-N [382, 384,385], hydrogenated N [382,384,385], pyrrolic-N [365], Fe/Fe_3C [383] facilitates $2e^-$ pathway. A study contrarily claimed that pyridinic-N fosters $2e^-$ reaction pathway [365]. Another source claimed graphitic N being effective to adsorb O_2 and reduce the ORR activation energy [386]. Nitrogen moieties e.g. pyridinic-N also help to chemisorb O_2 since charge delocalization is facilitated by nitrogen [364]. The presence of quaternary-N peak indicates some degree of graphitization [188]. Some studies also claimed pyrrolic-N to be the active sites toward ORR as well [264,387,388]. Edge defects are required to form active sites in N-doped carbon catalysts [389,390]. Metal and metal oxide nanoparticles encapsulated by carbon layer may lead to enhanced ORR catalytic activities [184] and higher corrosion resistance properties [391–394]. Inherent low conductivity of the metal oxides is considered as one of the drawbacks in their application and therefore highly conductive materials may be combined to prepare composite catalyst [127]. The electrode catalyst layer is generally comprised of ionomer, catalyst, and support materials. The catalyst support should have a high surface area, good stability, resistance to corrosion, surface functional groups, mesoporous structure, high electrical conductivity, etc. [54].

The optimization of catalyst loading is important since thickness, porosity, tortuosity, the interconnection between pores, etc. are dependent on it; thereby transport of water, reactant gases, and practically fuel cell performance also depend on the catalyst loading. Since the increment of Pt loading enhances the active sites for reaction and decreases ohmic resistances, fuel cell performance reached a PPD with the increase of Pt loading and diminished thereafter because of the poor dispersion and utilization of the catalyst sites [395]. Also, activation and ohmic losses become prominent for excessive thickness because electrons and ions have to travel longer [396]. The optimization of the cathode layer thickness depends on the ionomer properties and the partial pressure of the oxygen [397]. A thicker cathode catalyst layer with higher loading may be beneficial since it can hold back-diffused water more, and reduce the overall cell resistances [38].

A similar optimum effect was observed with PTFE content in GDE since PTFE integrates hydrophobicity, improves water management, and conversely increases ohmic resistances, decreases ionic conductivity [395]. The effect of the hydrophilicity of the cathode catalyst was studied based on its contact angle and wettability. The simulation result revealed that low contact angle or hydrophilic condition at cathode could occur a high performance since water is consumed at cathode and hydrophilicity helped to retain more water from the anode by back diffusion [398].

Ionomer loading in the catalyst ink was also optimized in previous studies. An optimum ionomer loading was also observed at 35–50 wt% for the maximum performances [86,194]. A low ionomer content leads to poor ionic conductivity, high internal resistance loss, and low accessible active sites. Although ionomer being hydrophilic may help retaining water, a high amount of ionomer may reduce pore volume, block the channel and the active sites for the reaction, and deteriorate the electronic conductivity of the catalyst layer [38,86]. It was observed that kinetic current was improved with the increase of ionomer content, but mass transport was declined due to flooding [399]. Although the optimum ionomer loading was commonly evaluated based on the performances, another methodology was also proposed using electrochemical impedance spectroscopy (EIS) technique previously [400,401].

Previously, Gokhale et al. claimed the surface area to be the major governing factor for ORR in alkaline environment [402,403]. It was reported that surface area surpasses the effect of elemental and chemical composition of the cathode catalysts in alkaline electrolytes, although the active sites has significant effects in acidic media [402,404]. Interconnection between the pores positively affect the mass transfer of the reactants and the products [405,406] and large pore sizes help to minimize the ohmic losses and mass transport losses [87,304,406]. It was observed in a study that the porosity, as well as the performance, was improved by increasing the carbon loading and reducing ionomer content at a definite value [312]. Both meso and microporous structures are important for the catalysts to attain enhanced ORR activity and AEMFC performance. It was suggested that mesopores and tortuosity were created by agglomeration of the catalyst which reduced the electrode volumetric current density [128]. Mesopores facilitates transportation of reactant molecules and accessibility to the electroactive species, whilst micropores hold the active sites [124,352,407]. A high percentage of micropores are helpful to attain high cell performance in the kinetic region, but not in high current density region, since micropores induce large mass-transfer resistance at this region [73].

3.2. Effect of membrane

In AEMFC, the membrane consisting of a hydrophobic polymer backbone with covalently attached cationic groups acts as an electronic barrier, selectively transports OH^- ions from the cathode to anode, and resists fuel crossover [21]. The properties of an ideal membrane include high OH^- conductivity, mechanical, chemical and thermal stability, flexibility, low gas permeability, availability, and low cost [54]. Over the years, a progressive pattern in the fuel cell performance was observed primarily because of the improvement in ionic conductivity and ion exchange capacity (IEC) of AEM [408]. In a study, it was revealed that fuel cell performance does not depend on OH^- conductivity alone and the membrane with relatively lower OH^- conductivity showed higher performance because of its lower water uptake [52]. The enhancement of the IEC can compensate low mobility of OH^- ions, but simultaneously it reduces the mechanical stability of the membrane, so a trade-off between these two must be balanced. The target of OH^- conductivity of AEM before 2010 was to exceed 10 mS/cm [22]. The rapid increase of OH^- conductivity now reaches at least 200 mS/cm [409–414]. Interestingly, the measurement procedure of OH^- conductivity is also improving [415]. Decades ago, although the ORR activity of the synthesized catalysts was high compared to recent works, the fuel cell performance was relatively lower because of the poor membrane properties [408,416].

In 2006, the first-ever all-solid-state H_2/O_2 AEMFC showed the PPD at 55 $mW.cm^{-2}$ using 4 $mg.cm^{-2}$ Pt-loading at 50ºC [417]. Recently, in 2019, the PPD of 3.4 $W.cm^{-2}$ was achieved with 1.5 $mg.cm^{-2}$ Pt-loading at 80ºC and relative humidity of 60% at the anode, 84% at the cathode [52]. In comparison, Varcoe et al. in 2006 considered the membrane issues with CO_2 and modified accordingly [417]; Kohl et al. in 2019 considered and optimized multiple issues like ionic conductivity and ion channel efficiency of the membrane, water uptake and swelling of the membrane, MEA stability, operating temperature, and relative humidity, membrane thickness, fuel crossover, etc. and therefore observed very high performance in fuel cell operation [52]. It was observed that light cross-linking in the membrane improved ionic conductivity, IEC, and mechanical properties [52,418,419]. A thin membrane is beneficial since it causes less ohmic losses and favors water back diffusion, although stability and fuel crossover may become issues, since fuel crossover is responsible for lower OCV values. The membrane interface may also have effect on the performance. Previously, a line patterned membrane or electrode interface with enlarged interface was developed using solvent-assisted molding technique and a higher cell performance was observed compared to the flat surface membrane due to an enhanced mass transport [420].

The membrane is required to uptake and transport water molecules for proper water management across MEA [421,422]. Ionic conductivity increases with water uptake, but excessive water uptake can deteriorate the performance and stability [51]. Swelling after water uptake is unwanted and needs to be minimized. The stability issue of the membrane in high pH conditions is still a challenge. In a study, two strategies were proposed to improve the durability of the membrane: (i) to increase molecular weight and glass transition temperature, (ii) to reduce the water uptake and swelling ratio [423]. The presence of CO_2 in the air forms a precipitate of CO_3^{2-} ions in contact with AEM, which degrade the fuel cell performance [424]. Since air is practically abundant and applicable in vehicles, so the upgrades of the membrane to be CO_2 tolerant are required, or the technology for the purification of air must be assured. Interestingly, at high current densities, the membrane purges the carbonate species and preserves its ionic conductivity [92,425].

Several cationic groups e.g. ammonium, phosphonium, imidazolium, sulphonium, organometallic cations, etc., and polymer backbones e.g. poly(ether-ether ketone), polysulfone, and poly(phenylene oxide), poly (arylene ether) etc. have already been employed in the construction of anion-exchange polyelectrolytes (AEPs) [53]. Several types of membranes have been synthesized which consist of high ionic conductivity such as QAPS-polysulfone copolymer [426], radiation-grafted ETFE [427], poly(benzimidazolium) [428], and interpenetrating network based membranes [429]. It was observed in a study that piperidinium functionalized long-side-chain type AEMs(LSCPi) shows lower conductivity than quaternary ammonium (QA)-based AEMs (LSCQA) [430]. Recently, PTFE reinforcement in composite membranes have been reported to be advantageous [52,76,431]. MEA including aryl ether-free AEPs comprising of alkyl-alkyl or aryl-aryl backbones showed excellent cell performance and high PPD over 1 $W.cm^{-2}$ up to 3.5 $W.cm^{-2}$ [52,75,76,312,409,432–435]. Few aryl ether based AEPs showed high performance up to 1.37 $W.cm^{-2}$ as well [436,437].

3.3. Effect of anion exchange ionomers (AEIs)

Although it is a common practice to use the same AEPs for both AEMs and AEIs, it is not always a good choice. The requirements for the individual properties may differ slightly as per application [53]. The high ionic conductivity, ion exchange capacity (IEC), and stability are essential for both of them. Ionic conductivity is related to the product of the ionic activity and effective mobility, where ionic activity or IEC indicates the ion content in ionomer and effective mobility inversely depends on the tortuosity [438,439]. The requirement for ionic conductivity in ionomer and membrane differs since the membrane is several thousand times thicker than the ionomer surrounding the catalyst or support agglomerates [73,440]. Ionomer generally forms few nanometers thick layer on the surface of catalyst particles [440–442]. For AEMs, low gas permeability, good mechanical strength, and low swelling ratio are important to control the fuel cross-over and hold the membrane structure. Unlikely, AEIs are required to have high gas and water permeability [443], reasonable molecular weight, and good

dispersion or solubility since AEIs are mixed in the catalyst inks and remain in the catalyst layers [53]. The optimization of ionomer content is important since it affects the structure, mechanical properties of the catalyst layer and the catalytic activity for ORR and HOR [444].

A suitable AEI is critical for the establishment of the triple-phase boundary and stability of the catalyst layer. The incorporation of chain-packing disrupters i.e. contorted spirobiindane units [445] or dimethyl groups [51] into the polymer backbone causes an increase of fractional free volume of the ionomer and thereby enhances gas permeability. It was observed in a study that a combination of hydrophilic ionomer at anode and hydrophobic ionomer at cathode resulted in the best performance compared to other combinations [446]. Contrarily, hydrophobic ionomer was suggested to be suitable for better performance at the anode catalyst [447–449]. It was proposed that for a small number of M-N_x sites, hydrophilic side chain of ionomer tends to face the pores and attract water molecules, whereas with the excess amount of M-N_x sites, hydrophobicity prevails in pores causing barrier to water and ion transport [450]. Hu et al. used fluorine containing ionomer (quaternary ammonia poly(arylene perfluoroalkylene)-QAPAF) which enhanced the hydrophobicity and conductivity of the anode catalyst layer [447]. The swelling and deswelling cycles in ionomer along with the pressure of gases may create cracks in the catalyst layer [451,452]. At lower hydration, oxidizable sites in ionomer is more susceptible to degradation by hydroxyl ions, so ionomer in cathodes is more vulnerable than anode side [68,73]. Currently, aryl ether-free AEPs such as benzyl-trimethyl-ammonium-functionalized poly (ethylene-co-tetrafluoro ethylene) (BTMA-ETFE), polyfluorene (FLN), Poly(terphenyl piperidinium) (PTP), poly(biphenyl piperidinium) (PBP) etc. are considered to be state of the art AEIs [53].

3.4. Effect of GDL

GDL is a highly permeable, porous carbon fiber structure that provides support for MEA, acts as a channel for transporting liquids/gases, conductor for transferring electrons, and an insulator to maintain temperature gradient so that steam may diffuse [38,453]. It may consist of two distinct layers i.e. microporous layer (MPL) and hydrophobic layer (PTFE). MPL consisting of carbon or graphite particles with 10–40 wt% of hydrophobic binder (pore sizes of less than 500 nm) enhances surface contact [454,455]. The optimization between hydrophobicity and hydrophilicity is required to eject water out of the cell by not getting completely dehydrated [454,456]. It was observed that the addition of PTFE by a small amount in anode GDL improved the flooding conditions and hence fuel transport as well as the performance [421,457,458]. The effect of the inclusion of MPL at the cathode, anode, or both sides on the performance was observed by Xie et al. [459]. It was revealed that MPL only on the anode side showed the highest performance, whereas MPL only on the cathode side showed the lowest performance. This is because that MPL being hydrophobic helped to expel water from both anode and cathode, but water removal is important for anode only. MPL in cathode also resists the diffusion of water from flow channels to catalyst layer [459]. Conversely, one study found that PTFE-treated GDL showed inferior performance and it was claimed that the porous network of the GDL was blocked by PTFE [460]. The conflict needs to be resolved by substantial researches since water management has a crucial effect on the fuel cell performance.

3.5. Effect of water management

Water management is crucial for AEMFC since both cathode and anode compartments deal with water. As it can be seen in Fig. 1, water is consumed at the cathode side and produced twice in an amount at the anode side, so cathode catalyst may confront dryness, and anode catalyst may get flooded for imbalanced water management [38]. Also, water fluxes were observed to be three times higher than the vapor fluxes in an investigation [461]. Proper hydration improves ionic conductivity of ionomers and membranes and reduces their resistances. Too much water can cause high internal stress in the membrane, influence the degradation in the membrane. Mass transport issues may also arise at high current density due to the blockage of the porous structure of catalyst layer by excess water at anode [52]. Two methods have been proposed to avoid anode flooding: (i) to increase the anode flow rate, (ii) to reduce the membrane thickness [422]. Also, increasing hydrophobicity of the anode catalyst layer is favorable to avid flooding. Contrarily, local drying-out may occur at the cathode at high current densities [462]. A low hydration in cell reduces ionic conductivity and may cause membrane degradation. Thus proper water management can imply a durable and stable cell performance [312]. Also, since AEMFC is sensitive to the relative humidity in the reactant streams, and water uptake in ionomer/membrane, it is essential to develop proper water management in MEA to obtain high performance [421]. In a study, after hours of operation, the reduction in fuel cell performance was observed due to the net loss of water which was mitigated by increasing the relative humidity [52].

3.6. Effect of fuel cell test conditions

It was observed that AEMFC showed much higher performance at higher temperatures, but the membrane stability at higher temperatures needs to be accounted [52]. Also, fuel cells operating at higher temperature conditions need higher humidification in the inlet gases [52]. Hydration of both the membrane and cathode catalyst is required for better performance in AEMFC as water is consumed at the cathode and ionic conductivity, membrane/ionomer stability depends on the hydration [21,63,463]. Water is generated at anode, so excessive humidification of the anode inlet may arise flooding conditions. Nonetheless, humidification at anode gas is also required since there is a significant loss of water by back diffusion and evaporation [464,465]. ORR kinetics, ion transport, the current density can be enhanced and ohmic loss, water diffusion loss can be reduced by humidifying gases at both anode and cathode [466]. Also, area-specific resistance (ASR) increases with the reduction of relative humidity below an optimum value [467].

It was contrarily claimed that mass transport limited current could be increased by reducing relative humidity [52]. Excessively high RH conditions can cause flooding and low RH conditions can degrade performance. Thus, the proper optimization of the relative humidity of inlet reactant gases is essential. Relative humidity has a negligible effect on the electrode kinetics but has a significant effect on the mass transport resistance [468]. It was reported that the optimization of the anode and cathode dew points or relative humidity improved the limiting current density by 33% and the PPD by 10% as shown in Fig. 29b [468]. The optimization depends on several factors such as pressure, temperature, current density, ionomer or membrane properties, stoichiometry, etc. [469]. From a study, partial humidification of the gases showed better performance than fully humidified conditions [421,470]. It was claimed that unsaturated humidification may accelerate back diffusion of water from anode to cathode by escalating the water gradient between two electrode compartments [73]. Partial or complete humidification affects the water accumulation in the form of the vapor phase or liquid [471].

The reactant gases are supplied at a higher extent to maintain homogeneity and to expel excess water from the electrode [421]. The high flow rate of gas at anode positively affects the performance particularly at high current density by facilitating the removal of water molecules with its exhaust [422]. Reduced cell performance was observed in a study by lowering the flow rates of both H_2 and O_2; although cathode mass transport losses, in this case, were claimed to be only attributable to the degradation in performance [421]. For maintaining a high flow rate, membrane gas permeability should be reduced by increasing its thickness to resist cross-flow [472]. Inlet gas flow direction has been found to have impacts on water management and local current density [473,474]. Counter-flow of H_2 and O_2 can help to drag more water from anode to cathode and thereby reduce anode flooding [474]. Although high gas flow and CO_2-free air are mostly supplied to achieve high

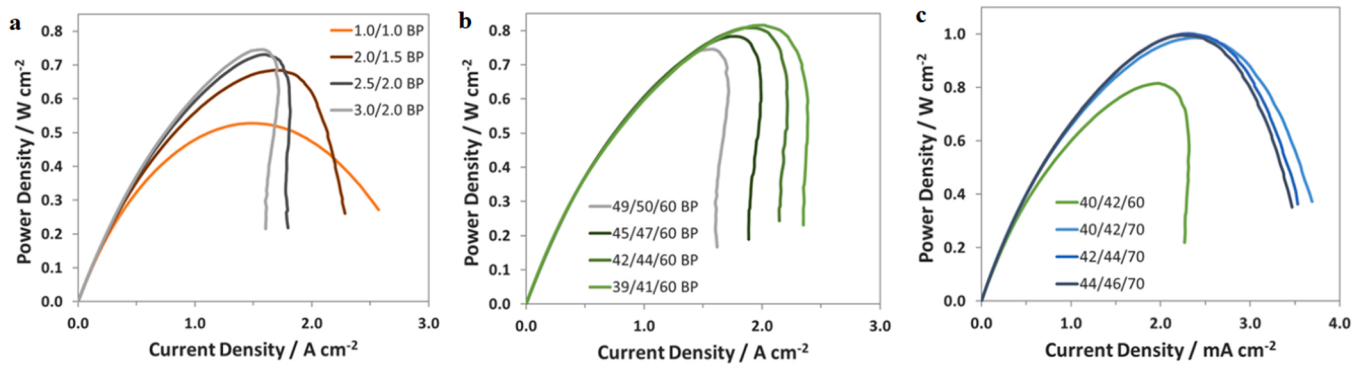

Fig. 29. Effect of a) backpressure ($BP_{anode}/BP_{cathode}$), b) dew points ($DP_{anode}/DP_{cathode}$/temerature), and c) temperature ($DP_{anode}/DP_{cathode}$/temerature) on the performance. Backpressure is in bar_a, dew points in °C, and temperature in °C. Reprinted and adapted with permission from ref. [468]. Copyright 2018, ECS.

performance in the cell, this would be unrealistic unless suitable technology is provided.

Backpressure indicates the pressure created by the gaseous molecules present in the cell. Backpressure can help to reduce the rate of convective water loss, OH^- transfer resistances, and kinetic overpotential, but it can also diminish the ability of the cell to eject water from anode [468]. The backpressure is generally kept the same at both sides of the membrane to retain its structure unless the membrane is durable enough. The asymmetric backpressure is beneficial because of the imbalanced water contents at the cathode and anode [38]. Omasta et al. optimized the backpressure conditions and applied 3.0 bar_a and 2.0 bar_a at anode and cathode respectively as shown in Fig. 29a [468]. Backpressure at the anode may promote the permeation of water from anode to cathode and thus it may help to achieve liquid saturation at the cathode and to control anode flooding [475]. An opposite phenomenon may arise due to the elevated boiling point at high backpressure at the anode and this may cause high retention of water at the anode. High backpressure at the cathode was claimed to be effective for water retention at the cathode and improving O_2 transport. It was suggested to keep the anode backpressure lower than the cathode for better performance [139,467].

The operating temperature significantly influences the AEMFC performance by affecting the electrode kinetics and the mass transfer resistance. In several studies, it was found that with the increase of the operating temperature, the enhanced AEMFC performance was achieved [154,421,458,468,476]. This is because that electrochemical kinetics, membrane hydration, ionic conductivity, mass transport through membrane, and water management through GDL are improved at higher temperatures [476–478]. The high vapor saturation pressure gradient at higher temperatures helps cleaning the pathway through GDL and thus improve the water management across the cell [38]. The limitation here is that most commercially available AEMs and ionomers are not stable over 60°C. Although few membranes such as quaternized poly(2, 6-dimethyl phenylene oxide) (QAPPO) [429], quaternary ammonia polysulfone [437], radiation-grafting onto poly (ethylene-co-tetrafluoroethylene) (ETFE) [427] are found to be stable up to 80 °C. Also, several AEPs have been reported to be stable up to 100°C [479–481], 140 °C [482], and 160°C [483].

It is claimed that catalyst's stability is dependent on the applied potential. In a study, it was found that in acidic medium, the catalyst at a potential range between 0.7 and 0.9 V showed good stability and no loss of Fe species. The potential excluding this range caused metal leaching and loss of the ORR activity [484]. Another study claimed similarly that demetallation mostly occurs at low potentials, whereas carbon corrosion and the loss of FeN_x active sites take place at higher potentials [485]. Carbon corrosion may lead to the loss of active sites, porosity, conductivity and cause flooding by increasing hydrophilicity through generating oxygen-functionalized groups. It was suggested that a higher level of graphitization may help to reduce carbon corrosion [128].

3.7. Effect of different compounds

The effect of different molecules on the ORR activity and the stability was studied previously. CO_2 poisoning is a common problem for the stability and performance of H_2 fed AEMFC since atmospheric air which always contains CO_2 is practically used as the feed gas. CO_2 poisoning causes an increase (i) in charge transfer resistance due to lower concentration of OH^- ions in anode, (ii) area-specific resistance due to a less mobility of carbonate ions, and (iii) anode potential due to the Nernstian thermodynamic shift caused by the carbonates accumulation [486]. It was also found that the presence of several compounds i.e. potassium thiocyanide, potassium cyanide, sodium fluoride, ethanethiol, urea, methanol, anions (N_3^-, Cl^-, PO_4^{3-}), benzene, toluene, SO_2, NO_2 showed no effect or negligible effect on the ORR activity of the PGM-free catalyst [400,487–490]. It was claimed that CO poising affects pyridinic and pyrrolic nitrogen containing FeN_4 sites but does not affect metal-free C-N_x sites [491].

4. Discussion on prospects

The catalysts are expected to have a high value of specific surface area, thermal and electrical conductivity. The water management is convenient for the catalysts belonging to high surface areas and interconnected micropores. To achieve a high surface area, the synthesis often requires pyrolysis at high temperatures. The heat-treatment also helps to coordinate N and O species on the metallic atoms. So, a higher melting point of the metals is expected for the synthesis. Also, the boiling of any elements may help to attain the microporous structure, therefore the boiling point of the sacrificial elements needs to be lower. In several cases, Zn as a sacrificial element was evaporated during high-temperature synthesis which created an interconnected hollow structure with higher surface area [130,159,492,493]. In sacrificial support method (SSM), a porous carbon structure containing active sites was created using fumed silica precursors which was removed by acid treatment after the pyrolysis [86,494–496].

For the electrochemical reaction to be accomplished, the catalysts must transport electrons to the current collector, so higher electrical conductivity is desired for catalysts and their support. The AEM often degrade at high temperatures, so the fuel cell must release heat at a faster rate, thus higher thermal conductivity of the catalysts and their supports is also expected. PGMs showed high catalytic activity for ORR, but are expensive and scarce. The endeavor is ongoing to identify the appropriate materials that are catalytically active, abundant, and of low price. Table S4 summarizes the data for few elements.

A preliminary selection can be conducted based on these data and a single metal or multiple metals can be chosen for the study. The catalytic activity cannot be assured from these data and thereby experimental observation is required. From Table S4, Cr, Fe, Co, Ni, Cu, Zn, Mo, W are identified as relatively abundant, inexpensive, and containing higher

melting point, thermal and electrical conductivity. Many of these elements are already studied. The modification of these metals and their combinations can be further studied to confirm their electrocatalytic activity for ORR.

To date, the most promising type of electrocatalysts for ORR are M-N-C materials with high number density of active sites and suitable porosity to enhance mass-transfer. These catalysts can be synthesized using various approaches. A common method is to use high-surface-area carbon substrate, which is doped with nitrogen and transition metals. The main advantage of this method is that the high BET surface area, overall porosity, pore size distribution and degree of graphitization are basically determined by the nanocarbon material used. A variety of nitrogen dopants can be employed, preferentially N-rich organic compounds. High-temperature pyrolysis is used to create the final electrocatalyst. It is desirable to optimize the preparation conditions to increase the density of active sites and thereby the ORR electrocatalytic activity.

Alternatively, the M-N-C catalysts can be prepared by heat-treatment of carbon, nitrogen and transition metal sources. In this way, a high number density of M-Nx sites can be created. However, the structure and porosity of this type of catalysts is difficult to control. A variation of M-N-C materials are MOF-derived electrocatalysts, the preparation of which is easily feasible. Also, the structure of the MOF-based catalysts is precisely controlled and therefore high-performing ORR catalysts have been synthesized by this method.

Template methods can be used for the preparation of catalysts of tuneable porosity. Both hard (for example silica) and soft (for example polymers) templates are frequently employed. A drawback of this approach is the application of etching agents to remove the hard template material after the pyrolysis, which might affect the electrocatalytic properties of the catalyst. Most importantly, hierarchical porosity created by the template approach is essential to facilitate mass-transfer of reactants and products in the catalyst material.

5. Conclusion

This article reviews, categorizes, and analyzes the previously synthesized non-platinum cathode catalysts for hydrogen-fueled AEMFC. This work summarizes the information of 203 catalysts since 2006. The catalysts are classified into broad categories. Among all types, it was observed that transition metal-nitrogen-carbon (M-N-C), transition metal oxides (TMO), carbon-supported transition metals (M-C), and non-metallic catalysts (NMC) were substantially studied. From the analysis, most of the catalysts showed high ORR activity, but poor AEMFC performances compared to the targets set by the U.S. Department of Energy. Only 13 catalysts from M-N-C, TMO, NMC, and MM-N-C groups containing Fe, Co, Mn elements were observed to cross the PPD value of 1000 $mW.cm^{-2}$. Each category except ceramics showed half-wave potentials over 0.8 V vs RHE. The effect of catalyst conditions, water management, fuel cell test conditions, properties of the membrane, ionomer, and GDL on the AEMFC performance are discussed briefly. For the proper selection of the catalyst materials, the information regarding material abundance, their price, electrical conductivity, and thermal conductivity are provided and the prospects are discussed.

CRediT authorship contribution statement

M.M. Hossen: Planning, Supervising, Data collection (15%), Graphing, Drawing, Analyzing, Writing; **M.S. Hasan**: Data collection (40%); **M.R.I. Sardar**: Data collection (40%); **J.B. Haider**: Planning, Data collection (5%); **Mottakin**: Planning, Proof reading; **K. Tammeveski**: Data analyzing, Proof reading, reviewing; **P. Atanassov:** Planning, Proof reading, Reviewing, Funding.

Declaration of Competing Interest

The authors declare the following financial interests/personal relationships which may be considered as potential competing interests: Plamen Atanassov has patent issued to Daihatsu Motor Co., a Toyota Motor Co. divison/subsidiary. The University of New Mexico (UNM) handles the patents filed and issued in collaboration with Daihatsu Motor Co., presently a division of Toyota Motor Co. These package is entirely managed by Rainforest Innovations LLC., UNM's technology transfer arm. All participation of Plamen Atanassov was as PI of the Daihatsu-funded research between 2008 and 2016. At present there is no activity on this project.

Data Availability

Data will be made available on request.

Appendix A. Supporting information

Supplementary data associated with this article can be found in the online version at doi:10.1016/j.apcatb.2022.121733.

References

[1] S. Pirani, Burning up: A global history of fossil fuel consumption, Pluto Press, 2018.
[2] F. Martins, C. Felgueiras, M. Smitkova, N. Caetano, Analysis of fossil fuel energy consumption and environmental impacts in european countries, Energies 12 (2019), 964, https://doi.org/10.3390/en12060964.
[3] J. Lelieveld, K. Klingmüller, A. Pozzer, R.T. Burnett, A. Haines, V. Ramanathan, Effects of fossil fuel and total anthropogenic emission removal on public health and climate 116 (2019), https://doi.org/10.1073/pnas.1819989116.
[4] F. Johnsson, J. Kjärstad, J. Rootzén, The threat to climate change mitigation posed by the abundance of fossil fuels, Clim. Policy 19 (2019) 258–274, https://doi.org/10.1080/14693062.2018.1483885.
[5] D.J. Wuebbles, A.K. Jain, Concerns about climate change and the role of fossil fuel use, Fuel Process. Technol. 71 (2001) 99–119, https://doi.org/10.1016/S0378-3820(01)00139-4.
[6] H. Ritchie, M. Roser, CO_2 and greenhouse gas emissions, Our World Data. (2017).
[7] B. Franta, Early oil industry knowledge of CO_2 and global warming, Nat. Clim. Chang 8 (2018) 1024–1025, https://doi.org/10.1038/s41558-018-0349-9.
[8] B.P. Statistical Review of World Energy 2020 | 69th edition, 2020.
[9] A.A. Vertes, N. Qureshi, H.P. Blaschek, H. Yukawa, Green energy to sustainability, Wiley Online Library, 2020.
[10] P. Balakrishnan, M.S. Shabbir, A.F. Siddiqi, X. Wang, Current status and future prospects of renewable energy: A case study, Energy Sources, Part A Recover. Util. Environ. Eff. 42 (2020) 2698–2703, https://doi.org/10.1080/15567036.2019.1618983.
[11] M.A. Bagherian, K. Mehranzamir, A comprehensive review on renewable energy integration for combined heat and power production, Energy Convers. Manag 224 (2020), 113454, https://doi.org/10.1016/j.enconman.2020.113454.
[12] L. Li, J. Lin, N. Wu, S. Xie, C. Meng, Y. Zheng, X. Wang, Y. Zhao, Review and outlook on the international renewable energy development, Energy Built Environ. 3 (2022) 139–157, https://doi.org/10.1016/j.enbenv.2020.12.002.
[13] J. Lindorfer, D.C. Rosenfeld, H. Böhm, 23 - Fuel Cells: Energy Conversion Technology, in: T.M.B.T.-F.E. (Third E. Letcher (Ed.), Elsevier, 2020: pp. 495–517. https://doi.org/10.1016/B978–0-08–102886-5.00023–2.
[14] A.G. Olabi, T. Wilberforce, M.A. Abdelkareem, Fuel cell application in the automotive industry and future perspective, Energy 214 (2021), 118955, https://doi.org/10.1016/j.energy.2020.118955.
[15] F. Zhao, Z. Mu, H. Hao, Z. Liu, X. He, S. Victor Przesmitzki, A. Ahmad Amer, Hydrogen Fuel Cell Vehicle Development in China: An Industry Chain Perspective, Energy Technol. 8 (2020) 2000179, https://doi.org/10.1002/ente.202000179.
[16] T. Wilberforce, A. Alaswad, A. Palumbo, M. Dassisti, A.G. Olabi, Advances in stationary and portable fuel cell applications, Int. J. Hydrog. Energy 41 (2016) 16509–16522, https://doi.org/10.1016/j.ijhydene.2016.02.057.
[17] S. Mekhilef, R. Saidur, A. Safari, Comparative study of different fuel cell technologies, Renew. Sustain. Energy Rev. 16 (2012) 981–989, https://doi.org/10.1016/j.rser.2011.09.020.
[18] Y. Manoharan, S.E. Hosseini, B. Butler, H. Alzhahrani, B.T. Senior, T. Ashuri, J. Krohn, Hydrogen fuel cell vehicles; current status and future prospect, Appl. Sci. 9 (2019), 2296, https://doi.org/10.3390/app9112296.
[19] A. Dicks, D.A.J. Rand, Fuel cell systems explained, Wiley Online Library, 2018.
[20] S.T. Revankar, P. Majumdar, Fuel cells: principles, design, and analysis, CRC Press, 2014.
[21] G. Merle, M. Wessling, K. Nijmeijer, Anion exchange membranes for alkaline fuel cells: a review, J. Memb. Sci. 377 (2011) 1–35, https://doi.org/10.1016/j.memsci.2011.04.043.

[22] J.R. Varcoe, R.C.T. Slade, Prospects for alkaline anion-exchange membranes in low temperature fuel cells, Fuel Cells 5 (2005) 187–200, https://doi.org/10.1002/fuce.200400045.
[23] S.H. Lee, J.C. Rasaiah, Proton transfer and the mobilities of the H+ and OH− ions from studies of a dissociating model for water, J. Chem. Phys. 135 (2011), 124505, https://doi.org/10.1063/1.3632990.
[24] S. Zhang, X.-Z. Yuan, J.N.C. Hin, H. Wang, K.A. Friedrich, M. Schulze, A review of platinum-based catalyst layer degradation in proton exchange membrane fuel cells, J. Power Sources 194 (2009) 588–600, https://doi.org/10.1016/j.jpowsour.2009.06.073.
[25] A.V. Virkar, Y. Zhou, Mechanism of catalyst degradation in proton exchange membrane fuel cells, J. Electrochem. Soc. 154 (2007) B540, https://doi.org/10.1149/1.2722563.
[26] M. Prokop, M. Drakselova, K. Bouzek, Review of the experimental study and prediction of Pt-based catalyst degradation during PEM fuel cell operation, Curr. Opin. Electrochem 20 (2020) 20–27, https://doi.org/10.1016/j.coelec.2020.01.016.
[27] P.G. Santori, A.N. Mondal, D.R. Dekel, F. Jaouen, The critical importance of ionomers on the electrochemical activity of platinum and platinum-free catalysts for anion-exchange membrane fuel cells, Sustain. Energy Fuels. 4 (2020) 3300–3307, https://doi.org/10.1039/d0se00483a.
[28] J.R. Varcoe, M. Beillard, D.M. Halepoto, J.P. Kizewski, S. Poynton, R.C.T. Slade, Membrane and electrode materials for alkaline membrane fuel cells, ECS Trans. 16 (2008) 1819–1834, https://doi.org/10.1149/1.2982023.
[29] S. Zhao, L. Yan, H. Luo, W. Mustain, H. Xu, Recent progress and perspectives of bifunctional oxygen reduction/evolution catalyst development for regenerative anion exchange membrane fuel cells, Nano Energy 47 (2018) 172–198, https://doi.org/10.1016/j.nanoen.2018.02.015.
[30] K. Kisand, A. Sarapuu, D. Danilian, A. Kikas, V. Kisand, M. Rähn, A. Treshchalov, M. Käärik, M. Merisalu, P. Paiste, J. Aruväli, J. Leis, V. Sammelselg, S. Holdcroft, K. Tammeveski, Transition metal-containing nitrogen-doped nanocarbon catalysts derived from 5-methylresorcinol for anion exchange membrane fuel cell application, J. Colloid Interface Sci. 584 (2021) 263–274, https://doi.org/10.1016/j.jcis.2020.09.114.
[31] D.R. Dekel, Review of cell performance in anion exchange membrane fuel cells, J. Power Sources 375 (2018) 158–169, https://doi.org/10.1016/j.jpowsour.2017.07.117.
[32] G. Bae, M.W. Chung, S.G. Ji, F. Jaouen, C.H. Choi, pH effect on the H2O2-induced deactivation of Fe-N-C catalysts, ACS Catal. 10 (2020) 8485–8495, https://doi.org/10.1021/acscatal.0c00948.
[33] N. Ramaswamy, S. Mukerjee, Fundamental mechanistic understanding of electrocatalysis of oxygen reduction on Pt and Non-Pt surfaces: acid versus alkaline media, Adv. Phys. Chem. 2012 (2012), 491604, https://doi.org/10.1155/2012/491604.
[34] H.A. Firouzjaie, W.E. Mustain, Catalytic advantages, challenges, and priorities in alkaline membrane fuel cells, ACS Catal. 10 (2020) 225–234, https://doi.org/10.1021/acscatal.9b03892.
[35] Y.S. Li, T.S. Zhao, Understanding the performance degradation of anion-exchange membrane direct ethanol fuel cells, Int. J. Hydrog. Energy 37 (2012) 4413–4421, https://doi.org/10.1016/j.ijhydene.2011.11.086.
[36] Y. Li, H. Wu, Y. He, Y. Liu, L. Jin, Performance of direct formate-peroxide fuel cells, J. Power Sources 287 (2015) 75–80, https://doi.org/10.1016/j.jpowsour.2015.04.014.
[37] Y.S. Li, T.S. Zhao, Z.X. Liang, Performance of alkaline electrolyte-membrane-based direct ethanol fuel cells, J. Power Sources 187 (2009) 387–392, https://doi.org/10.1016/j.jpowsour.2008.10.132.
[38] R. Gutru, Z. Turtayeva, F. Xu, G. Maranzana, B. Vigolo, A. Desforges, A comprehensive review on water management strategies and developments in anion exchange membrane fuel cells, Int. J. Hydrog. Energy 45 (2020) 19642–19663, https://doi.org/10.1016/j.ijhydene.2020.05.026.
[39] E.F. Holby, P. Zelenay, Linking structure to function: the search for active sites in non-platinum group metal oxygen reduction reaction catalysts, Nano Energy 29 (2016) 54–64, https://doi.org/10.1016/j.nanoen.2016.05.025.
[40] S. Kabir, K. Lemire, K. Artyushkova, A. Roy, M. Odgaard, D. Schlueter, A. Oshchepkov, A. Bonnefont, E. Savinova, D.C. Sabarirajan, P. Mandal, E. J. Crumlin, I.V. Zenyuk, P. Atanassov, A. Serov, Platinum group metal-free NiMo hydrogen oxidation catalysts: high performance and durability in alkaline exchange membrane fuel cells, J. Mater. Chem. A 5 (2017) 24433–24443, https://doi.org/10.1039/C7TA08718G.
[41] F.T. Wagner, B. Lakshmanan, M.F. Mathias, Electrochemistry and the future of the automobile, J. Phys. Chem. Lett. 1 (2010) 2204–2219, https://doi.org/10.1021/jz100553m.
[42] S. Hanif, N. Iqbal, X. Shi, T. Noor, G. Ali, A.M. Kannan, NiCo–N-doped carbon nanotubes based cathode catalyst for alkaline membrane fuel cell, Renew. Energy 154 (2020) 508–516, https://doi.org/10.1016/j.renene.2020.03.060.
[43] K. Khan, A.K. Tareen, M. Aslam, Q. Khan, R. Wang, S.A. Khan, A.S. Saleemi, Q. U. Khan, Y. Zhang, Z. Ouyang, Novel two dimensional carbon-chromium nitride based composite as an electrocatalyst for Oxygen Reduction Reaction, Front. Chem. 7 (2019) 738.
[44] X. Peng, T.J. Omasta, J.M. Roller, W.E. Mustain, Highly active and durable Pd-Cu catalysts for oxygen reduction in alkaline exchange membrane fuel cells, Front. Energy 11 (2017) 299–309.
[45] B.P. Setzler, Z. Zhuang, J.A. Wittkopf, Y. Yan, Activity targets for nanostructured platinum-group-metal-free catalysts in hydroxide exchange membrane fuel cells, Nat. Nanotechnol. 11 (2016) 1020–1025, https://doi.org/10.1038/nnano.2016.265.
[46] J. Lilloja, E. Kibena-Põldsepp, A. Sarapuu, M. Kodali, Y. Chen, T. Asset, M. Kaarik, M. Merisalu, P.P. Paiste, J. Aruväli, M. Kaärik, M. Merisalu, P.P. Paiste, J. Aruväli, A. Treshchalov, M. Rähn, J. Leis, V. Sammelselg, S. Holdcroft, P. Atanassov, K. Tammeveski, Cathode catalysts based on cobalt and nitrogen-doped nanocarbon composites for anion exchange membrane fuel cells, ACS Appl. Energy Mater. 3 (2020) 5375–5384, https://doi.org/10.1021/acsaem.0c00381.
[47] J. Zhang, W. Zhu, Y. Pei, Y. Liu, Y. Qin, X. Zhang, Q. Wang, Y. Yin, M.D. Guiver, Hierarchically porous Co− N− C cathode catalyst layers for anion exchange membrane fuel cells, ChemSusChem 12 (2019) 4165–4169.
[48] H. Wang, H.D. Abruña, Rh and Rh alloy nanoparticles as highly active H2 oxidation catalysts for alkaline fuel cells, ACS Catal. 9 (2019) 5057–5062, https://doi.org/10.1021/acscatal.9b00906.
[49] Y. Xue, L. Shi, X. Liu, J. Fang, X. Wang, B.P. Setzler, W. Zhu, Y. Yan, Z. Zhuang, A highly-active, stable and low-cost platinum-free anode catalyst based on RuNi for hydroxide exchange membrane fuel cells, Nat. Commun. 11 (2020) 5651, https://doi.org/10.1038/s41467-020-19413-5.
[50] R. Ren, X. Wang, H. Chen, H.A. Miller, I. Salam, J.R. Varcoe, L. Wu, Y. Chen, H.-G. Liao, E. Liu, F. Bartoli, F. Vizza, Q. Jia, Q. He, Reshaping the cathodic catalyst layer for anion exchange membrane fuel cells: from heterogeneous catalysis to homogeneous catalysis, Angew. Chem. Int. Ed. 60 (2021) 4049–4054, https://doi.org/10.1002/anie.202012547.
[51] W. You, K.J.T. Noonan, G.W. Coates, Alkaline-stable anion exchange membranes: a review of synthetic approaches, Prog. Polym. Sci. 100 (2020), 101177, https://doi.org/10.1016/j.progpolymsci.2019.101177.
[52] G. Huang, M. Mandal, X. Peng, A.C. Yang-Neyerlin, B.S. Pivovar, W.E. Mustain, P. A. Kohl, Composite poly(norbornene) anion conducting membranes for achieving durability, water management and high power (3.4 W/cm2) in hydrogen/oxygen alkaline fuel cells, J. Electrochem. Soc. 166 (2019) F637–F644, https://doi.org/10.1149/2.1301910jes.
[53] N. Chen, Y.M. Lee, Anion exchange polyelectrolytes for membranes and ionomers, Prog. Polym. Sci. 113 (2021), 101345, https://doi.org/10.1016/j.progpolymsci.2020.101345.
[54] M. Hren, M. Božič, D. Fakin, K.S. Kleinschek, S. Gorgieva, Alkaline membrane fuel cells: anion exchange membranes and fuels, Sustain. Energy Fuels 5 (2021) 604–637.
[55] X. Gao, H. Yu, J. Jia, J. Hao, F. Xie, J. Chi, B. Qin, L. Fu, W. Song, Z. Shao, High performance anion exchange ionomer for anion exchange membrane fuel cells, RSC Adv. 7 (2017) 19153–19161.
[56] N. Chen, C. Hu, H.H. Wang, S.P. Kim, H.M. Kim, W.H. Lee, J.Y. Bae, J.H. Park, Y. M. Lee, Poly(alkyl-terphenyl piperidinium) ionomers and membranes with an outstanding alkaline-membrane fuel-cell performance of 2.58W cm−2, Angew. Chem. Int. Ed. 60 (2021) 7710–7718, https://doi.org/10.1002/anie.202013395.
[57] D. Li, H.T. Chung, S. Maurya, I. Matanovic, Y.S. Kim, Impact of ionomer adsorption on alkaline hydrogen oxidation activity and fuel cell performance, Curr. Opin. Electrochem 12 (2018) 189–195, https://doi.org/10.1016/j.coelec.2018.11.012.
[58] Y.S. Ham, M.J. Kim, T. Lim, D.-K. Kim, S.-K. Kim, J.J. Kim, Direct formation of dendritic Ag catalyst on a gas diffusion layer for electrochemical CO_2 reduction to CO and H2, Int. J. Hydrog. Energy 43 (2018) 11315–11325, https://doi.org/10.1016/j.ijhydene.2017.12.067.
[59] K. Yang, R. Kas, W.A. Smith, T. Burdyny, Role of the carbon-based gas diffusion layer on flooding in a gas diffusion electrode cell for electrochemical CO_2 reduction, ACS Energy Lett. 6 (2021) 33–40, https://doi.org/10.1021/acsenergylett.0c02184.
[60] N. Pilinski, C. Käding, A. Dushina, T. Hickmann, A. Dyck, P. Wagner, Investigation of corrosion methods for bipolar plates for high temperature polymer electrolyte membrane fuel cell application, Energies 13 (2020), 235, https://doi.org/10.3390/en13010235.
[61] S. Witpathomwong, M. Okhawilai, C. Jubsilp, P. Karagiannidis, S. Rimdusit, Highly filled graphite/graphene/carbon nanotube in polybenzoxazine composites for bipolar plate in PEMFC, Int. J. Hydrog. Energy 45 (2020) 30898–30910, https://doi.org/10.1016/j.ijhydene.2020.08.006.
[62] S. Porstmann, T. Wannemacher, W.-G. Drossel, A comprehensive comparison of state-of-the-art manufacturing methods for fuel cell bipolar plates including anticipated future industry trends, J. Manuf. Process 60 (2020) 366–383, https://doi.org/10.1016/j.jmapro.2020.10.041.
[63] Y. Chang, Y. Qin, Y. Yin, J. Zhang, X. Li, Humidification strategy for polymer electrolyte membrane fuel cells – a review, Appl. Energy 230 (2018) 643–662, https://doi.org/10.1016/j.apenergy.2018.08.125.
[64] J.C. Douglin, J.R. Varcoe, D.R. Dekel, A high-temperature anion-exchange membrane fuel cell, J. Power Sources Adv. 5 (2020), 100023, https://doi.org/10.1016/j.powera.2020.100023.
[65] K. Yassin, K. Rasin, S. Brandon, D.R. Dekel, Quantifying the critical effect of water diffusivity in anion exchange membranes for fuel cell applications, J. Memb. Sci. 608 (2020), 118206, https://doi.org/10.1016/j.memsci.2020.118206.
[66] S. Huo, J. Zhou, T. Wang, R. Chen, K. Jiao, Experimental and analytical analysis of polarization and water transport behaviors of hydrogen alkaline membrane fuel cell, J. Power Sources 382 (2018) 1–12, https://doi.org/10.1016/j.jpowsour.2018.02.020.
[67] W.E. Mustain, M. Chatenet, M. Page, Y.S. Kim, Durability challenges of anion exchange membrane fuel cells, Energy Environ. Sci. 13 (2020) 2805–2838.
[68] D.R. Dekel, M. Amar, S. Willdorf, M. Kosa, S. Dhara, C.E. Diesendruck, Effect of water on the stability of quaternary ammonium groups for anion exchange membrane fuel cell applications, Chem. Mater. 29 (2017) 4425–4431, https://doi.org/10.1021/acs.chemmater.7b00958.

[69] H. Zhu, Z. Sun, M. Chen, H. Cao, K. Li, Y. Cai, F. Wang, Highly porous composite based on tungsten carbide and N-doped carbon aerogels for electrocatalyzing oxygen reduction reaction in acidic and alkaline media, Electrochim. Acta 236 (2017) 154–160, https://doi.org/10.1016/j.electacta.2017.02.156.

[70] H. Zhang, H. Osgood, X. Xie, Y. Shao, G. Wu, Engineering nanostructures of PGM-free oxygen-reduction catalysts using metal-organic frameworks, Nano Energy 31 (2017) 331–350, https://doi.org/10.1016/j.nanoen.2016.11.033.

[71] J. Wang, F. Chen, Y. Jin, Y. Lei, R.L. Johnston, One-pot synthesis of dealloyed auni nanodendrite as a bifunctional electrocatalyst for oxygen reduction and borohydride oxidation reaction, Adv. Funct. Mater. 27 (2017), https://doi.org/10.1002/adfm.201700260.

[72] L. Shang, H. Yu, X. Huang, T. Bian, R. Shi, Y. Zhao, G.I.N. Waterhouse, L.Z. Wu, C. H. Tung, T. Zhang, Well-dispersed ZIF-derived Co,N-Co-doped carbon nanoframes through mesoporous-silica-protected calcination as efficient oxygen reduction electrocatalysts, Adv. Mater. 28 (2016) 1668–1674, https://doi.org/10.1002/adma.201505045.

[73] J. Zhang, W. Zhu, T. Huang, C. Zheng, Y. Pei, G. Shen, Z. Nie, D. Xiao, Y. Yin, M. D. Guiver, Recent insights on catalyst layers for anion exchange membrane fuel cells, Adv. Sci. 8 (2021) 2100284, https://doi.org/10.1002/advs.202100284.

[74] Y. Wang, G. Wang, G. Li, B. Huang, J. Pan, Q. Liu, J. Han, L. Xiao, J. Lu, L. Zhuang, Pt-Ru catalyzed hydrogen oxidation in alkaline media: Oxophilic effect or electronic effect? Energy Environ. Sci. 8 (2015) 177–181, https://doi.org/10.1039/c4ee02564d.

[75] Q. Li, H. Peng, Y. Wang, L. Xiao, J. Lu, L. Zhuang, The comparability of Pt to Pt-Ru in catalyzing the hydrogen oxidation reaction for alkaline polymer electrolyte fuel cells operated at 80 °C, Angew. Chem. Int. Ed. 58 (2019) 1442–1446, https://doi.org/10.1002/anie.201812662.

[76] M. Mandal, G. Huang, N.U. Hassan, X. Peng, T. Gu, A.H. Brooks-Starks, B. Bahar, W.E. Mustain, P.A. Kohl, The importance of water transport in high conductivity and high-power alkaline fuel cells, J. Electrochem. Soc. 167 (2020), 054501, https://doi.org/10.1149/2.0022005jes.

[77] A. Sarapuu, E. Kibena-Põldsepp, M. Borghei, K. Tammeveski, Electrocatalysis of oxygen reduction on heteroatom-doped nanocarbons and transition metal-nitrogen-carbon catalysts for alkaline membrane fuel cells, J. Mater. Chem. A 6 (2018) 776–804, https://doi.org/10.1039/c7ta08690c.

[78] H. Erikson, A. Sarapuu, J. Solla-Gullón, K. Tammeveski, Recent progress in oxygen reduction electrocatalysis on Pd-based catalysts, J. Electroanal. Chem. 780 (2016) 327–336, https://doi.org/10.1016/j.jelechem.2016.09.034.

[79] Q. He, E.J. Cairns, Review—recent progress in electrocatalysts for oxygen reduction suitable for alkaline anion exchange membrane fuel cells, J. Electrochem. Soc. 162 (2015) F1504–F1539, https://doi.org/10.1149/2.0551514jes.

[80] D. Liu, L. Tao, D. Yan, Y. Zou, S. Wang, Recent advances on non-precious metal porous carbon-based electrocatalysts for oxygen reduction reaction, ChemElectroChem 5 (2018) 1775–1785, https://doi.org/10.1002/celc.201800086.

[81] J. Wu, H. Yang, Platinum-based oxygen reduction electrocatalysts, Acc. Chem. Res. 46 (2013) 1848–1857, https://doi.org/10.1021/ar300359w.

[82] A. Arunchander, M. Vivekanantha, S.G. Peera, A.K. Sahu, MnO-nitrogen doped graphene as a durable non-precious hybrid catalyst for the oxygen reduction reaction in anion exchange membrane fuel cells †, RSC Adv. 16 (2016) 95592–95600, https://doi.org/10.1039/c6ra20627a.

[83] K.-C. Wang, H.-C. Huang, S.-T. Chang, C.-H. Wu, I. Yamanaka, J.-F. Lee, C.-H. Wang, Hybrid porous catalysts derived from metal–organic framework for oxygen reduction reaction in an anion exchange membrane fuel cell, ACS Sustain. Chem. Eng. 7 (2019) 9143–9152.

[84] M.J. Kim, S. Kim, J.E. Park, C.C. Hwang, S. Lee, S.Y. Kang, D. Jung, Y.H. Cho, J. Kim, K.S. Lee, Y.E. Sung, Controlling active sites of Fe–N–C electrocatalysts for oxygen electrocatalysis, Nano Energy 78 (2020), 105395, https://doi.org/10.1016/j.nanoen.2020.105395.

[85] S. Hanif, N. Iqbal, X. Shi, T. Noor, G. Ali, A.M. Kannan, NiCo-N-doped carbon nanotubes based cathode catalyst for alkaline membrane fuel cell, Renew, Energy 154 (2020) 508–516.

[86] M.M. Hossen, K. Artyushkova, P. Atanassov, A. Serov, Synthesis and characterization of high performing Fe-N-C catalyst for oxygen reduction reaction (ORR) in Alkaline Exchange Membrane Fuel Cells, J. Power Sources 375 (2018) 214–221, https://doi.org/10.1016/j.jpowsour.2017.08.036.

[87] Y. Mun, M.J. Kim, S.A. Park, E. Lee, Y. Ye, S. Lee, Y.T. Kim, S. Kim, O.H. Kim, Y. H. Cho, Y.E. Sung, J. Lee, Soft-template synthesis of mesoporous non-precious metal catalyst with Fe-Nx/C active sites for oxygen reduction reaction in fuel cells, Appl. Catal. B Environ. 222 (2018) 191–199, https://doi.org/10.1016/j.apcatb.2017.10.015.

[88] S. Sarkar, S. Patel, S. Sampath, Efficient oxygen reduction activity on layered palladium phosphosulphide and its application in alkaline fuel cells, J. Power Sources 445 (2020), 227280.

[89] S. Ratso, A. Zitolo, M. Käärik, M. Merisalu, A. Kikas, V. Kisand, M. Rähn, P. Paiste, J. Leis, V. Sammelselg, S. Holdcroft, F. Jaouen, K. Tammeveski, Non-precious metal cathodes for anion exchange membrane fuel cells from ball-milled iron and nitrogen doped carbide-derived carbons, Renew. Energy 167 (2021) 800–810, https://doi.org/10.1016/j.renene.2020.11.154.

[90] U.S. DOE, DOE Technical Targets for Polymer Electrolyte Membrane Fuel Cell Components, (2020). https://www.energy.gov/eere/fuelcells/doe-technical-targets-polymer-electrolyte-membrane-fuel-cell-components.

[91] H. Yanagi, K. Fukuta, Anion exchange membrane and ionomer for alkaline membrane fuel cells (AMFCs, ECS Trans. 16 (2008) 257–262, https://doi.org/10.1149/1.2981860.

[92] S. Suzuki, H. Muroyama, T. Matsui, K. Eguchi, Influence of CO_2 dissolution into anion exchange membrane on fuel cell performance, Electrochim. Acta 88 (2013) 552–558, https://doi.org/10.1016/j.electacta.2012.10.105.

[93] N. Ziv, A.N. Mondal, T. Weissbach, S. Holdcroft, D.R. Dekel, Effect of CO_2 on the properties of anion exchange membranes for fuel cell applications, J. Memb. Sci. 586 (2019) 140–150, https://doi.org/10.1016/j.memsci.2019.05.053.

[94] B.A. Pinaud, A. Bonakdarpour, L. Daniel, J. Sharman, D.P. Wilkinson, Key considerations for high current fuel cell catalyst testing in an electrochemical half-cell, J. Electrochem. Soc. 164 (2017) F321–F327, https://doi.org/10.1149/2.0891704jes.

[95] H.A. Gasteiger, S.S. Kocha, B. Sompalli, F.T. Wagner, Activity benchmarks and requirements for Pt, Pt-alloy, and non-Pt oxygen reduction catalysts for PEMFCs, Appl. Catal. B Environ. 56 (2005) 9–35, https://doi.org/10.1016/j.apcatb.2004.06.021.

[96] Y. Garsany, O.A. Baturina, K.E. Swider-Lyons, S.S. Kocha, Experimental methods for quantifying the activity of platinum electrocatalysts for the oxygen reduction reaction, Anal. Chem. 82 (2010) 6321–6328, https://doi.org/10.1021/ac100306c.

[97] K. Shinozaki, J.W. Zack, R.M. Richards, B.S. Pivovar, S.S. Kocha, Oxygen reduction reaction measurements on platinum electrocatalysts utilizing rotating disk electrode technique, J. Electrochem. Soc. 162 (2015) F1144–F1158, https://doi.org/10.1149/2.1071509jes.

[98] C.M. Zalitis, D. Kramer, A.R. Kucernak, Electrocatalytic performance of fuel cell reactions at low catalyst loading and high mass transport, Phys. Chem. Chem. Phys. 15 (2013) 4329–4340, https://doi.org/10.1039/C3CP44431G.

[99] E. Antolini, L. Giorgi, A. Pozio, E. Passalacqua, Influence of Nafion loading in the catalyst layer of gas-diffusion electrodes for PEFC, J. Power Sources 77 (1999) 136–142, https://doi.org/10.1016/S0378-7753(98)00186-4.

[100] Y.-X. Chen, M.-F. Li, L.-W. Liao, J. Xu, S. Ye, A thermostatic cell with gas diffusion electrode for oxygen reduction reaction under fuel cell relevant conditions, Electrochem. Commun. 11 (2009) 1434–1436, https://doi.org/10.1016/j.elecom.2009.05.023.

[101] L.G. Austin, S. Almaula, An experimental study of the mode of operation of porous gas-diffusion electrodes with hydrogen fuel, J. Electrochem. Soc. 114 (1967) 927, https://doi.org/10.1149/1.2426780.

[102] J. Giner, J.M. Parry, S. Smith, M. Turchan, Methods for characterizing the structure and electrochemical behavior of teflon-bonded Pt electrodes, J. Electrochem. Soc. 116 (1969) 1692, https://doi.org/10.1149/1.2411664.

[103] K. Ehelebe, D. Seeberger, M.T.Y. Paul, S. Thiele, K.J.J. Mayrhofer, S. Cherevko, Evaluating electrocatalysts at relevant currents in a half-cell: the impact of Pt loading on oxygen reduction reaction, J. Electrochem. Soc. 166 (2019) F1259–F1268, https://doi.org/10.1149/2.0911915jes.

[104] A.J. Bard, L.R. Faulkner, ELECTROCHEMICAL METHODS: Fundamentals and applications, 2nd ed, Wiley, New York (2001) pp. 580–632.

[105] H. Grimler, A. Carlson, H. Ekström, C. Lagergren, R.W. Lindström, G. Lindbergh, Determination of kinetic parameters for the oxygen reduction reaction on platinum in an AEMFC, J. Electrochem. Soc. 168 (2021), 124501, https://doi.org/10.1149/1945-7111/ac38f8.

[106] M. Moore, A. Putz, M. Secanell, Investigation of the ORR using the double-trap intrinsic kinetic model, J. Electrochem. Soc. 160 (2013) F670–F681, https://doi.org/10.1149/2.123306jes.

[107] A. Muthukrishnan, Y. Nabae, Estimation of the inherent kinetic parameters for oxygen reduction over a Pt-Free cathode catalyst by resolving the quasi-four-electron reduction, J. Phys. Chem. C. 120 (2016) 22515–22525, https://doi.org/10.1021/acs.jpcc.6b07905.

[108] S. Martens, L. Asen, G. Ercolano, F. Dionigi, C. Zalitis, A. Hawkins, A. Martinez Bonastre, L. Seidl, A.C. Knoll, J. Sharman, P. Strasser, D. Jones, O. Schneider, A comparison of rotating disc electrode, floating electrode technique and membrane electrode assembly measurements for catalyst testing, J. Power Sources 392 (2018) 274–284, https://doi.org/10.1016/j.jpowsour.2018.04.084.

[109] D. Yang, H. Yu, G. Li, Y. Zhao, Y. Liu, C. Zhang, W. Song, Z. Shao, Fine microstructure of high performance electrode in alkaline anion exchange membrane fuel cells, J. Power Sources 267 (2014) 39–47, https://doi.org/10.1016/j.jpowsour.2014.04.053.

[110] B. Britton, S. Holdcroft, The control and effect of pore size distribution in AEMFC catalyst layers, J. Electrochem. Soc. 163 (2016) F353–F358, https://doi.org/10.1149/2.0421605jes.

[111] M.-S. Shin, Y.-J. Byun, Y.-W. Choi, M.-S. Kang, J.-S. Park, On-site crosslinked quaternized poly(vinyl alcohol) as ionomer binder for solid alkaline fuel cells, Int. J. Hydrog. Energy 39 (2014) 16556–16561, https://doi.org/10.1016/j.ijhydene.2014.03.181.

[112] W.E. Mustain, Understanding how high-performance anion exchange membrane fuel cells were achieved: Component, interfacial, and cell-level factors, Curr. Opin. Electrochem 12 (2018) 233–239, https://doi.org/10.1016/j.coelec.2018.11.010.

[113] R.L. McCreery, Advanced carbon electrode materials for molecular electrochemistry, Chem. Rev. 108 (2008) 2646–2687, https://doi.org/10.1021/cr068076m.

[114] H. Jahnke, M. Schönborn, G. Zimmermann, Organic dyestuffs as catalysts for fuel cells BT - Physical and Chemical Applications of Dyestuffs, in: F.P. Schäfer, H. Gerischer, F. Willig, H. Meier, H. Jahnke, M. Schönborn, G. Zimmermann (Eds.), Springer Berlin Heidelberg, Berlin, Heidelberg, 1976: pp. 133–181.

[115] N. Alexeyeva, E. Shulga, V. Kisand, I. Kink, K. Tammeveski, Electroreduction of oxygen on nitrogen-doped carbon nanotube modified glassy carbon electrodes in acid and alkaline solutions, J. Electroanal. Chem. 648 (2010) 169–175, https://doi.org/10.1016/j.jelechem.2010.07.014.

[116] J. Lilloja, E. Kibena-Põldsepp, M. Merisalu, P. Rauwel, L. Matisen, A. Niilisk, E.S. F. Cardoso, G. Maia, V. Sammelselg, K. Tammeveski, An oxygen reduction study of graphene-based nanomaterials of different origin, Catalysis 6 (2016), 108, https://doi.org/10.3390/catal6070108.
[117] E. Kibena, M. Mooste, J. Kozlova, M. Marandi, V. Sammelselg, K. Tammeveski, Surface and electrochemical characterisation of CVD grown graphene sheets, Electrochem. Commun. 35 (2013) 26–29, https://doi.org/10.1016/j.elecom.2013.07.034.
[118] H. Wang, H. Dai, Strongly coupled inorganic–nano-carbon hybrid materials for energy storage, Chem. Soc. Rev. 42 (2013) 3088–3113, https://doi.org/10.1039/C2CS35307E.
[119] Y. Liang, Y. Li, H. Wang, J. Zhou, J. Wang, T. Regier, H. Dai, Co3O4 nanocrystals on graphene as a synergistic catalyst for oxygen reduction reaction, Nat. Mater. 10 (2011) 780–786, https://doi.org/10.1038/nmat3087.
[120] Y. Liang, H. Wang, J. Zhou, Y. Li, J. Wang, T. Regier, H. Dai, Covalent hybrid of spinel manganese–cobalt oxide and graphene as advanced oxygen reduction electrocatalysts, J. Am. Chem. Soc. 134 (2012) 3517–3523, https://doi.org/10.1021/ja210924t.
[121] K. Gong, F. Du, Z. Xia, M. Durstock, L. Dai, Nitrogen-doped carbon nanotube arrays with high electrocatalytic activity for oxygen reduction, Science 323 (2009) 760–764, https://doi.org/10.1126/science.1168049.
[122] S. Zhang, H. Liu, N. Zhang, R. Xia, S. Kuang, G. Yin, X. Ma, Tuning the electronic structure of platinum nanocrystals towards high efficient ethanol oxidation, Chin. J. Catal. 40 (2019) 1904–1911, https://doi.org/10.1016/S1872-2067(19)63442-X.
[123] L. Qu, Y. Liu, J.-B. Baek, L. Dai, Nitrogen-doped graphene as efficient metal-free electrocatalyst for oxygen reduction in fuel cells, ACS Nano 4 (2010) 1321–1326, https://doi.org/10.1021/nn901850u.
[124] R. Sibul, E. Kibena-Põldsepp, S. Ratso, M. Kook, M.T. Sougrati, M. Käärik, M. Merisalu, J. Aruväli, P. Paiste, A. Treshchalov, J. Leis, V. Kisand, V. Sammelselg, S. Holdcroft, F. Jaouen, K. Tammeveski, Iron-and nitrogen-doped graphene-based catalysts for fuel cell application, ChemElectroChem 7 (2020) 1739–1747.
[125] C.H. Choi, H.-K. Lim, M.W. Chung, G. Chon, N. Ranjbar Sahraie, A. Altin, M.-T. Sougrati, L. Stievano, H.S. Oh, E.S. Park, F. Luo, P. Strasser, G. Dražić, K.J. J. Mayrhofer, H. Kim, F. Jaouen, The Achilles' heel of iron-based catalysts during oxygen reduction in an acidic medium, Energy Environ. Sci. 11 (2018) 3176–3182, https://doi.org/10.1039/C8EE01855C.
[126] J. Tong, W. Ma, L. Bo, T. Li, W. Li, Y. Li, Q. Zhang, Nitrogen-doped hollow carbon spheres as highly effective multifunctional electrocatalysts for fuel cells, Zn–air batteries, and water-splitting electrolyzers, J. Power Sources 441 (2019), 227166.
[127] Q. Li, R. Cao, J. Cho, G. Wu, Nanocarbon electrocatalysts for oxygen reduction in alkaline media for advanced energy conversion and storage, Adv. Energy Mater. 4 (2014) 1301415, https://doi.org/10.1002/aenm.201301415.
[128] U. Martinez, S. Komini Babu, E.F. Holby, H.T. Chung, X. Yin, P. Zelenay, Progress in the development of Fe-based PGM-free electrocatalysts for the oxygen reduction reaction, Adv. Mater. 31 (2019) 1806545, https://doi.org/10.1002/adma.201806545.
[129] H.M. Barkholtz, D.-J. Liu, Advancements in rationally designed PGM-free fuel cell catalysts derived from metal–organic frameworks, Mater. Horiz. 4 (2017) 20–37, https://doi.org/10.1039/C6MH00344C.
[130] E. Proietti, F. Jaouen, M. Lefèvre, N. Larouche, J. Tian, J. Herranz, J.P. Dodelet, Iron-based cathode catalyst with enhanced power density in polymer electrolyte membrane fuel cells, Nat. Commun. 2 (2011), 416, https://doi.org/10.1038/ncomms1427.
[131] V. Bambagioni, C. Bianchini, J. Filippi, A. Lavacchi, W. Oberhauser, A. Marchionni, S. Moneti, F. Vizza, R. Psaro, V. Dal Santo, A. Gallo, S. Recchia, L. Sordelli, Single-site and nanosized Fe–Co electrocatalysts for oxygen reduction: Synthesis, characterization and catalytic performance, J. Power Sources 196 (2011) 2519–2529, https://doi.org/10.1016/j.jpowsour.2010.11.030.
[132] M. Ferrandon, A.J. Kropf, D.J. Myers, K. Artyushkova, U. Kramm, P. Bogdanoff, G. Wu, C.M. Johnston, P. Zelenay, Multitechnique characterization of a polyaniline–iron–carbon oxygen reduction catalyst, J. Phys. Chem. C 116 (2012) 16001–16013, https://doi.org/10.1021/jp302396g.
[133] J. Sanetuntikul, S. Shanmugam, High pressure pyrolyzed non-precious metal oxygen reduction catalysts for alkaline polymer electrolyte membrane fuel cells, Nanoscale 7 (2015) 7644–7650.
[134] P. Bogdanoff, I. Herrmann, M. Hilgendorff, I. Dorbandt, S. Fiechter, H. Tributsch, Probing structural effects of pyrolysed CoTMPP-based electrocatalysts for oxygen reduction via new preparation strategies, J. New Mater. Electrochem. Syst. 7 (2004) 85–92.
[135] R.W. Joyner, J.A.R. van Veen, W.M.H. Sachtler, Extended X-ray absorption fine structure (EXAFS) study of cobalt–porphyrin catalysts supported on active carbon, J. Chem. Soc. Faraday Trans. 1 Phys. Chem. Condens. Phases 78 (1982) 1021–1028, https://doi.org/10.1039/F19827801021.
[136] B. van Wingerden, J.A.R. van Veen, C.T.J. Mensch, An extended X-ray absorption fine structure study of heat-treated cobalt porphyrin catalysts supported on active carbon, J. Chem. Soc. Faraday Trans. 1 Phys. Chem. Condens. Phases 84 (1988) 65–74, https://doi.org/10.1039/F19888400065.
[137] G. Faubert, G. Lalande, R. Côté, D. Guay, J.P. Dodelet, L.T. Weng, P. Bertrand, G. Dénès, Heat-treated iron and cobalt tetraphenylporphyrins adsorbed on carbon black: Physical characterization and catalytic properties of these materials for the reduction of oxygen in polymer electrolyte fuel cells, Electrochim. Acta 41 (1996) 1689–1701, https://doi.org/10.1016/0013-4686(95)00423-8.
[138] J.-P. Dodelet, Oxygen reduction in PEM fuel cell conditions: heat-treated non-precious metal-N 4 macrocycles and beyond, in: N4-Macrocyclic Met. Complexes, Springer, 2006, pp. 83–147.
[139] H. Adabi, A. Shakouri, N. Ul Hassan, J.R. Varcoe, B. Zulevi, A. Serov, J. R. Regalbuto, W.E. Mustain, High-performing commercial Fe–N–C cathode electrocatalyst for anion-exchange membrane fuel cells, Nat. Energy 6 (2021) 834–843, https://doi.org/10.1038/s41560-021-00878-7.
[140] A. Serov, M.H. Robson, K. Artyushkova, P. Atanassov, Templated non-PGM cathode catalysts derived from iron and poly(ethyleneimine) precursors, Appl. Catal. B Environ. 127 (2012) 300–306, https://doi.org/10.1016/j.apcatb.2012.08.040.
[141] M.H. Robson, A. Serov, K. Artyushkova, P. Atanassov, A mechanistic study of 4-aminoantipyrine and iron derived non-platinum group metal catalyst on the oxygen reduction reaction, Electrochim. Acta 90 (2013) 656–665, https://doi.org/10.1016/j.electacta.2012.11.025.
[142] H. Adabi, P.G. Santori, A. Shakouri, X. Peng, K. Yassin, I.G. Rasin, S. Brandon, D. R. Dekel, N.U. Hassan, M.-T. Sougrati, A. Zitolo, J.R. Varcoe, J.R. Regalbuto, F. Jaouen, W.E. Mustain, Understanding how single-atom site density drives the performance and durability of PGM-free Fe–N–C cathodes in anion exchange membrane fuel cells, Mater. Today Adv. 12 (2021), 100179, https://doi.org/10.1016/j.mtadv.2021.100179.
[143] X. Peng, V. Kashyap, B. Ng, S. Kurungot, L. Wang, J.R. Varcoe, W.E. Mustain, High-performing pgm-free aemfc cathodes from carbon-supported cobalt ferrite nanoparticles, Catalysts 9 (2019), 264, https://doi.org/10.3390/catal9030264.
[144] N. Ramaswamy, U. Tylus, Q. Jia, S. Mukerjee, Activity descriptor identification for oxygen reduction on nonprecious electrocatalysts: linking surface science to coordination chemistry, J. Am. Chem. Soc. 135 (2013) 15443–15449, https://doi.org/10.1021/ja405149m.
[145] F. Jaouen, F. Charreteur, J.P. Dodelet, Fe-based catalysts for oxygen reduction in PEMFCs, J. Electrochem. Soc. 153 (2006) A689, https://doi.org/10.1149/1.2168418.
[146] Q. He, L. Zeng, J. Wang, J. Jiang, L. Zhang, J. Wang, W. Ding, Z. Wei, Polymer-coating-induced synthesis of FeNx enriched carbon nanotubes as cathode that exceeds 1.0 W cm−2 peak power in both proton and anion exchange membrane fuel cells, J. Power Sources 489 (2021), 229499, https://doi.org/10.1016/j.jpowsour.2021.229499.
[147] S. Park, M. Her, H. Shin, W. Hwang, Y.-E. Sung, Maximizing the active site densities of single-atomic Fe–N–C electrocatalysts for high-performance anion membrane fuel cells, ACS Appl. Energy Mater. 4 (2021) 1459–1466, https://doi.org/10.1021/acsaem.0c02650.
[148] H. Zhang, H.T. Chung, D.A. Cullen, S. Wagner, U.I. Kramm, K.L. More, P. Zelenay, G. Wu, High-performance fuel cell cathodes exclusively containing atomically dispersed iron active sites, Energy Environ. Sci. 12 (2019) 2548–2558, https://doi.org/10.1039/C9EE00877B.
[149] K. Strickland, E. Miner, Q. Jia, U. Tylus, N. Ramaswamy, W. Liang, M.T. Sougrati, F. Jaouen, S. Mukerjee, Highly active oxygen reduction non-platinum group metal electrocatalyst without direct metal-nitrogen coordination, Nat. Commun. 6 (2015), 7343, https://doi.org/10.1038/ncomms8343.
[150] X. Ma, X. Zhao, J. Huang, L. Sun, Q. Li, X. Yang, Fine Co nanoparticles encapsulated in a N-doped porous carbon matrix with superficial N-doped porous carbon nanofibers for efficient oxygen reduction, ACS Appl. Mater. Interfaces 9 (2017) 21747–21755, https://doi.org/10.1021/acsami.7b02490.
[151] J. Lilloja, E. Kibena-Põldsepp, A. Sarapuu, J.C. Douglin, M. Käärik, J. Kozlova, P. Paiste, A. Kikas, J. Aruväli, J. Leis, V. Sammelselg, D.R. Dekel, K. Tammeveski, Transition-metal- and nitrogen-doped carbide-derived carbon/carbon nanotube composites as cathode catalysts for anion-exchange membrane fuel cells, ACS Catal. 11 (2021) 1920–1931, https://doi.org/10.1021/acscatal.0c03511.
[152] Y. Lu, L. Wang, K. Preuß, M. Qiao, M.-M. Titirici, J. Varcoe, Q. Cai, Halloysite-derived nitrogen doped carbon electrocatalysts for anion exchange membrane fuel cells, J. Power Sources 372 (2017) 82–90.
[153] S. Ratso, I. Kruusenberg, M. Käärik, M. Kook, R. Saar, M. Pärs, J. Leis, K. Tammeveski, Highly efficient nitrogen-doped carbide-derived carbon materials for oxygen reduction reaction in alkaline media, Carbon 113 (2017) 159–169, https://doi.org/10.1016/j.carbon.2016.11.037.
[154] J.C. Douglin, R.K. Singh, S. Haj-Bsoul, S. Li, J. Biemolt, N. Yan, J.R. Varcoe, G. Rothenberg, D.R. Dekel, A high-temperature anion-exchange membrane fuel cell with a critical raw material-free cathode, Chem. Eng. J. Adv. 8 (2021), 100153, https://doi.org/10.1016/j.ceja.2021.100153.
[155] J. Woo, S.Y. Yang, Y.J. Sa, W.-Y. Choi, M.-H. Lee, H.-W. Lee, T.J. Shin, T.-Y. Kim, S.H. Joo, Promoting oxygen reduction reaction activity of Fe–N/C electrocatalysts by silica-coating-mediated synthesis for anion-exchange membrane fuel cells, Chem. Mater. 30 (2018) 6684–6701.
[156] V.M. Truong, M.K. Yang, H. Yang, Functionalized carbon black supported silver (Ag/C) catalysts in cathode electrode for alkaline anion exchange membrane fuel cells, Int. J. Precis. Eng. Manuf. Green. Technol. 6 (2019) 711–721, https://doi.org/10.1007/s40684-019-00123-3.
[157] C. Van Pham, B. Britton, T. Böhm, S. Holdcroft, S. Thiele, Doped, defect-enriched carbon nanotubes as an efficient oxygen reduction catalyst for anion exchange membrane fuel cells, Adv. Mater. Interfaces 5 (2018) 1800184.
[158] X. Huang, X. Zhang, W. Hu, S. Lv, Y. Huang, Altering the MOF-74 derivatives for efficient oxygen electrocatalysis through synergistic multi-metals and nitrogen modification, J. Mater. Sci. 55 (2020) 10733–10784.
[159] S. Ma, G.A. Goenaga, A.V. Call, D.-J. Liu, Cobalt imidazolate framework as precursor for oxygen reduction reaction electrocatalysts, Chem. – A Eur. J. 17 (2011) 2063–2067, https://doi.org/10.1002/chem.201003080.

[160] T. Palaniselvam, B.P. Biswal, R. Banerjee, S. Kurungot, Zeolitic imidazolate framework (ZIF)-derived, hollow-core, nitrogen-doped carbon nanostructures for oxygen-reduction reactions in PEFCs, Chem. – A Eur. J. 19 (2013) 9335–9342, https://doi.org/10.1002/chem.201300145.
[161] X. Wang, J. Zhou, H. Fu, W. Li, X. Fan, G. Xin, J. Zheng, X. Li, MOF derived catalysts for electrochemical oxygen reduction, J. Mater. Chem. A. 2 (2014) 14064–14070, https://doi.org/10.1039/C4TA01506A.
[162] X. Peng, T.J.T.J. Omasta, E. Magliocca, L. Wang, J.R. Varcoe, W.E. Mustain, Nitrogen-doped carbon–CoOx nanohybrids: a precious metal free cathode that exceeds 1.0 W cm−2 peak power and 100h life in anion-exchange membrane, Fuel Cells, Angew. Chem. 58 (2019) 1046–1051, https://doi.org/10.1002/ange.201811099.
[163] M. Mooste, E. Kibena-Põldsepp, V. Vassiljeva, A. Kikas, M. Käärik, J. Kozlova, V. Kisand, M. Külaviir, S. Cavaliere, J. Leis, A. Krumme, V. Sammelselg, S. Holdcroft, K. Tammeveski, Electrospun polyacrylonitrile-derived Co or Fe containing nanofibre catalysts for oxygen reduction reaction at the alkaline membrane fuel cell cathode, ChemCatChem 12 (2020) 4568–4581.
[164] M. Sharma, J.J.-H. Jang, D.Y. Shin, J.A. Kwon, D.-H. Lim, D. Choi, H. Sung, J.J.-H. Jang, S.-Y. Lee, K.Y. Lee, Work function-tailored graphene via transition metal encapsulation as a highly active and durable catalyst for the oxygen reduction reaction, Energy Environ. Sci. 12 (2019) 2200–2211.
[165] P.G. Santori, F.D. Speck, S. Cherevko, H.A. Firouzjaie, X. Peng, W.E. Mustain, F. Jaouen, High performance FeNC and Mn-oxide/FeNC Layers for AEMFC cathodes, J. Electrochem. Soc. 167 (2020), 134505, https://doi.org/10.1149/1945-7111/abb7e0.
[166] P. Faubert, I. Kondov, D. Qazzazie, O. Yurchenko, C. Müller, A non-noble Cr-Ni-based catalyst for the oxygen reduction reaction in alkaline polymer electrolyte fuel cells, MRS Commun. 8 (2018) 160.
[167] G.A. Goenaga, A.L. Roy, N.M. Cantillo, S. Foister, T.A. Zawodzinski Jr, A family of platinum group metal-free catalysts for oxygen reduction in alkaline media, J. Power Sources 395 (2018) 148–157.
[168] M.J. Dzara, J.M. Christ, P. Joghee, C. Ngo, C.A. Cadigan, G. Bender, R. M. Richards, R. O'Hayre, S. Pylypenko, La and Al co-doped CaMnO3 perovskite oxides: From interplay of surface properties to anion exchange membrane fuel cell performance, J. Power Sources 375 (2018) 265–276.
[169] P. Moni, M.G. Pollachini, M. Wilhelm, J. Lorenz, C. Harms, M.M. Murshed, K. Rezwan, Metal-containing ceramic composite with in situ grown carbon nanotube as a cathode catalyst for anion exchange membrane fuel cell and rechargeable zinc-air battery, ACS Appl. Energy Mater. 2 (2019) 6078–6086, https://doi.org/10.1021/acsaem.9b01276.
[170] X. Yang, W. Zou, Y. Su, Y. Zhu, H. Jiang, J. Shen, C. Li, Activated nitrogen-doped carbon nanofibers with hierarchical pore as efficient oxygen reduction reaction catalyst for microbial fuel cells, J. Power Sources 266 (2014) 36–42.
[171] M. Wang, H. Zhang, G. Thirunavukkarasu, I. Salam, J.R. Varcoe, P. Mardle, X. Li, S. Mu, S. Du, Ionic liquid-modified microporous ZnCoNC-based electrocatalysts for polymer electrolyte fuel cells, ACS Energy Lett. 4 (2019) 2104–2110.
[172] Z. Chang, F. Meng, H. Zhong, X. Zhang, Anchoring Iron-EDTA complex on graphene toward the synthesis of highly efficient Fe-N-C oxygen reduction electrocatalyst for fuel cells, Chin. J. Chem. 36 (2018) 287–292.
[173] Y.-M. Zhao, P.-C. Zhang, C. Xu, X.-Y. Zhou, L.-M. Liao, P.-J. Wei, E. Liu, H. Chen, Q. He, J.-G. Liu, Design and preparation of Fe–N5 catalytic sites in single-atom catalysts for enhancing the oxygen reduction reaction in fuel cells, ACS Appl. Mater. Interfaces 12 (2020) 17334–17342.
[174] Y. Yang, H. Peng, Y. Xiong, Q. Li, J. Lu, L. Xiao, F.J. DiSalvo, L. Zhuang, H. D. Abruña, High-loading composition-tolerant Co–Mn spinel oxides with performance beyond 1 W/cm2 in alkaline polymer electrolyte fuel cells, ACS Energy Lett. 4 (2019) 1251–1257.
[175] R. Praats, M. Käärik, A. Kikas, V. Kisand, J. Aruväli, P. Paiste, M. Merisalu, A. Sarapuu, J. Leis, V. Sammelselg, J.C. Douglin, D.R. Dekel, K. Tammeveski, Electroreduction of oxygen on cobalt phthalocyanine-modified carbide-derived carbon/carbon nanotube composite catalysts, J. Solid State Electrochem 25 (2021) 57–71.
[176] R. Praats, M. Käärik, A. Kikas, V. Kisand, J. Aruväli, P. Paiste, M. Merisalu, J. Leis, V. Sammelselg, J.H. Zagal, S. Holdcroft, N. Nakashima, K. Tammeveski, Electrocatalytic oxygen reduction reaction on iron phthalocyanine-modified carbide-derived carbon/carbon nanotube composite electrocatalysts, Electrochim. Acta 334 (2020), 135575.
[177] Y. Wang, Y. Yang, S. Jia, X. Wang, K. Lyu, Y. Peng, H. Zheng, X. Wei, H. Ren, L. Xiao, J. Wang, D.A. Muller, H.D. Abruña, B.J. Hwang, J. Lu, L. Zhuang, Synergistic Mn-Co catalyst outperforms Pt on high-rate oxygen reduction for alkaline polymer electrolyte fuel cells, Nat. Commun. 10 (2019) 1506, https://doi.org/10.1038/s41467-019-09503-4.
[178] S.N. Bhange, R. Soni, G. Singla, T.G. Ajithkumar, S. Kurungot, FeN x/FeS x-anchored carbon sheet–carbon nanotube composite electrocatalysts for oxygen reduction, ACS Appl. Nano Mater. 3 (2020) 2234–2245.
[179] S.N. Bhange, S.M. Unni, S. Kurungot, Graphene with Fe and S coordinated active centers: an active competitor for the Fe–N–C active center for oxygen reduction reaction in acidic and basic pH conditions, ACS Appl. Energy Mater. 1 (2018) 368–376.
[180] H.-C. Huang, C.-Y. Su, K.-C. Wang, H.-Y. Chen, Y.-C. Chang, Y.-L. Chen, K.C.-W. Wu, C.-H. Wang, Nanostructured cementite/ferrous sulfide encapsulated carbon with heteroatoms for oxygen reduction in alkaline environment, ACS Sustain. Chem. Eng. 7 (2019) 3185–3194.
[181] Z. Li, B. Li, Z. Liu, Z. Liu, D. Li, A tungsten carbide/iron sulfide/FePt nanocomposite supported on nitrogen-doped carbon as an efficient electrocatalyst for oxygen reduction reaction, RSC Adv. 5 (2015) 106245–106251.
[182] Y. Xu, W. Li, F. Zhang, X. Zhang, W. Zhang, C.-S. Lee, Y. Tang, In situ incorporation of FeS nanoparticles/carbon nanosheets composite with an interconnected porous structure as a high-performance anode for lithium ion batteries, J. Mater. Chem. A 4 (2016) 3697–3703.
[183] C. Xing, D. Zhang, K. Cao, S. Zhao, X. Wang, H. Qin, J. Liu, Y. Jiang, L. Meng, In situ growth of FeS microsheet networks with enhanced electrochemical performance for lithium-ion batteries, J. Mater. Chem. A 3 (2015) 8742–8749.
[184] U. Tylus, Q. Jia, K. Strickland, N. Ramaswamy, A. Serov, P. Atanassov, S. Mukerjee, Elucidating oxygen reduction active sites in pyrolyzed metal–nitrogen coordinated non-precious-metal electrocatalyst systems, J. Phys. Chem. C. 118 (2014) 8999–9008.
[185] J. Yang, J. Tao, T. Isomura, H. Yanagi, I. Moriguchi, N. Nakashima, A comparative study of iron phthalocyanine electrocatalysts supported on different nanocarbons for oxygen reduction reaction, Carbon 145 (2019) 565–571, https://doi.org/10.1016/j.carbon.2019.01.022.
[186] V. Parthiban, B. Bhuvaneshwari, J. Karthikeyan, P. Murugan, A.K. Sahu, Fluorine-enriched mesoporous carbon as efficient oxygen reduction catalyst: understanding the defects in porous matrix and fuel cell applications, Nanoscale Adv. 1 (2019) 4926–4937.
[187] S. Akula, B. Balasubramaniam, P. Varathan, A.K. Sahu, Nitrogen–fluorine dual doped porous carbon derived from silk cotton as efficient oxygen reduction catalyst for polymer electrolyte fuel cells, ACS Appl. Energy Mater. 2 (2019) 3253–3263.
[188] M. Karuppannan, J.E. Park, H.E. Bae, Y.-H. Cho, O.J. Kwon, A nitrogen and fluorine enriched Fe/Fe 3C@ C oxygen reduction reaction electrocatalyst for anion/proton exchange membrane fuel cells, Nanoscale 12 (2020) 2542–2554.
[189] Y. Hao, X. Zhang, Q. Yang, K. Chen, J. Guo, D. Zhou, L. Feng, Z. Slanina, Highly porous defective carbons derived from seaweed biomass as efficient electrocatalysts for oxygen reduction in both alkaline and acidic media, Carbon 137 (2018) 93–103, https://doi.org/10.1016/j.carbon.2018.05.007.
[190] N. Wang, T. Li, Y. Song, J. Liu, F. Wang, Metal-free nitrogen-doped porous carbons derived from pomelo peel treated by hypersaline environments for oxygen reduction reaction, Carbon 130 (2018) 692–700, https://doi.org/10.1016/j.carbon.2018.01.068.
[191] A. Srinu, S.G. Peera, V. Parthiban, B. Bhuvaneshwari, A.K. Sahu, Heteroatom engineering and Co–Doping of N and P to porous carbon derived from spent coffee grounds as an efficient electrocatalyst for oxygen reduction reactions in alkaline medium, ChemistrySelect 3 (2018) 690–702, https://doi.org/10.1002/slct.201702042.
[192] H.-W. Liang, X. Zhuang, S. Brüller, X. Feng, K. Müllen, Hierarchically porous carbons with optimized nitrogen doping as highly active electrocatalysts for oxygen reduction, Nat. Commun. 5 (2014) 4973, https://doi.org/10.1038/ncomms5973.
[193] J. Herranz, M. Lefèvre, N. Larouche, B. Stansfield, J.-P. Dodelet, Step-by-step synthesis of non-noble metal electrocatalysts for O2 reduction under proton exchange membrane fuel cell conditions, J. Phys. Chem. C. 111 (2007) 19033–19042, https://doi.org/10.1021/jp0764438.
[194] D.W. Lee, J.H.J. Jang, I. Jang, Y.S. Kang, S. Jang, K.Y. Lee, J.H.J. Jang, H. Kim, S. J. Yoo, Bio-derived Co2P nanoparticles supported on nitrogen-doped carbon as promising oxygen reduction reaction electrocatalyst for anion exchange membrane fuel cells, Small 15 (2019) 1902090.
[195] S. Abinaya, P. Moni, V. Parthiban, A.K. Sahu, M. Wilhelm, Metal silicide nanosphere decorated carbon-rich polymer-derived ceramics: bifunctional electrocatalysts towards oxygen and their application in anion exchange membrane fuel cells, ChemElectroChem 6 (2019) 3268–3278.
[196] V.M. Truong, N.B. Duong, H. Yang, Comparison of carbon supports in anion exchange membrane fuel cells, Mater. (Basel) 13 (2020) 5370, https://doi.org/10.3390/ma13235370.
[197] N. Chen, S.P. Kim, C. Hu, H.H. Wang, J.H. Park, H.M. Kim, Y.M. Lee, High-performance poly(fluorenyl aryl piperidinium)-based anion exchange membrane fuel cells with realistic hydrogen supply, J. Power Sources 512 (2021), 230474, https://doi.org/10.1016/j.jpowsour.2021.230474.
[198] C. He, A.C. Yang-Neyerlin, B.S. Pivovar, Probing anion exchange membrane fuel cell cathodes by varying electrocatalysts and electrode processing, J. Electrochem. Soc. 169 (2022) 24507, https://doi.org/10.1149/1945-7111/ac4daa.
[199] S. Kim, J. Choi, Y.-E. Sung, M. Choi, S. Jang, Fabrication of an ionomer-free electrode containing vertically aligned one-dimensional nanostructures for alkaline membrane fuel cells, J. Electrochem. Soc. 168 (2021), 114505, https://doi.org/10.1149/1945-7111/ac3595.
[200] L. Osmieri, C. Zafferoni, L. Wang, A.H.A. Monteverde Videla, A. Lavacchi, S. Specchia, Polypyrrole-derived Fe− Co− N− C catalyst for the oxygen reduction reaction: performance in alkaline hydrogen and ethanol fuel cells, ChemElectroChem 5 (2018) 1954–1965.
[201] A. Sokka, M. Mooste, M. Käärik, V. Gudkova, J. Kozlova, A. Kikas, V. Kisand, A. Treshchalov, A. Tamm, P. Paiste, J. Aruväli, J. Leis, A. Krumme, S. Holdcroft, S. Cavaliere, F. Jaouen, K. Tammeveski, Iron and cobalt containing electrospun carbon nanofibre-based cathode catalysts for anion exchange membrane fuel cell, Int. J. Hydrog. Energy 46 (2021), https://doi.org/10.1016/j.ijhydene.2021.07.025.
[202] Y. Kumar, E. Kibena-Põldsepp, J. Kozlova, M. Rähn, A. Treshchalov, A. Kikas, V. Kisand, J. Aruväli, A. Tamm, J.C. Douglin, S.J. Folkman, I. Gelmetti, F. A. Garcés-Pineda, J.R. Galán-Mascarós, D.R. Dekel, K. Tammeveski, Bifunctional oxygen electrocatalysis on mixed metal phthalocyanine-modified carbon nanotubes prepared via pyrolysis, ACS Appl. Mater. Interfaces 13 (2021) 41507–41516, https://doi.org/10.1021/acsami.1c06737.

[203] W. Zhu, Y. Pei, J.C. Douglin, J. Zhang, H. Zhao, J. Xue, Q. Wang, R. Li, Y. Qin, Y. Yin, D.R. Dekel, M.D. Guiver, Multi-scale study on bifunctional Co/Fe–N–C cathode catalyst layers with high active site density for the oxygen reduction reaction, Appl. Catal. B Environ. 299 (2021), 120656, https://doi.org/10.1016/j.apcatb.2021.120656.
[204] J. Lilloja, E. Kibena-Põldsepp, A. Sarapuu, M. Käärik, J. Kozlova, P. Paiste, A. Kikas, A. Treshchalov, J. Leis, A. Tamm, V. Kisand, S. Holdcroft, K. Tammeveski, Transition metal and nitrogen-doped mesoporous carbons as cathode catalysts for anion-exchange membrane fuel cells, Appl. Catal. B Environ. 306 (2022), 121113, https://doi.org/10.1016/j.apcatb.2022.121113.
[205] J.G. Kim, J. Cho, S. Han, H. Lee, E. Yuk, B. Bae, S.S. Jang, C. Pak, Boosting activity toward oxygen reduction reaction of a mesoporous FeCuNC catalyst via heteroatom doping-induced electronic state modulation, J. Mater. Chem. A 10 (2022) 5361–5372, https://doi.org/10.1039/D1TA07264A.
[206] H.S. Kim, J. Lee, J.-H. Jang, H. Jin, V.K. Paidi, S.-H. Lee, K.-S. Lee, P. Kim, S. J. Yoo, Waste pig blood-derived 2D Fe single-atom porous carbon as an efficient electrocatalyst for zinc–air batteries and AEMFCs, Appl. Surf. Sci. 563 (2021), 150208, https://doi.org/10.1016/j.apsusc.2021.150208.
[207] H.S. Kim, C.H. Lee, J.-H. Jang, M.S. Kang, H. Jin, K.-S. Lee, S.U. Lee, S.J. Yoo, W. C. Yoo, Single-atom oxygen reduction reaction electrocatalysts of Fe, Si, and N co-doped carbon with 3D interconnected mesoporosity, J. Mater. Chem. A 9 (2021) 4297–4309, https://doi.org/10.1039/D0TA11208A.
[208] J. Lilloja, M. Mooste, E. Kibena-Põldsepp, A. Sarapuu, B. Zulevi, A. Kikas, H.-M. Piirsoo, A. Tamm, V. Kisand, S. Holdcroft, A. Serov, K. Tammeveski, Mesoporous iron-nitrogen co-doped carbon material as cathode catalyst for the anion exchange membrane fuel cell, J. Power Sources Adv. 8 (2021), 100052, https://doi.org/10.1016/j.powera.2021.100052.
[209] S. Ratso, I. Kruusenberg, M. Käärik, M. Kook, L. Puust, R. Saar, J. Leis, K. Tammeveski, Highly efficient transition metal and nitrogen co-doped carbide-derived carbon electrocatalysts for anion exchange membrane fuel cells, J. Power Sources 375 (2018) 233–243, https://doi.org/10.1016/j.jpowsour.2017.08.046.
[210] J. Zhang, Y. Liu, Z. Yu, M. Huang, C. Wu, C. Jin, L. Guan, Boosting the performance of the Fe–N–C catalyst for the oxygen reduction reaction by introducing single-walled carbon nanohorns as branches on carbon fibers, J. Mater. Chem. A 7 (2019) 23182–23190.
[211] M. Kim, J.M. Yoo, C. Ahn, J. Jang, Y.J. Son, H. Shin, J. Kang, Y.S. Kang, S.J. Yoo, K. Lee, Rational generation of Fe− Nx Active Sites in Fe− N− C electrocatalysts facilitated by fe− n coordinated precursors for the oxygen reduction reaction, ChemCatChem 11 (2019) 5982–5988.
[212] Y. Liang, H. Zhang, J. Zhang, X. Cheng, Y. Zhu, L. Luo, S. Lu, J. Wei, H. Wang, Porous 2D carbon nanosheets synthesized via organic groups triggered polymer particles exfoliation: an effective cathode catalyst for polymer electrolyte membrane fuel cells, Electrochim. Acta 332 (2020), 135397.
[213] S. Ratso, M. Käärik, M. Kook, P. Paiste, V. Kisand, S. Vlassov, J. Leis, K. Tammeveski, Iron and nitrogen Co-doped carbide-derived carbon and carbon nanotube composite catalysts for oxygen reduction reaction, ChemElectroChem 5 (2018) 1827–1836, https://doi.org/10.1002/celc.201800132.
[214] N. Zion, J.C. Douglin, D.A. Cullen, P. Zelenay, D.R. Dekel, L. Elbaz, Porphyrin aerogel catalysts for oxygen reduction reaction in anion-exchange membrane fuel cells, Adv. Funct. Mater. 31 (2021), 2100963, https://doi.org/10.1002/adfm.202100963.
[215] J. Feng, R. Cai, E. Magliocca, H. Luo, L. Higgins, G.L.F. Romario, X. Liang, A. Pedersen, Z. Xu, Z. Guo, A. Periasamy, D. Brett, T.S. Miller, S.J. Haigh, B. Mishra, M.-M. Titirici, Iron, nitrogen Co-doped carbon spheres as low cost, scalable electrocatalysts for the oxygen reduction reaction, Adv. Funct. Mater. 31 (2021) 2102974, https://doi.org/10.1002/adfm.202102974.
[216] J. Woo, H. Choi, Y.J. Sa, H.Y. Kim, T. Lim, J.-H. Jang, S.J. Yoo, J.Y. Kim, C.S. Kim, S.H. Joo, Structural evolution of atomically dispersed fe species in Fe–N/C catalysts probed by X-ray absorption and 57Fe mössbauer spectroscopies, J. Phys. Chem. C. 125 (2021) 11928–11938, https://doi.org/10.1021/acs.jpcc.1c01333.
[217] T.-H. Hsieh, S.-N. Chen, Y.-Z. Wang, K.-S. Ho, J.-K. Chuang, L.-C. Ho, Cobalt-doped carbon nitride frameworks obtained from calcined aromatic polyimines as cathode catalyst of anion exchange membrane fuel cells, Membr 12 (2022), https://doi.org/10.3390/membranes12010074.
[218] M. Rauf, J. Wang, S. Handschuh-Wang, Z. Zhou, Waheed Iqbal, S.A. Khan, L. Zhuang, X. Ren, Y. Li, S. Sun, Highly stable N-containing polymer-based Fe/Nx/C electrocatalyst for alkaline anion exchange membrane fuel cell applications, Prog. Nat. Sci. Mater. Int 32 (2022) 27–33, https://doi.org/10.1016/j.pnsc.2021.10.016.
[219] R. Zeng, Y. Yang, X.R. Feng, H. Li, L.M. Gibbs, F.J. DiSalvo, H.D. Abruna, Nonprecious transition metal nitrides as efficient oxygen reduction electrocatalysts for alkaline fuel cells, Sci. Adv. 8 (2022) eabj1584, https://doi.org/10.1126/sciadv.abj1584.
[220] J. Zhang, Y. Pei, W. Zhu, Y. Liu, Y. Yin, Y. Qin, M.D. Guiver, Ionomer dispersion solvent influence on the microstructure of Co–N–C catalyst layers for anion exchange membrane fuel cell, J. Power Sources 484 (2021), 229259, https://doi.org/10.1016/j.jpowsour.2020.229259.
[221] R. Soni, S.N. Bhange, S. Kurungot, A 3-D nanoribbon-like Pt-free oxygen reduction reaction electrocatalyst derived from waste leather for anion exchange membrane fuel cells and zinc-air batteries, Nanoscale 11 (2019) 7893–7902.
[222] J. Lee, H.S. Kim, J.-H. Jang, E.-H. Lee, H.-W. Jeong, K.-S. Lee, P. Kim, S.J. Yoo, Atomic-scale engineered Fe single-atom electrocatalyst based on waste Pig blood for high-performance AEMFCs, ACS Sustain. Chem. Eng. 9 (2021) 7863–7872, https://doi.org/10.1021/acssuschemeng.1c01590.
[223] K. Im, D. Kim, J.-H. Jang, J. Kim, S.J. Yoo, Hollow-sphere Co-NC synthesis by incorporation of ultrasonic spray pyrolysis and pseudomorphic replication and its enhanced activity toward oxygen reduction reaction, Appl. Catal. B Environ. 260 (2020), 118192.
[224] G. Singla, S.N. Bhange, M. Mahajan, S. Kurungot, Facile synthesis of CNT interconnected PVP-ZIF-8 derived hierarchical porous Zn/N Co-doped carbon frameworks for oxygen reduction, Nanoscale 13 (2021) 6248–6258, https://doi.org/10.1039/D0NR09156A.
[225] J.H. Lee, J. Jang, J. Kim, S.J. Yoo, Bimetallic ZIFs derived nitrogen-doped hollow carbon with carbon nanotube bridges as a superior oxygen reduction reaction electrocatalyst, J. Ind. Eng. Chem. 97 (2021) 466–475, https://doi.org/10.1016/j.jiec.2021.03.004.
[226] M. Mooste, T. Tkesheliadze, J. Kozlova, A. Kikas, V. Kisand, A. Treshchalov, A. Tamm, J. Aruväli, J.H. Zagal, A.M. Kannan, K. Tammeveski, Transition metal phthalocyanine-modified shungite-based cathode catalysts for alkaline membrane fuel cell, Int. J. Hydrog. Energy 46 (2021) 4365–4377, https://doi.org/10.1016/j.ijhydene.2020.10.231.
[227] G.-S. Kang, J.-H. Jang, S.-Y. Son, C.-H. Lee, Y.-K. Lee, D.C. Lee, S.J. Yoo, S. Lee, H.-I. Joh, Fe-based non-noble metal catalysts with dual active sites of nanosized metal carbide and single-atomic species for oxygen reduction reaction, J. Mater. Chem. A 8 (2020) 22379–22388.
[228] L. Cui, L. Cui, Z. Li, J. Zhang, H. Wang, S. Lu, Y. Xiang, A copper single-atom catalyst towards efficient and durable oxygen reduction for fuel cells, J. Mater. Chem. A 7 (2019) 16690–16695, https://doi.org/10.1039/C9TA03518D.
[229] J.Y. Jung, J.-H. Jang, J.-G. Kim, K.-S. Lee, H.-K. Lim, P. Kim, R.P.H. Chang, J.-W. Park, S.J. Yoo, N.D. Kim, Flash bottom-up arc synthesis of nanocarbons as a universal route for fabricating single-atom electrocatalysts, Small Methods 5 (2021) 2100239, https://doi.org/10.1002/smtd.202100239.
[230] L. Liao, Y.M. Zhao, C. Xu, X.Y. Zhou, P.J. Wei, J.G. Liu, B. N-codoped, Cu–N/B–C composite as an efficient electrocatalyst for oxygen-reduction reaction in alkaline media, ChemistrySelect 5 (2020) 3647–3654, https://doi.org/10.1002/slct.202000523.
[231] Y. Zhao, L. Liao, G. Yu, P. Wei, J. Liu, B-doped Fe/N/C porous catalyst for high-performance oxygen reduction in anion-exchange membrane fuel cells, ChemElectroChem 6 (2019) 1754–1760.
[232] A. Friedman, M. Mizrahi, N. Levy, N. Zion, M. Zachman, L. Elbaz, Application of molecular catalysts for the oxygen reduction reaction in alkaline fuel cells, ACS Appl. Mater. Interfaces 13 (2021) 58532–58538, https://doi.org/10.1021/acsami.1c16311.
[233] X. Shi, S. Ahmad, K. Pérez-Salcedo, B. Escobar, H. Zheng, A.M. Kannan, Maximization of quadruple phase boundary for alkaline membrane fuel cell using non-stoichiometric α-MnO2 as cathode catalyst, Int. J. Hydrog. Energy 44 (2019) 1166–1173, https://doi.org/10.1016/j.ijhydene.2018.11.042.
[234] P. Anandha Ganesh, A.N. Prakrthi, S. Selva Chandrasekaran, D. Jeyakumar, Shape-tuned, surface-active and support-free silver oxygen reduction electrocatalyst enabled high performance fully non-PGM alkaline fuel cell, RSC Adv. 11 (2021) 24872–24882, https://doi.org/10.1039/D1RA02718B.
[235] S. Akula, A.K. Sahu, Heteroatoms co-doping (N, F) to the porous carbon derived from spent coffee grounds as an effective catalyst for oxygen reduction reaction in polymer electrolyte fuel cells, J. Electrochem. Soc. 166 (2019) F93.
[236] S. Akula, P. Varathan, R.S. Menon, A.K. Sahu, Rationally constructing nitrogen–fluorine heteroatoms on porous carbon derived from pomegranate fruit peel waste towards an efficient oxygen reduction catalyst for polymer electrolyte membrane fuel cells, Sustain. Energy Fuels 5 (2021) 886–899, https://doi.org/10.1039/D0SE01214A.
[237] S. Akula, A.K. Sahu, Structurally modulated graphitic carbon nanofiber and heteroatom (N, F) engineering toward metal-free ORR electrocatalysts for polymer electrolyte membrane fuel cells, ACS Appl. Mater. Interfaces 12 (2020) 11438–11449.
[238] J. Lilloja, E. Kibena-Põldsepp, A. Sarapuu, A. Kikas, V. Kisand, M. Käärik, M. Merisalu, A. Treshchalov, J. Leis, V. Sammelselg, Q. Wei, S. Holdcroft, K. Tammeveski, Nitrogen-doped carbide-derived carbon/carbon nanotube composites as cathode catalysts for anion exchange membrane fuel cell application, Appl. Catal. B Environ. 272 (2020), 119012.
[239] J. Biemolt, J.C. Douglin, R.K. Singh, E.S. Davydova, N. Yan, G. Rothenberg, D. R. Dekel, An anion-exchange membrane fuel cell containing only abundant and affordable materials, Energy Technol. (2021) 2000909, https://doi.org/10.1002/ente.202000909.
[240] D. Bosubabu, V. Parthiban, A.K. Sahu, K. Ramesha, Nitrogen-doped graphene-like carbon from bio-waste as efficient low-cost electrocatalyst for fuel cell application, Bull. Mater. Sci. 44 (2021) 135, https://doi.org/10.1007/s12034-021-02367-9.
[241] M. Vagin, V. Gueskine, E. Mitraka, S. Wang, A. Singh, I. Zozoulenko, M. Berggren, S. Fabiano, X. Crispin, Negatively-doped conducting polymers for oxygen reduction reaction, Adv. Energy Mater. 11 (2021) 2002664, https://doi.org/10.1002/aenm.202002664.
[242] M.-J. Kim, J.E. Park, S. Kim, M.S. Lim, A. Jin, O.-H. Kim, M.J. Kim, K.-S. Lee, J. Kim, S.-S. Kim, Biomass-derived air cathode materials: pore-controlled S, N-co-doped carbon for fuel cells and metal–air batteries, ACS Catal. 9 (2019) 3389–3398.
[243] A. Arunchander, S.G. Peera, V.V. Giridhar, A.K. Sahu, Synthesis of cobalt sulfide-graphene as an efficient oxygen reduction catalyst in alkaline medium and its application in anion exchange membrane fuel cells, J. Electrochem. Soc. 164 (2016) F71–F80.
[244] A. Arunchander, S.G. Peera, A.K. Sahu, Synthesis of flower-like molybdenum sulfide/graphene hybrid as an efficient oxygen reduction electrocatalyst for anion exchange membrane fuel cells, J. Power Sources 353 (2017) 104–114.

[245] A. Arunchander, S.G. Peera, A.K. Sahu, Self-assembled manganese sulfide nanostructures on graphene as an oxygen reduction catalyst for anion exchange membrane fuel cells, ChemElectroChem 4 (2017) 1544–1553, https://doi.org/10.1002/celc.201700160.
[246] L. Zeng, T.S. Zhao, L. An, A high-performance supportless silver nanowire catalyst for anion exchange membrane fuel cells, J. Mater. Chem. A. (2015) 1410–1416, https://doi.org/10.1039/c0xx00000x.
[247] L. Xin, Z. Zhang, Z. Wang, J. Qi, W. Li, Carbon supported Ag nanoparticles as high performance cathode catalyst for H2/O2 anion exchange membrane fuel cell, Front. Chem. 1 (2013), 16, https://doi.org/10.3389/fchem.2013.00016.
[248] A. Fazil, R. Chetty, Synthesis and evaluation of carbon nanotubes supported silver catalyst for alkaline fuel cell, Electroanalysis 26 (2014) 2380–2387, https://doi.org/10.1002/elan.201400246.
[249] R. Vinodh, D. Sangeetha, Carbon supported silver (Ag/C) electrocatalysts for alkaline membrane fuel cells, J. Mater. Sci. 47 (2012) 852–859, https://doi.org/10.1007/s10853-011-5863-3.
[250] S. Maheswari, P. Sridhar, S. Pitchumani, Carbon-supported silver as cathode electrocatalyst for alkaline polymer electrolyte membrane fuel cells, Electrocatalysis 3 (2012) 13–21, https://doi.org/10.1007/s12678-011-0071-0.
[251] S.D. Poynton, J.P. Kizewski, R.C.T. Slade, J.R. Varcoe, Novel electrolyte membranes and non-Pt catalysts for low temperature fuel cells (https://doi.org/https://doi.org/), Solid State Ion. 181 (2010) 219–222, https://doi.org/10.1016/j.ssi.2009.01.019.
[252] O.V. Korchagin, V.A. Bogdanovskaya, M.R. Tarasevich, A.V. Kuzov, G. V. Zhutaeva, M.V. Radina, V.T. Novikov, V.V. Zharikov, Characteristics of non-platinum cathode catalysts for a hydrogen–oxygen fuel cell with proton- and anion-conducting electrolytes, Catal. Ind. 8 (2016) 265–273, https://doi.org/10.1134/S2070050416030053.
[253] J.R. Varcoe, R.C.T. Slade, G.L. Wright, Y. Chen, Steady-state dc and impedance investigations of H2/O2 alkaline membrane fuel cells with commercial Pt/C, Ag/C, and Au, /C. Cathodes, J. Phys. Chem. B. 110 (2006) 21041–21049, https://doi.org/10.1021/jp064898b.
[254] S. Gu, W.C. Sheng, R. Cai, S.M. Alia, S.Q. Song, K.O. Jensen, Y.S. Yan, An efficient Ag–ionomer interface for hydroxide exchange membrane fuel cells, Chem. Commun. 49 (2013) 131–133, https://doi.org/10.1039/c2cc34862d.
[255] M. Mamlouk, S.M.S. Kumar, P. Gouerec, K. Scott, Electrochemical and fuel cell evaluation of Co based catalyst for oxygen reduction in anion exchange polymer membrane fuel cells, J. Power Sources 196 (2011) 7594–7600.
[256] M. Piana, M. Boccia, A. Filpi, E. Flammia, H.A. Miller, M. Orsini, F. Salusti, S. Santiccioli, F. Ciardelli, A. Pucci, H2/air alkaline membrane fuel cell performance and durability, using novel ionomer and non-platinum group metal cathode catalyst, J. Power Sources 195 (2010) 5875–5881.
[257] S.K. Singh, V. Kashyap, N. Manna, S.N. Bhange, R. Soni, R. Boukherroub, S. Szunerits, S. Kurungot, Efficient and durable oxygen reduction electrocatalyst based on CoMn alloy oxide nanoparticles supported over N-doped porous graphene, ACS Catal. 7 (2017) 6700–6710.
[258] T. Palaniselvam, V. Kashyap, S.N. Bhange, J. Baek, S. Kurungot, Nanoporous graphene enriched with Fe/Co-N active sites as a promising oxygen reduction electrocatalyst for anion exchange membrane fuel cells, Adv. Funct. Mater. 26 (2016) 2150–2162.
[259] X. Li, B.N. Popov, T. Kawahara, H. Yanagi, Non-precious metal catalysts synthesized from precursors of carbon, nitrogen, and transition metal for oxygen reduction in alkaline fuel cells, J. Power Sources 196 (2011) 1717–1722.
[260] R. Jiang, D. Chu, Comparative study of CoFeNx/C catalyst obtained by pyrolysis of hemin and cobalt porphyrin for catalytic oxygen reduction in alkaline and acidic electrolytes, J. Power Sources 245 (2014) 352–361.
[261] H.B. Aiyappa, S.N. Bhange, V.P. Sivasankaran, S. Kurungot, Single cell fabrication towards the realistic evaluation of a CNT-strung zif-derived electrocatalyst as a cathode material in alkaline fuel cells and metal− air batteries, ChemElectroChem 4 (2017) 2928–2933.
[262] T. Van MEN, C.-W. YANG, H. YANG, Carbon black and multi-walled carbon nanotubes supported cobalt for anion exchange membrane fuel cell, 3rd ASEAN Smart Grid Congr. 5th Int. Conf. Sustain. Energy (2017) 15.
[263] H.-C. Huang, Y.-C. Lin, S.-T. Chang, C.-C. Liu, K.-C. Wang, H.-P. Jhong, J.-F. Lee, C.-H. Wang, Effect of sulfur and nitrogen dual-doped Fe-N-S, Electro Oxyg. Reduct. React., J. Mater. Chem. A 5 (2017), https://doi.org/10.1039/C7TA05030E.
[264] S.M. Unni, S. Ramadas, R. Illathvalappil, S.N. Bhange, S. Kurungot, Surface-modified single wall carbon nanohorn as an effective electrocatalyst for platinum-free fuel cell cathodes, J. Mater. Chem. A 3 (2015) 4361–4367.
[265] I. Kruusenberg, L. Matisen, Q. Shah, A.M. Kannan, K. Tammeveski, Non-platinum cathode catalysts for alkaline membrane fuel cells, Int. J. Hydrog. Energy 37 (2012) 4406–4412.
[266] J. Sanetuntikul, C. Chuaicham, Y.-W. Choi, S. Shanmugam, Investigation of hollow nitrogen-doped carbon spheres as non-precious Fe–N4 based oxygen reduction catalysts, J. Mater. Chem. A 3 (2015) 15473–15481, https://doi.org/10.1039/C5TA02677F.
[267] Y.J. Sa, D.-J. Seo, J. Woo, J.T. Lim, J.Y. Cheon, S.Y. Yang, J.M. Lee, D. Kang, T. J. Shin, H.S. Shin, H.Y Yeong, C.S. Kim, M.G. Kim, T.-Y. Kim, S.H. Joo, A general approach to preferential formation of active Fe–N x sites in Fe–N/C electrocatalysts for effricient oxygen reduction reaction, J. Am. Chem. Soc. 138 (2016) 15046–15056.
[268] J. Guo, H. He, D. Chu, R. Chen, OH−-binding effects on metallophthalocyanine catalysts for O 2 reduction reaction in anion exchange membrane fuel cells, Electrocatalysis 3 (2012) 252–264.
[269] P. Song, H.M. Barkholtz, Y. Wang, W. Xu, D. Liu, L. Zhuang, High-performance oxygen reduction catalysts in both alkaline and acidic fuel cells based on pre-treating carbon material and iron precursor, Sci. Bull. 62 (2017) 1602–1608.
[270] L. Chen, Y. Xing, S. Cai, R. Wang, S. Li, J. Li, W. Guo, H. Tang, Ordered iron-and nitrogen-doped carbon framework as a carbon monoxide-tolerant alkaline anion-exchange membrane fuel cell catalyst, Energy Technol. 6 (2018) 1003–1010.
[271] F. Meng, Z. Wang, H. Zhong, J. Wang, J. Yan, X. Zhang, Reactive multifunctional template-induced preparation of fe-N-doped mesoporous carbon microspheres towards highly efficient electrocatalysts for oxygen reduction, Adv. Mater. 28 (2016) 7948–7955.
[272] H. Lee, M.J. Kim, T. Lim, Y.-E. Sung, H.-J. Kim, H.-N. Lee, O.J. Kwon, Y.-H. Cho, A facile synthetic strategy for iron, aniline-based non-precious metal catalysts for polymer electrolyte membrane fuel cells, Sci. Rep. 7 (2017) 1–8, https://doi.org/10.1038/s41598-017- 05830-y.
[273] R. Gokhale, Y. Chen, A. Serov, K. Artyushkova, P. Atanassov, Novel dual templating approach for preparation of highly active Fe-NC electrocatalyst for oxygen reduction, Electrochim. Acta 224 (2017) 49–55.
[274] I. Kruusenberg, D. Ramani, S. Ratso, U. Joost, R. Saar, P. Rauwel, A.M. Kannan, K. Tammeveski, Cobalt–nitrogen Co-doped carbon nanotube cathode catalyst for alkaline membrane fuel cells, ChemElectroChem 3 (2016) 1455–1465.
[275] T. Zhu, X. Qing, P. Xu, Y. Song, J. Qiao, H2/O2 alkaline membrane fuel cell performances using carbon-supported metal phthalocyanine (MPc/C, M= Co, Cu, Zn, Ni) as cathode catalysts, ECS Trans. 66 (2015) 105.
[276] H.A. Miller, M. Bellini, W. Oberhauser, X. Deng, H. Chen, Q. He, M. Passaponti, M. Innocenti, R. Yang, F. Sun, Heat treated carbon supported iron (ii) phthalocyanine oxygen reduction catalysts: elucidation of the structure–activity relationship using X-ray absorption spectroscopy, Phys. Chem. Chem. Phys. 18 (2016) 33142–33151.
[277] P. Song, Y. Zhang, J. Pan, L. Zhuang, W. Xu, Cheap carbon black-based high-performance electrocatalysts for oxygen reduction reaction, Chem. Commun. 51 (2015) 1972–1975.
[278] G.A. Ferrero, K. Preuss, A. Marinovic, A.B. Jorge, N. Mansor, D.J.L. Brett, A. B. Fuertes, M. Sevilla, M.-M. Titirici, Fe–N-doped carbon capsules with outstanding electrochemical performance and stability for the oxygen reduction reaction in both acid and alkaline conditions, ACS Nano 10 (2016) 5922–5932.
[279] D.Y. Chung, M.J. Kim, N. Kang, J.M. Yoo, H. Shin, O.-H. Kim, Y.-E. Sung, Low-temperature and gram-scale synthesis of two-dimensional Fe–N–C carbon sheets for robust electrochemical oxygen reduction reaction, Chem. Mater. 29 (2017) 2890–2898.
[280] F.R. Brushett, M.S. Thorum, N.S. Lioutas, M.S. Naughton, C. Tornow, H.-R. "Molly" Jhong, A.A. Gewirth, P.J.A. Kenis, A carbon-supported copper complex of 3,5-diamino-1,2,4-triazole as a cathode catalyst for alkaline fuel cell applications, J. Am. Chem. Soc. 132 (2010) 12185–12187, https://doi.org/10.1021/ja104767w.
[281] H. Ren, Y. Wang, Y. Yang, X. Tang, Y. Peng, H. Peng, L. Xiao, J. Lu, H.D. Abruña, L. Zhuang, Fe/N/C nanotubes with atomic Fe sites: a highly active cathode catalyst for alkaline polymer electrolyte fuel cells, ACS Catal. 7 (2017) 6485–6492, https://doi.org/10.1021/acscatal.7b02340.
[282] M. Xu, C. Li, H. Ren, L. Ding, K. Xu, J. Geng, Carbon-supported Co-phthalocyanine modified with pyridine, 2-acid pyridine and 2-methyl pyridine as novel cathode catalysts for alkaline PEM fuel cells, J. Mol. Catal. A Chem. 390 (2014) 69–75, https://doi.org/10.1016/j.molcata.2014.03.007.
[283] C. Chen, X.-D. Yang, Z.-Y. Zhou, Y.-J. Lai, M. Rauf, Y. Wang, J. Pan, L. Zhuang, Q. Wang, Y.-C. Wang, Aminothiazole-derived N, S, Fe-doped graphene nanosheets as high performance electrocatalysts for oxygen reduction, Chem. Commun. 51 (2015) 17092–17095.
[284] J.W.D. Ng, Y. Gorlin, D. Nordlund, T.F. Jaramillo, Nanostructured manganese oxide supported onto particulate glassy carbon as an active and stable oxygen reduction catalyst in alkaline-based fuel cells, J. Electrochem. Soc. 161 (2014) D3105–D3112, https://doi.org/10.1149/2.014407jes.
[285] A. Arunchander, M. Vivekanantha, S.G. Peera, A.K. Sahu, MnO–nitrogen doped graphene as a durable non-precious hybrid catalyst for the oxygen reduction reaction in anion exchange membrane fuel cells, RSC Adv. 6 (2016) 95590–95600.
[286] Q. He, Q. Li, S. Khene, X. Ren, F.E. López-Suárez, D. Lozano-Castelló, A. Bueno-López, G. Wu, High-loading cobalt oxide coupled with nitrogen-doped graphene for oxygen reduction in anion-exchange-membrane alkaline fuel cells, J. Phys. Chem. C. 117 (2013) 8697–8707.
[287] C.-H. Wang, C.-W. Yang, Y.-C. Lin, S.-T. Chang, S.L.Y. Chang, Cobalt–iron (II, III) oxide hybrid catalysis with enhanced catalytic activities for oxygen reduction in anion exchange membrane fuel cell, J. Power Sources 277 (2015) 147–154.
[288] V.M. Dhavale, S.K. Singh, A. Nadeema, S.S. Gaikwad, S. Kurungot, Nanocrystalline Fe–Fe2O3 particle-deposited N-doped graphene as an activity-modulated Pt-free electrocatalyst for oxygen reduction reaction, Nanoscale 7 (2015) 20117–20125.
[289] D. Huang, Y. Luo, S. Li, B. Zhang, Y. Shen, M. Wang, Active catalysts based on cobalt oxide@cobalt/N-C nanocomposites for oxygen reduction reaction in alkaline solutions, Nano Res. 7 (2014) 1054–1064, https://doi.org/10.1007/s12274-014-0468-1.
[290] M. Wang, Y. Hou, R.C.T. Slade, J. Wang, D. Shi, D. Wexler, H. Liu, J. Chen, Core-shell Co/CoO integrated on 3D nitrogen doped reduced graphene oxide aerogel as an enhanced electrocatalyst for the oxygen reduction reaction, Front. Chem. 4 (2016) 36.
[291] M. Saito, T. Takakuwa, T. Kenko, H. Daimon, A. Tasaka, M. Inaba, H. Shiroishi, T. Hatai, J. Kuwano, New oxygen reduction electrocatalysts based on lanthanum

manganite oxides and their application to the cathode of AEMFCs, ECS Trans. 58 (2013) 1335.
[292] T. Takakuwa, M. Akiyoshi, T. Kenko, M. Saito, H. Daimon, A. Tasaka, M. Inaba, H. Shiroishi, T. Hatai, J. Kuwano, Development of oxygen reduction electrocatalysts based on manganese oxides for AEMFCs, ECS Trans. 41 (2011) 2185.
[293] T. Kenko, T. Takakuwa, M. Saito, H. Daimon, A. Tasaka, M. Inaba, Y. Kadoma, N. Kumagai, H. Shiroishi, T. Hatai, J. Kuwano, Oxygen reduction catalytic activity of hollandite-type manganese oxides, Key Eng. Mater., Trans. Tech. Publ. Ltd (2013) 253–257, https://doi.org/10.4028/www.scientific.net/KEM.566.253.
[294] Y.J. Sa, C. Park, H.Y. Jeong, S. Park, Z. Lee, K.T. Kim, G. Park, S.H. Joo, Carbon nanotubes/heteroatom-doped carbon core–sheath nanostructures as highly active, metal-free oxygen reduction electrocatalysts for alkaline fuel cells, Angew, Chemie 126 (2014) 4186–4190.
[295] C. Van Pham, M. Klingele, B. Britton, K.R. Vuyyuru, T. Unmuessig, S. Holdcroft, A. Fischer, S. Thiele, Tridoped reduced graphene oxide as a metal-free catalyst for oxygen reduction reaction demonstrated in acidic and alkaline polymer electrolyte fuel cells, Adv. Sustain. Syst. 1 (2017) 1600038, https://doi.org/10.1002/adsu.201600038.
[296] C. Venkateswara Rao, Y. Ishikawa, Activity, selectivity, and anion-exchange membrane fuel cell performance of virtually metal-free nitrogen-doped carbon nanotube electrodes for oxygen reduction reaction, J. Phys. Chem. C. 116 (2012) 4340–4346.
[297] O.-H. Kim, Y.-H. Cho, D.Y. Chung, M.J. Kim, J.M. Yoo, J.E. Park, H. Choe, Y.-E. Sung, Facile and gram-scale synthesis of metal-free catalysts: toward realistic applications for fuel cells, Sci. Rep. 5 (2015) 1–8.
[298] J.W.F. To, J.W.D. Ng, S. Siahrostami, A.L. Koh, Y. Lee, Z. Chen, K.D. Fong, S. Chen, J. He, W.-G. Bae, High-performance oxygen reduction and evolution carbon catalysis: From mechanistic studies to device integration, Nano Res. 10 (2017) 1163–1177.
[299] S.M. Unni, S.N. Bhange, R. Illathvalappil, N. Mutneja, K.R. Patil, S. Kurungot, Nitrogen-induced surface area and conductivity modulation of carbon nanohorn and its function as an efficient metal-free oxygen reduction electrocatalyst for anion-exchange membrane fuel cells, Small 11 (2015) 352–360.
[300] M. Wang, J. Wang, Y. Hou, D. Shi, D. Wexler, S.D. Poynton, R.C.T. Slade, W. Zhang, H. Liu, J. Chen, N-doped crumpled graphene derived from vapor phase deposition of PPy on graphene aerogel as an efficient oxygen reduction reaction electrocatalyst, ACS Appl. Mater. Interfaces 7 (2015) 7066–7072.
[301] D.C. Higgins, Z. Chen, Nitrogen doped carbon nanotube thin films as efficient oxygen reduction catalyst for alkaline anion exchange membrane fuel cell, ECS Trans. 28 (2010) 63.
[302] M.P. Kumar, M.M. Raju, A. Arunchander, S. Selvaraj, G. Kalita, T.N. Narayanan, A.K. Sahu, D.K. Pattanayak, Nitrogen doped graphene as metal free electrocatalyst for efficient oxygen reduction reaction in alkaline media and its application in anion exchange membrane fuel cells, J. Electrochem. Soc. 163 (2016) F848–F855.
[303] T. Palaniselvam, M.O. Valappil, R. Illathvalappil, S. Kurungot, Nanoporous graphene by quantum dots removal from graphene and its conversion to a potential oxygen reduction electrocatalyst via nitrogen doping, Energy Environ. Sci. 7 (2014) 1059–1067.
[304] S. Lee, M. Choun, Y. Ye, J. Lee, Y. Mun, E. Kang, J. Hwang, Y.H. Lee, C.H. Shin, S. H. Moon, S.K. Kim, E. Lee, J. Lee, Designing a highly active metal-free oxygen reduction catalyst in membrane electrode assemblies for alkaline fuel cells: effects of pore size and doping-site position, Angew. Chem. - Int. Ed. 54 (2015) 9230–9234, https://doi.org/10.1002/anie.201501590.
[305] M. Klingele, C. Pham, K.R. Vuyyuru, B. Britton, S. Holdcroft, A. Fischer, S. Thiele, Sulfur doped reduced graphene oxide as metal-free catalyst for the oxygen reduction reaction in anion and proton exchange fuel cells, Electrochem. Commun. 77 (2017) 71–75, https://doi.org/10.1016/j.elecom.2017.02.015.
[306] A. Arunchander, S.G. Peera, S.K. Panda, S. Chellammal, A.K. Sahu, Simultaneous co-doping of N and S by a facile in-situ polymerization of 6-N, N-dibutylamine-1, 3, 5-triazine-2, 4-dithiol on graphene framework: an efficient and durable oxygen reduction catalyst in alkaline medium, Carbon 118 (2017) 531–544.
[307] N. Xu, T. Zhu, J. Qiao, F. Zhang, Z. Chen, Nitrogen and sulfur co-doped mesoporous carbon as cathode catalyst for H2/O2 alkaline membrane fuel cell–effect of catalyst/bonding layer loading, Int. J. Hydrog. Energy 41 (2016) 9159–9166.
[308] F. Jaouen, J. Herranz, M. Lefèvre, J.-P. Dodelet, U.I. Kramm, I. Herrmann, P. Bogdanoff, J. Maruyama, T. Nagaoka, A. Garsuch, J.R. Dahn, T. Olson, S. Pylypenko, P. Atanassov, E.A. Ustinov, Cross-laboratory experimental study of non-noble-metal electrocatalysts for the oxygen reduction reaction, ACS Appl. Mater. Interfaces 1 (2009) 1623–1639, https://doi.org/10.1021/am900219g.
[309] F. Jaouen, M. Lefèvre, J.-P. Dodelet, M. Cai, Heat-treated Fe/N/C catalysts for O2 electroreduction: are active sites hosted in micropores, ?, J. Phys. Chem. B. 110 (2006) 5553–5558, https://doi.org/10.1021/jp057135h.
[310] M. Wang, W. Zhang, J. Wang, D. Wexler, S.D. Poynton, R.C.T. Slade, H. Liu, B. Winther-Jensen, R. Kerr, D. Shi, PdNi hollow nanoparticles for improved electrocatalytic oxygen reduction in alkaline environments, ACS Appl. Mater. Interfaces 5 (2013) 12708–12715.
[311] S. Kabir, A. Serov, K. Artyushkova, P. Atanassov, Nitrogen-doped three-dimensional graphene-supported palladium nanocomposites: high-performance cathode catalysts for oxygen reduction reactions, ACS Catal. (2017), https://doi.org/10.1021/acscatal.7b02071.
[312] T.J. Omasta, A.M. Park, J.M. LaManna, Y. Zhang, X. Peng, L. Wang, D. L. Jacobson, J.R. Varcoe, D.S. Hussey, B.S. Pivovar, W.E. Mustain, Beyond catalysis and membranes: visualizing and solving the challenge of electrode water accumulation and flooding in AEMFCs, Energy Environ. Sci. 11 (2018) 551–558, https://doi.org/10.1039/C8EE00122G.
[313] I. Verhaert, S. Verhelst, G. Janssen, G. Mulder, M. De Paepe, Water management in an alkaline fuel cell, Int. J. Hydrog. Energy 36 (2011) 11011–11024, https://doi.org/10.1016/j.ijhydene.2011.05.172.
[314] G. Wu, K.L. More, P. Xu, H.-L. Wang, M. Ferrandon, A.J. Kropf, D.J. Myers, S. Ma, C.M. Johnston, P. Zelenay, A carbon-nanotube-supported graphene-rich non-precious metal oxygen reduction catalyst with enhanced performance durability, Chem. Commun. 49 (2013) 3291–3293, https://doi.org/10.1039/C3CC39121C.
[315] X. Fu, Y. Liu, X. Cao, J. Jin, Q. Liu, J. Zhang, FeCo–Nx embedded graphene as high performance catalysts for oxygen reduction reaction, Appl. Catal. B Environ. 130–131 (2013) 143–151, https://doi.org/10.1016/j.apcatb.2012.10.028.
[316] S. Shanmugam, T. Osaka, Efficient electrocatalytic oxygen reduction over metal free-nitrogen doped carbon nanocapsules, Chem. Commun. 47 (2011) 4463–4465, https://doi.org/10.1039/C1CC10361J.
[317] J. Sanetuntikul, T. Hang, S. Shanmugam, Hollow nitrogen-doped carbon spheres as efficient and durable electrocatalysts for oxygen reduction, Chem. Commun. 50 (2014) 9473–9476, https://doi.org/10.1039/C4CC03437F.
[318] C. Zhang, N. Mahmood, H. Yin, F. Liu, Y. Hou, Synthesis of phosphorus-doped graphene and its multifunctional applications for oxygen reduction reaction and lithium ion batteries, Adv. Mater. 25 (2013) 4932–4937, https://doi.org/10.1002/adma.201301870.
[319] G. Jo, J. Sanetuntikul, S. Shanmugam, Boron and phosphorous-doped graphene as a metal-free electrocatalyst for the oxygen reduction reaction in alkaline medium, RSC Adv. 5 (2015) 53637–53643, https://doi.org/10.1039/C5RA06952A.
[320] R. Li, Z. Wei, X. Gou, W. Xu, Phosphorus-doped graphene nanosheets as efficient metal-free oxygen reduction electrocatalysts, RSC Adv. 3 (2013) 9978–9984, https://doi.org/10.1039/C3RA41079J.
[321] D.-S. Yang, D. Bhattacharjya, M.Y. Song, J.-S. Yu, Highly efficient metal-free phosphorus-doped platelet ordered mesoporous carbon for electrocatalytic oxygen reduction, Carbon 67 (2014) 736–743, https://doi.org/10.1016/j.carbon.2013.10.065.
[322] Z.-H. Sheng, H.-L. Gao, W.-J. Bao, F.-B. Wang, X.-H. Xia, Synthesis of boron doped graphene for oxygen reduction reaction in fuel cells, J. Mater. Chem. 22 (2012) 390–395, https://doi.org/10.1039/C1JM14694G.
[323] G. Jo, S. Shanmugam, Single-step synthetic approach for boron-doped carbons as a non-precious catalyst for oxygen reduction in alkaline medium, Electrochem. Commun. 25 (2012) 101–104, https://doi.org/10.1016/j.elecom.2012.09.025.
[324] X. Bo, L. Guo, Ordered mesoporous boron-doped carbons as metal-free electrocatalysts for the oxygen reduction reaction in alkaline solution, Phys. Chem. Chem. Phys. 15 (2013) 2459–2465, https://doi.org/10.1039/C2CP43541A.
[325] J. Su, X. Cao, J. Wu, C. Jin, J.-H. Tian, R. Yang, One-pot synthesis of boron-doped ordered mesoporous carbons as efficient electrocatalysts for the oxygen reduction reaction, RSC Adv. 6 (2016) 24728–24737, https://doi.org/10.1039/C6RA01296E.
[326] Y. Zhao, L. Yang, S. Chen, X. Wang, Y. Ma, Q. Wu, Y. Jiang, W. Qian, Z. Hu, Can boron and nitrogen Co-doping improve oxygen reduction reaction activity of carbon nanotubes, J. Am. Chem. Soc. 135 (2013) 1201–1204, https://doi.org/10.1021/ja310566z.
[327] L. Yang, S. Jiang, Y. Zhao, L. Zhu, S. Chen, X. Wang, Q. Wu, J. Ma, Y. Ma, Z. Hu, Boron-doped carbon nanotubes as metal-free electrocatalysts for the oxygen reduction reaction, Angew. Chem. Int. Ed. 50 (2011) 7132–7135, https://doi.org/10.1002/anie.201101287.
[328] S. Wang, E. Iyyamperumal, A. Roy, Y. Xue, D. Yu, L. Dai, Vertically aligned BCN nanotubes as efficient metal-free electrocatalysts for the oxygen reduction reaction: a synergetic effect by Co-doping with boron and nitrogen, Angew. Chem. Int. Ed. 50 (2011) 11756–11760, https://doi.org/10.1002/anie.201105204.
[329] J. Liang, Y. Jiao, M. Jaroniec, S.Z. Qiao, Sulfur and nitrogen dual-doped mesoporous graphene electrocatalyst for oxygen reduction with synergistically enhanced performance, Angew. Chem. Int. Ed. 51 (2012) 11496–11500, https://doi.org/10.1002/anie.201206720.
[330] C. You, S. Liao, H. Li, S. Hou, H. Peng, X. Zeng, F. Liu, R. Zheng, Z. Fu, Y. Li, Uniform nitrogen and sulfur co-doped carbon nanospheres as catalysts for the oxygen reduction reaction, Carbon 69 (2014) 294–301, https://doi.org/10.1016/j.carbon.2013.12.028.
[331] Q. Shi, F. Peng, S. Liao, H. Wang, H. Yu, Z. Liu, B. Zhang, D. Su, Sulfur and nitrogen co-doped carbon nanotubes for enhancing electrochemical oxygen reduction activity in acidic and alkaline media, J. Mater. Chem. A. 1 (2013) 14853–14857, https://doi.org/10.1039/C3TA12647A.
[332] J. Li, Y. Zhang, X. Zhang, J. Huang, J. Han, Z. Zhang, X. Han, P. Xu, B. Song, S, N dual-doped graphene-like carbon nanosheets as efficient oxygen reduction reaction electrocatalysts, ACS Appl. Mater. Interfaces 9 (2017) 398–405, https://doi.org/10.1021/acsami.6b12547.
[333] Z.K. Yang, L. Lin, Y.-N. Liu, X. Zhou, C.-Z. Yuan, A.-W. Xu, Supramolecular polymers-derived nonmetal N, S-codoped carbon nanosheets for efficient oxygen reduction reaction, RSC Adv. 6 (2016) 52937–52944, https://doi.org/10.1039/C6RA05523K.
[334] M. Seredych, T.J. Bandosz, Confined space reduced graphite oxide doped with sulfur as metal-free oxygen reduction catalyst, Carbon 66 (2014) 227–233, https://doi.org/10.1016/j.carbon.2013.08.062.
[335] T. Ishizaki, Y. Wada, S. Chiba, S. Kumagai, H. Lee, A. Serizawa, O.L. Li, G. Panomsuwan, Effects of halogen doping on nanocarbon catalysts synthesized by a solution plasma process for the oxygen reduction reaction, Phys. Chem. Chem. Phys. 18 (2016) 21843–21851, https://doi.org/10.1039/C6CP03579E.

[336] Y.-G. Lee, H.-J. Ahn, Tri (Fe/N/F)-doped mesoporous carbons as efficient electrocatalysts for the oxygen reduction reaction, Appl. Surf. Sci. 487 (2019) 389–397.
[337] G. Liu, Z. Liu, J. Li, M. Zeng, Z. Li, L. He, F. Li, Chitosan/phytic acid hydrogel as a platform for facile synthesis of heteroatom-doped porous carbon frameworks for electrocatalytic oxygen reduction, Carbon 137 (2018) 68–77, https://doi.org/10.1016/j.carbon.2018.05.027.
[338] J. Wang, Z. Wu, L. Han, R. Lin, W. Xiao, C. Xuan, H.L. Xin, D. Wang, Nitrogen and sulfur co-doping of partially exfoliated MWCNTs as 3-D structured electrocatalysts for the oxygen reduction reaction, J. Mater. Chem. A. 4 (2016) 5678–5684, https://doi.org/10.1039/C6TA00490C.
[339] J. Zhang, L. Dai, Nitrogen, phosphorus, and fluorine tri-doped graphene as a multifunctional catalyst for self-powered electrochemical water splitting, Angew. Chem. Int. Ed. 55 (2016) 13296–13300.
[340] S. Akula, V. Parthiban, S.G. Peera, B.P. Singh, S.R. Dhakate, A.K. Sahu, Simultaneous Co-doping of nitrogen and fluorine into MWCNTs: an in-situ conversion to graphene like sheets and its electro-catalytic activity toward oxygen reduction reaction, J. Electrochem. Soc. 164 (2017) F568–F576, https://doi.org/10.1149/2.0501706jes.
[341] M. Wu, Y. Wang, Z. Wei, L. Wang, M. Zhuo, J. Zhang, X. Han, J. Ma, Ternary doped porous carbon nanofibers with excellent ORR and OER performance for zinc–air batteries, J. Mater. Chem. A 6 (2018) 10918–10925, https://doi.org/10.1039/C8TA02416B.
[342] K. Meng, Q. Liu, Y. Huang, Y. Wang, Facile synthesis of nitrogen and fluorine co-doped carbon materials as efficient electrocatalysts for oxygen reduction reactions in air-cathode microbial fuel cells, J. Mater. Chem. A. 3 (2015) 6873–6877, https://doi.org/10.1039/C4TA06500J.
[343] M. Wu, K. Wang, M. Yi, Y. Tong, Y. Wang, S. Song, A facile activation strategy for an mof-derived metal-free oxygen reduction reaction catalyst: direct access to optimized pore structure and nitrogen species, ACS Catal. 7 (2017) 6082–6088, https://doi.org/10.1021/acscatal.7b01649.
[344] C. Zhai, M. Sun, M. Zhu, S. Song, S. Jiang, A new method to synthesize sulfur-doped graphene as effective metal-free electrocatalyst for oxygen reduction reaction, Appl. Surf. Sci. 407 (2017) 503–508, https://doi.org/10.1016/j.apsusc.2017.02.191.
[345] S. Zhao, J. Liu, C. Li, W. Ji, M. Yang, H. Huang, Y. Liu, Z. Kang, Tunable Ternary (N, P, B)-doped porous nanocarbons and their catalytic properties for oxygen reduction reaction, ACS Appl. Mater. Interfaces 6 (2014) 22297–22304, https://doi.org/10.1021/am506284k.
[346] D.C. Higgins, M.A. Hoque, F. Hassan, J.-Y. Choi, B. Kim, Z. Chen, Oxygen reduction on graphene–carbon nanotube composites doped sequentially with nitrogen and sulfur, ACS Catal. 4 (2014) 2734–2740, https://doi.org/10.1021/cs5003806.
[347] J. Yang, H. Sun, H. Liang, H. Ji, L. Song, C. Gao, H. Xu, A highly efficient metal-free oxygen reduction electrocatalyst assembled from carbon nanotubes and graphene, Adv. Mater. 28 (2016) 4606–4613, https://doi.org/10.1002/adma.201505855.
[348] N.R. Sahraie, U.I. Kramm, J. Steinberg, Y. Zhang, A. Thomas, T. Reier, J.-P. Paraknowitsch, P. Strasser, Quantifying the density and utilization of active sites in non-precious metal oxygen electroreduction catalysts, Nat. Commun. 6 (2015) 8618, https://doi.org/10.1038/ncomms9618.
[349] R. Zhang, S. He, Y. Lu, W. Chen, Fe, Co, N-functionalized carbon nanotubes in situ grown on 3D porous N-doped carbon foams as a noble metal-free catalyst for oxygen reduction, J. Mater. Chem. A 3 (2015) 3559–3567, https://doi.org/10.1039/C4TA05735J.
[350] G. Wu, M. Nelson, S. Ma, H. Meng, G. Cui, P.K. Shen, Synthesis of nitrogen-doped onion-like carbon and its use in carbon-based CoFe binary non-precious-metal catalysts for oxygen-reduction, Carbon 49 (2011) 3972–3982, https://doi.org/10.1016/j.carbon.2011.05.036.
[351] N. Brun, S.A. Wohlgemuth, P. Osiceanu, M.M. Titirici, Original design of nitrogen-doped carbon aerogels from sustainable precursors: application as metal-free oxygen reduction catalysts, Green. Chem. 15 (2013) 2514–2524, https://doi.org/10.1039/C3GC40904J.
[352] G.A. Ferrero, K. Preuss, A.B. Fuertes, M. Sevilla, M.-M. Titirici, The influence of pore size distribution on the oxygen reduction reaction performance in nitrogen doped carbon microspheres, J. Mater. Chem. A 4 (2016) 2581–2589.
[353] G.A. Ferrero, A.B. Fuertes, M. Sevilla, M.-M. Titirici, Efficient metal-free N-doped mesoporous carbon catalysts for ORR by a template-free approach, Carbon 106 (2016) 179–187, https://doi.org/10.1016/j.carbon.2016.04.080.
[354] C. Tang, H.-F. Wang, X. Chen, B.-Q. Li, T.-Z. Hou, B. Zhang, Q. Zhang, M.-M. Titirici, F. Wei, Topological Defects in Metal-Free Nanocarbon for Oxygen Electrocatalysis (https://doi.org/https://doi.org/), Adv. Mater. 28 (2016) 6845–6851, https://doi.org/10.1002/adma.201601406.
[355] K. Preuss, L.C. Tănase, C.M. Teodorescu, I. Abrahams, M.-M. Titirici, Sustainable metal-free carbogels as oxygen reduction electrocatalysts, J. Mater. Chem. A 5 (2017) 16336–16343, https://doi.org/10.1039/C7TA02001E.
[356] Z. Chen, D. Higgins, H. Tao, R.S. Hsu, Z. Chen, Highly active nitrogen-doped carbon nanotubes for oxygen reduction reaction in fuel cell applications, J. Phys. Chem. C. 113 (2009) 21008–21013, https://doi.org/10.1021/jp908067v.
[357] M. Borghei, P. Kanninen, M. Lundahl, T. Susi, J. Sainio, I. Anoshkin, A. Nasibulin, T. Kallio, K. Tammeveski, E. Kauppinen, V. Ruiz, High oxygen reduction activity of few-walled carbon nanotubes with low nitrogen content, Appl. Catal. B Environ. 158–159 (2014) 233–241, https://doi.org/10.1016/j.apcatb.2014.04.027.
[358] J. Wu, D. Zhang, Y. Wang, B. Hou, Electrocatalytic activity of nitrogen-doped graphene synthesized via a one-pot hydrothermal process towards oxygen reduction reaction, J. Power Sources 227 (2013) 185–190, https://doi.org/10.1016/j.jpowsour.2012.11.074.
[359] L. Lai, J.R. Potts, D. Zhan, L. Wang, C.K. Poh, C. Tang, H. Gong, Z. Shen, J. Lin, R. S. Ruoff, Exploration of the active center structure of nitrogen-doped graphene-based catalysts for oxygen reduction reaction, Energy Environ. Sci. 5 (2012) 7936–7942.
[360] Z.-J. Lu, S.-J. Bao, Y.-T. Gou, C.-J. Cai, C.-C. Ji, M.-W. Xu, J. Song, R. Wang, Nitrogen-doped reduced-graphene oxide as an efficient metal-free electrocatalyst for oxygen reduction in fuel cells, RSC Adv. 3 (2013) 3990–3995, https://doi.org/10.1039/C3RA22161J.
[361] G. Liu, X. Li, J.-W. Lee, B.N. Popov, A review of the development of nitrogen-modified carbon-based catalysts for oxygen reduction at USC, Catal. Sci. Technol. 1 (2011) 207–217.
[362] A. Zhao, J. Masa, W. Schuhmann, W. Xia, Activation and stabilization of nitrogen-doped carbon nanotubes as electrocatalysts in the oxygen reduction reaction at strongly alkaline conditions, J. Phys. Chem. C. 117 (2013) 24283–24291, https://doi.org/10.1021/jp4059438.
[363] S. Liu, C. Deng, L. Yao, H. Zhong, H. Zhang, The key role of metal dopants in nitrogen-doped carbon xerogel for oxygen reduction reaction, J. Power Sources 269 (2014) 225–235, https://doi.org/10.1016/j.jpowsour.2014.06.148.
[364] S.K. Singh, K. Takeyasu, J. Nakamura, Active sites and mechanism of oxygen reduction reaction electrocatalysis on nitrogen-doped carbon materials, Adv. Mater. 31 (2019) 1804297, https://doi.org/10.1002/adma.201804297.
[365] K. Artyushkova, A. Serov, S. Rojas-Carbonell, P. Atanassov, Chemistry of multitudinous active sites for oxygen reduction reaction in transition metal–nitrogen–carbon electrocatalysts, J. Phys. Chem. C. 119 (2015) 25917–25928, https://doi.org/10.1021/acs.jpcc.5b07653.
[366] J.H. Zagal, M.T.M. Koper, Reactivity descriptors for the activity of molecular mn4 catalysts for the oxygen reduction reaction, Angew. Chem. Int. Ed. 55 (2016) 14510–14521, https://doi.org/10.1002/anie.201604311.
[367] K. Tammeveski, J.H. Zagal, Electrocatalytic oxygen reduction on transition metal macrocyclic complexes for anion exchange membrane fuel cell application, , Curr. Opin. Electrochem 9 (2018) 207–213, https://doi.org/10.1016/j.coelec.2018.04.001.
[368] B. Jeong, D. Shin, H. Jeon, J.D. Ocon, B.S. Mun, J. Baik, H.-J. Shin, J. Lee, Excavated Fe-N-C Sites for Enhanced Electrocatalytic Activity in the Oxygen Reduction Reaction, ChemSusChem 7 (2014) 1289–1294, https://doi.org/10.1002/cssc.201301374.
[369] Y. Wang, Y. Nie, W. Ding, S.G. Chen, K. Xiong, X.Q. Qi, Y. Zhang, J. Wang, Z. D. Wei, Unification of catalytic oxygen reduction and hydrogen evolution reactions: highly dispersive Co nanoparticles encapsulated inside Co and nitrogen co-doped carbon, Chem. Commun. 51 (2015) 8942–8945, https://doi.org/10.1039/C5CC02400E.
[370] T. Xing, Y. Zheng, L.H. Li, B.C.C. Cowie, D. Gunzelmann, S.Z. Qiao, S. Huang, Y. Chen, Observation of Active Sites for Oxygen Reduction Reaction on Nitrogen-Doped Multilayer Graphene, ACS Nano 8 (2014) 6856–6862, https://doi.org/10.1021/nn501506p.
[371] J. Chen, X. Wang, X. Cui, G. Yang, W. Zheng, Amorphous carbon enriched with pyridinic nitrogen as an efficient metal-free electrocatalyst for oxygen reduction reaction, Chem. Commun. 50 (2014) 557–559, https://doi.org/10.1039/C3CC47519K.
[372] K. Parvez, S. Yang, Y. Hernandez, A. Winter, A. Turchanin, X. Feng, K. Müllen, Nitrogen-doped graphene and its iron-based composite as efficient electrocatalysts for oxygen reduction reaction, ACS Nano 6 (2012) 9541–9550, https://doi.org/10.1021/nn302674k.
[373] J.A. Varnell, E.C.M. Tse, C.E. Schulz, T.T. Fister, R.T. Haasch, J. Timoshenko, A. I. Frenkel, A.A. Gewirth, Identification of carbon-encapsulated iron nanoparticles as active species in non-precious metal oxygen reduction catalysts, Nat. Commun. 7 (2016) 12582, https://doi.org/10.1038/ncomms12582.
[374] D. Guo, R. Shibuya, C. Akiba, S. Saji, T. Kondo, J. Nakamura, Active sites of nitrogen-doped carbon materials for oxygen reduction reaction clarified using model catalysts 351 (2016), https://doi.org/10.1126/science.aad0832.
[375] W. Ding, Z. Wei, S. Chen, X. Qi, T. Yang, J. Hu, D. Wang, L. Wan, S.F. Alvi, L. Li, Space-confinement-induced synthesis of pyridinic-and pyrrolic-nitrogen-doped graphene for the catalysis of oxygen reduction, Angew. Chem. 125 (2013) 11971–11975.
[376] A. Zhao, J. Masa, M. Muhler, W. Schuhmann, W. Xia, N-doped carbon synthesized from N-containing polymers as metal-free catalysts for the oxygen reduction under alkaline conditions, Electrochim. Acta 98 (2013) 139–145, https://doi.org/10.1016/j.electacta.2013.03.043.
[377] H. Li, X. Cheng, F.-B. Weng, A. Su, Y.-C. Chiang, Nitrogen-doped carbon nanotubes prepared at different temperatures for oxygen reduction reaction, J. Electrochem. Soc. 161 (2014) F1140–F1145, https://doi.org/10.1149/2.0171412jes.
[378] W. Wei, H. Ge, L. Huang, M. Kuang, A.M. Al-Enizi, L. Zhang, G. Zheng, Hierarchically tubular nitrogen-doped carbon structures for the oxygen reduction reaction, J. Mater. Chem. A. 5 (2017) 13634–13638, https://doi.org/10.1039/C7TA02658G.
[379] S.-H. Liu, J.-R. Wu, F.-S. Zheng, J.-M. Guo, Impact of iron precursors on the properties and activities of carbon-supported Fe-N oxygen reduction catalysts, J. Solid State Electrochem 19 (2015) 1381–1391.
[380] Z. Lin, G.H. Waller, Y. Liu, M. Liu, C. Wong, 3D Nitrogen-doped graphene prepared by pyrolysis of graphene oxide with polypyrrole for electrocatalysis of oxygen reduction reaction, Nano Energy 2 (2013) 241–248.
[381] C.-T. Hung, N. Yu, C.-T. Chen, P.-H. Wu, X. Han, Y.-S. Kao, T.-C. Liu, Y. Chu, F. Deng, A. Zheng, S.-B. Liu, Highly nitrogen-doped mesoscopic carbons as

efficient metal-free electrocatalysts for oxygen reduction reactions, J. Mater. Chem. A 2 (2014) 20030–20037, https://doi.org/10.1039/C4TA04403G.
[382] K. Artyushkova, I. Matanovic, B. Halevi, P. Atanassov, Oxygen binding to active sites of Fe–N–C ORR electrocatalysts observed by ambient-pressure XPS, J. Phys. Chem. C. 121 (2017) 2836–2843, https://doi.org/10.1021/acs.jpcc.6b11721.
[383] J.H. Kim, Y.J. Sa, H.Y. Jeong, S.H. Joo, Roles of Fe−Nx and Fe−Fe3C@C species in Fe−N/C electrocatalysts for oxygen reduction reaction, ACS Appl. Mater. Interfaces 9 (2017) 9567–9575, https://doi.org/10.1021/acsami.6b13417.
[384] S. Kabir, K. Artyushkova, A. Serov, P. Atanassov, Role of nitrogen moieties in N-doped 3D-graphene nanosheets for oxygen electroreduction in acidic and alkaline media, ACS Appl. Mater. Interfaces 10 (2018) 11623–11632, https://doi.org/10.1021/acsami.7b18651.
[385] S. Yasuda, L. Yu, J. Kim, K. Murakoshi, Selective nitrogen doping in graphene for oxygen reduction reactions, Chem. Commun. 49 (2013) 9627–9629, https://doi.org/10.1039/C3CC45641B.
[386] C.V. Rao, C.R. Cabrera, Y. Ishikawa, In search of the active site in nitrogen-doped carbon nanotube electrodes for the oxygen reduction reaction, J. Phys. Chem. Lett. 1 (2010) 2622–2627, https://doi.org/10.1021/jz100971v.
[387] A.C. Ramírez-Pérez, J. Quílez-Bermejo, J.M. Sieben, E. Morallón, D. Cazorla-Amorós, Effect of nitrogen-functional groups on the ORR activity of activated carbon fiber-polypyrrole-based electrodes, Electrocatalysis 9 (2018) 697–705, https://doi.org/10.1007/s12678-018-0478-y.
[388] M. Mooste, E. Kibena-Põldsepp, V. Vassiljeva, M. Merisalu, M. Kook, A. Treshchalov, V. Kisand, M. Uibu, A. Krumme, V. Sammelselg, K. Tammeveski, Electrocatalysts for oxygen reduction reaction based on electrospun polyacrylonitrile, styrene–acrylonitrile copolymer and carbon nanotube composite fibres, J. Mater. Sci. 54 (2019) 11618–11634, https://doi.org/10.1007/s10853-019-03725-z.
[389] Q. Wang, Y. Ji, Y. Lei, Y. Wang, Y. Wang, Y. Li, S. Wang, Pyridinic-N-dominated doped defective graphene as a superior oxygen electrocatalyst for ultrahigh-energy-density Zn–Air batteries, ACS Energy Lett. 3 (2018) 1183–1191, https://doi.org/10.1021/acsenergylett.8b00303.
[390] Q. Wang, Y. Lei, Y. Zhu, H. Wang, J. Feng, G. Ma, Y. Wang, Y. Li, B. Nan, Q. Feng, Z. Lu, H. Yu, Edge defect engineering of nitrogen-doped carbon for oxygen electrocatalysts in Zn–Air batteries, ACS Appl. Mater. Interfaces 10 (2018) 29448–29456, https://doi.org/10.1021/acsami.8b07863.
[391] G. Lalande, R. Cote, G. Tamizhmani, D. Guay, J.P. Dodelet, L. Dignard-Bailey, L. T. Weng, P. Bertrand, Physical, chemical and electrochemical characterization of heat-treated tetracarboxylic cobalt phthalocyanine adsorbed on carbon black as electrocatalyst for oxygen reduction in polymer electrolyte fuel cells, Electrochim. Acta 40 (1995) 2635–2646.
[392] M.Y. Song, H.Y. Park, D. Yang, D. Bhattacharjya, J. Yu, Seaweed-derived heteroatom-doped highly porous carbon as an electrocatalyst for the oxygen reduction reaction, ChemSusChem 7 (2014) 1755–1763.
[393] Y. Zhu, B. Zhang, X. Liu, D. Wang, D.S. Su, Unravelling the structure of electrocatalytically active Fe–N complexes in carbon for the oxygen reduction reaction, Angew. Chem. 126 (2014) 10849–10853.
[394] G. Wu, K.L. More, C.M. Johnston, P. Zelenay, High-performance electrocatalysts for oxygen reduction derived from polyaniline, iron, and cobalt, Science 332 (2011) 443–447, https://doi.org/10.1126/science.1200832.
[395] D. Yang, H. Yu, G. Li, W. Song, Y. Liu, Z. Shao, Effect of gas diffusion electrode parameters on anion exchange membrane fuel cell performance, Chin. J. Catal. 35 (2014) 1091–1097, https://doi.org/10.1016/S1872-2067(14)60050-4.
[396] J. Cheng, G. He, F. Zhang, A mini-review on anion exchange membranes for fuel cell applications: stability issue and addressing strategies, Int. J. Hydrog. Energy 40 (2015) 7348–7360, https://doi.org/10.1016/j.ijhydene.2015.04.040.
[397] M. Mamlouk, K. Scott, Phosphoric acid-doped electrodes for a PBI polymer membrane fuel cell, Int. J. Energy Res 35 (2011) 507–519, https://doi.org/10.1002/er.1708.
[398] S. Huo, J.W. Park, P. He, D. Wang, K. Jiao, Analytical modeling of liquid saturation jump effect for hydrogen alkaline anion exchange membrane fuel cell, Int. J. Heat. Mass Transf. 112 (2017) 891–902, https://doi.org/10.1016/j.ijheatmasstransfer.2017.04.137.
[399] S. Komini Babu, H.T. Chung, P. Zelenay, S. Litster, Resolving electrode morphology's impact on platinum group metal-free cathode performance using nano-CT of 3D hierarchical pore and ionomer distribution, ACS Appl. Mater. Interfaces 8 (2016) 32764–32777, https://doi.org/10.1021/acsami.6b08844.
[400] D. Malko, T. Lopes, E.A. Ticianelli, A. Kucernak, A catalyst layer optimisation approach using electrochemical impedance spectroscopy for PEM fuel cells operated with pyrolysed transition metal-N-C catalysts, J. Power Sources 323 (2016) 189–200, https://doi.org/10.1016/j.jpowsour.2016.05.035.
[401] D. Banham, T. Kishimoto, Y. Zhou, T. Sato, K. Bai, J. Ozaki, Y. Imashiro, S. Ye, Critical advancements in achieving high power and stable nonprecious metal catalyst–based MEAs for real-world proton exchange membrane fuel cell applications, Sci. Adv. 4 (2018) eaar7180, https://doi.org/10.1126/sciadv.aar7180.
[402] R. Gokhale, L.K. Tsui, K. Roach, Y. Chen, M.M. Hossen, K. Artyushkova, F. Garzon, P. Atanassov, Hydrothermal synthesis of platinum-group-metal-free catalysts: structural elucidation and oxygen reduction catalysis, ChemElectroChem 5 (2018) 1848–1853, https://doi.org/10.1002/celc.201700949.
[403] R. Gokhale, Y. Chen, A. Serov, K. Artyushkova, P. Atanassov, Direct synthesis of platinum group metal-free Fe-N-C catalyst for oxygen reduction reaction in alkaline media, Electrochem. Commun. 72 (2016) 140–143, https://doi.org/10.1016/j.elecom.2016.09.013.
[404] N. Ramaswamy, S. Mukerjee, Influence of inner- and outer-sphere electron transfer mechanisms during electrocatalysis of oxygen reduction in alkaline media, J. Phys. Chem. C 115 (2011) 18015–18026, https://doi.org/10.1021/jp204680p.
[405] T.V. Reshetenko, H.-T. Kim, H.-J. Kweon, Modification of cathode structure by introduction of CNT for air-breathing DMFC, Electrochim. Acta 53 (2008) 3043–3049, https://doi.org/10.1016/j.electacta.2007.11.021.
[406] Y.-H. Cho, N. Jung, Y.S. Kang, D.Y. Chung, J.W. Lim, H. Choe, Y.-H. Cho, Y.-E. Sung, Improved mass transfer using a pore former in cathode catalyst layer in the direct methanol fuel cell, Int. J. Hydrog. Energy 37 (2012) 11969–11974, https://doi.org/10.1016/j.ijhydene.2012.05.031.
[407] S.H. Lee, J. Kim, D.Y. Chung, J.M. Yoo, H.S. Lee, M.J. Kim, B.S. Mun, S.G. Kwon, Y.-E. Sung, T. Hyeon, Design principle of Fe–N–C electrocatalysts: how to optimize multimodal porous structures, ?, J. Am. Chem. Soc. 141 (2019) 2035–2045, https://doi.org/10.1021/jacs.8b11129.
[408] D.R. Dekel, Review of cell performance in anion exchange membrane fuel cells, J. Power Sources 375 (2018) 158–169, https://doi.org/10.1016/j.jpowsour.2017.07.117.
[409] L. Wang, X. Peng, W.E. Mustain, J.R. Varcoe, Radiation-grafted anion-exchange membranes: the switch from low-to high-density polyethylene leads to remarkably enhanced fuel cell performance, Energy Environ. Sci. 12 (2019) 1575–1579.
[410] L. Zhu, X. Yu, X. Peng, T.J. Zimudzi, N. Saikia, M.T. Kwasny, S. Song, D. I. Kushner, Z. Fu, G.N. Tew, W.E. Mustain, M.A. Yandrasits, M.A. Hickner, Poly (olefin)-based anion exchange membranes prepared using ziegler–natta polymerization, Macromolecules 52 (2019) 4030–4041, https://doi.org/10.1021/acs.macromol.8b02756.
[411] R. He, P. Wen, H.-N. Zhang, S. Guan, G. Xie, L.-Z. Li, M.-H. Lee, X.-D. Li, In-situ photocrosslinked hydroxide conductive membranes based on photosensitive poly (arylene ether sulfone) block copolymers for anion exchange membrane fuel cells, J. Memb. Sci. 556 (2018) 73–84, https://doi.org/10.1016/j.memsci.2018.03.088.
[412] W. Chen, M. Mandal, G. Huang, X. Wu, G. He, P.A. Kohl, Highly conducting anion-exchange membranes based on cross-linked poly(norbornene): ring opening metathesis polymerization, ACS Appl. Energy Mater. 2 (2019) 2458–2468, https://doi.org/10.1021/acsaem.8b02052.
[413] L. Wang, M. Bellini, H.A. Miller, J.R. Varcoe, A high conductivity ultrathin anion-exchange membrane with 500+ h alkali stability for use in alkaline membrane fuel cells that can achieve 2 W cm-2 at 80 °c, J. Mater. Chem. A 6 (2018) 15404–15412, https://doi.org/10.1039/c8ta04783a.
[414] J. Wang, Y. Zhao, B.P. Setzler, S. Rojas-Carbonell, C. Ben Yehuda, A. Amel, M. Page, L. Wang, K. Hu, L. Shi, S. Gottesfeld, B. Xu, Y. Yan, Poly(aryl piperidinium) membranes and ionomers for hydroxide exchange membrane fuel cells, Nat. Energy 4 (2019) 392–398, https://doi.org/10.1038/s41560-019-0372-8.
[415] N. Ziv, D.R. Dekel, A practical method for measuring the true hydroxide conductivity of anion exchange membranes, Electrochem. Commun. 88 (2018) 109–113, https://doi.org/10.1016/j.elecom.2018.01.021.
[416] K.F.L. Hagesteijn, S. Jiang, B.P. Ladewig, A review of the synthesis and characterization of anion exchange membranes, J. Mater. Sci. 53 (2018) 11131–11150, https://doi.org/10.1007/s10853-018-2409-y.
[417] J.R. Varcoe, R.C.T. Slade, E. Lam How Yee, An alkaline polymer electrochemical interface: a breakthrough in application of alkaline anion-exchange membranes in fuel cells, Chem. Commun. (2006) 1428–1429, https://doi.org/10.1039/B600838K.
[418] M. Mandal, G. Huang, P.A. Kohl, Highly conductive anion-exchange membranes based on cross-linked poly(norbornene): vinyl addition polymerization, ACS Appl. Energy Mater. 2 (2019) 2447–2457, https://doi.org/10.1021/acsaem.8b02051.
[419] N. Chen, C. Lu, Y. Li, C. Long, Z. Li, H. Zhu, Tunable multi-cations-crosslinked poly(arylene piperidinium)-based alkaline membranes with high ion conductivity and durability, J. Memb. Sci. 588 (2019), 117120, https://doi.org/10.1016/j.memsci.2019.05.044.
[420] S. Jang, M. Her, S. Kim, J.-H. Jang, J.E. Chae, J. Choi, M. Choi, S.M. Kim, H.-J. Kim, Y.-H. Cho, Y.-E. Sung, S.J. Yoo, Membrane/electrode interface design for effective water management in alkaline membrane fuel cells, ACS Appl. Mater. Interfaces 11 (2019) 34805–34811, https://doi.org/10.1021/acsami.9b08075.
[421] T.J. Omasta, L. Wang, X. Peng, C.A. Lewis, J.R. Varcoe, W.E. Mustain, Importance of balancing membrane and electrode water in anion exchange membrane fuel cells, J. Power Sources 375 (2018) 205–213, https://doi.org/10.1016/j.jpowsour.2017.05.006.
[422] Y. Oshiba, J. Hiura, Y. Suzuki, T. Yamaguchi, Improvement in the solid-state alkaline fuel cell performance through efficient water management strategies, J. Power Sources 345 (2017) 221–226, https://doi.org/10.1016/j.jpowsour.2017.01.111.
[423] Y. Luo, J. Guo, C. Wang, D. Chu, Fuel cell durability enhancement by crosslinking alkaline anion exchange membrane electrolyte, Electrochem. Commun. 16 (2012) 65–68, https://doi.org/10.1016/j.elecom.2012.01.005.
[424] I. Gunasekara, M. Lee, D. Abbott, S. Mukerjee, Mass transport and oxygen reduction kinetics at an anion exchange membrane interface: microelectrode studies on effect of carbonate exchange, ECS Electrochem. Lett. 1 (2012) F16–F19, https://doi.org/10.1149/2.007202eel.
[425] N. Ziv, W.E. Mustain, D.R. Dekel, The effect of ambient carbon dioxide on anion-exchange membrane fuel cells, ChemSusChem 11 (2018) 1136–1150, https://doi.org/10.1002/cssc.201702330.

[426] C. Chen, J. Pan, J. Han, Y. Wang, L. Zhu, M.A. Hickner, L. Zhuang, Varying the microphase separation patterns of alkaline polymer electrolytes, J. Mater. Chem. A 4 (2016) 4071–4081, https://doi.org/10.1039/C5TA09438K.
[427] J. Ponce-González, D.K. Whelligan, L. Wang, R. Bance-Soualhi, Y. Wang, Y. Peng, H. Peng, D.C. Apperley, H.N. Sarode, T.P. Pandey, High performance aliphatic-heterocyclic benzyl-quaternary ammonium radiation-grafted anion-exchange membranes, Energy Environ. Sci. 9 (2016) 3724–3735.
[428] A.G. Wright, J. Fan, B. Britton, T. Weissbach, H.-F. Lee, E.A. Kitching, T. J. Peckham, S. Holdcroft, Hexamethyl-p-terphenyl poly(benzimidazolium): a universal hydroxide-conducting polymer for energy conversion devices, Energy Environ. Sci. 9 (2016) 2130–2142, https://doi.org/10.1039/C6EE00656F.
[429] J. Pan, L. Zhu, J. Han, M.A. Hickner, Mechanically tough and chemically stable anion exchange membranes from rigid-flexible semi-interpenetrating networks, Chem. Mater. 27 (2015) 6689–6698, https://doi.org/10.1021/acs.chemmater.5b02557.
[430] X. Chu, Y. Shi, L. Liu, Y. Huang, N. Li, Piperidinium-functionalized anion exchange membranes and their application in alkaline fuel cells and water electrolysis, J. Mater. Chem. A 7 (2019) 7717–7727, https://doi.org/10.1039/C9TA01167F.
[431] M. Mandal, G. Huang, P.A. Kohl, Anionic multiblock copolymer membrane based on vinyl addition polymerization of norbornenes: applications in anion-exchange membrane fuel cells, J. Memb. Sci. 570–571 (2019) 394–402, https://doi.org/10.1016/j.memsci.2018.10.041.
[432] H. Peng, Q. Li, M. Hu, L. Xiao, J. Lu, L. Zhuang, Alkaline polymer electrolyte fuel cells stably working at 80 °C, J. Power Sources 390 (2018) 165–167, https://doi.org/10.1016/j.jpowsour.2018.04.047.
[433] T.J. Omasta, Y. Zhang, A.M. Park, X. Peng, B. Pivovar, J.R. Varcoe, W.E. Mustain, Strategies for reducing the PGM loading in high power AEMFC anodes, J. Electrochem. Soc. 165 (2018) F710–F717, https://doi.org/10.1149/2.1401809jes.
[434] S. Maurya, S. Noh, I. Matanovic, E.J. Park, C. Narvaez Villarrubia, U. Martinez, J. Han, C. Bae, Y.S. Kim, Rational design of polyaromatic ionomers for alkaline membrane fuel cells with >1 W cm−2 power density, Energy Environ. Sci. 11 (2018) 3283–3291, https://doi.org/10.1039/C8EE02192A.
[435] E.J. Park, S. Maurya, A.S. Lee, D.P. Leonard, D. Li, J.Y. Jeon, C. Bae, Y.S. Kim, How does a small structural change of anode ionomer make a big difference in alkaline membrane fuel cell performance, ?, J. Mater. Chem. A 7 (2019) 25040–25046, https://doi.org/10.1039/C9TA10157H.
[436] X. Liang, M.A. Shehzad, Y. Zhu, L. Wang, X. Ge, J. Zhang, Z. Yang, L. Wu, J. R. Varcoe, T. Xu, Ionomer cross-linking immobilization of catalyst nanoparticles for high performance alkaline membrane fuel cells, Chem. Mater. 31 (2019) 7812–7820, https://doi.org/10.1021/acs.chemmater.9b00999.
[437] J. Pan, C. Chen, Y. Li, L. Wang, L. Tan, G. Li, X. Tang, L. Xiao, J. Lu, L. Zhuang, Constructing ionic highway in alkaline polymer electrolytes, Energy Environ. Sci. 7 (2014) 354–360.
[438] T.J. Peckham, S. Holdcroft, Structure-morphology-property relationships of non-perfluorinated proton-conducting membranes, Adv. Mater. 22 (2010) 4667–4690, https://doi.org/10.1002/adma.201001164.
[439] J.R. Varcoe, P. Atanassov, D.R. Dekel, A.M. Herring, M.A. Hickner, P.A. Kohl, A. R. Kucernak, W.E. Mustain, K. Nijmeijer, K. Scott, T. Xu, L. Zhuang, Anion-exchange membranes in electrochemical energy systems, Energy Environ. Sci. 7 (2014) 3135–3191, https://doi.org/10.1039/c4ee01303d.
[440] Z. Siroma, R. Kakitsubo, N. Fujiwara, T. Ioroi, S. Yamazaki, K. Yasuda, Depression of proton conductivity in recast Nafion® film measured on flat substrate, J. Power Sources 189 (2009) 994–998, https://doi.org/10.1016/j.jpowsour.2008.12.141.
[441] Y. Kurihara, T. Mabuchi, T. Tokumasu, Molecular analysis of structural effect of ionomer on oxygen permeation properties in PEFC, J. Electrochem. Soc. 164 (2017) F628–F637, https://doi.org/10.1149/2.1301706jes.
[442] L. Fan, Y. Wang, K. Jiao, Oxygen transport routes in ionomer film on polyhedral platinum nanoparticles, ACS Nano 14 (2020) 17487–17495, https://doi.org/10.1021/acsnano.0c07856.
[443] G. Gupta, K. Scott, M. Mamlouk, Soluble Polystyrene-b-poly (ethylene/butylene)-b-polystyrene based ionomer for anion exchange membrane fuel cells operating at 70 °C, Fuel Cells 18 (2018) 137–147, https://doi.org/10.1002/fuce.201700176.
[444] A. Hernández-Flores, M.I. Salazar-Gastélum, S. Pérez-Sicairos, T. Romero-Castañón, J.R. Flores-Hernández, Preparation of membrane-electrode assemblies for alkaline fuel cells: effect of the ionomeric solution, Mater. Lett. 303 (2021), 130494, https://doi.org/10.1016/j.matlet.2021.130494.
[445] J. Choi, M.-H. Kim, J.Y. Han, J.E. Chae, W.H. Lee, Y.M. Lee, S.Y. Lee, J.H. Jang, J. Y. Kim, D. Henkensmeier, S.J. Yoo, Y.-E. Sung, H.-J. Kim, Application of spirobiindane-based microporous poly(ether sulfone)s as polymeric binder on solid alkaline exchange membrane fuel cells (https://doi.org/https://doi.org/), J. Memb. Sci. 568 (2018) 67–75, https://doi.org/10.1016/j.memsci.2018.09.048.
[446] N. Ul Hassan, M. Mandal, G. Huang, H.A. Firouzjaie, P.A. Kohl, W.E. Mustain, Achieving high-performance and 2000h stability in anion exchange membrane fuel cells by manipulating ionomer properties and electrode optimization, Adv. Energy Mater. 10 (2020) 2001986, https://doi.org/10.1002/aenm.202001986.
[447] M. Hu, Q. Li, H. Peng, H. Ma, L. Xiao, G. Wang, J. Lu, L. Zhuang, Alkaline polymer electrolyte fuel cells without anode humidification and H2 emission, J. Power Sources 472 (2020), 228471, https://doi.org/10.1016/j.jpowsour.2020.228471.
[448] S.D. Poynton, R.C.T. Slade, T.J. Omasta, W.E. Mustain, R. Escudero-Cid, P. Ocón, J.R. Varcoe, Preparation of radiation-grafted powders for use as anion exchange ionomers in alkaline polymer electrolyte fuel cells, J. Mater. Chem. A. 2 (2014) 5124–5130, https://doi.org/10.1039/C4TA00558A.
[449] D.P. Leonard, S. Maurya, E.J. Park, L. Delfin Manriquez, S. Noh, X. Wang, C. Bae, E.D. Baca, C. Fujimoto, Y.S. Kim, Asymmetric electrode ionomer for low relative humidity operation of anion exchange membrane fuel cells, J. Mater. Chem. A 8 (2020) 14135–14144, https://doi.org/10.1039/D0TA05807F.
[450] K. Artyushkova, M.J. Workman, I. Matanovic, M.J. Dzara, C. Ngo, S. Pylypenko, A. Serov, P. Atanassov, Role of surface chemistry on catalyst/ionomer interactions for transition metal–nitrogen–carbon electrocatalysts, ACS Appl. Energy Mater. 1 (2018) 68–77, https://doi.org/10.1021/acsaem.7b00002.
[451] Y. Yin, R. Li, F. Bai, W. Zhu, Y. Qin, Y. Chang, J. Zhang, M.D. Guiver, Ionomer migration within PEMFC catalyst layers induced by humidity changes, Electrochem. Commun. 109 (2019), 106590, https://doi.org/10.1016/j.elecom.2019.106590.
[452] Y. Chang, J. Liu, R. Li, J. Zhao, Y. Qin, J. Zhang, Y. Yin, X. Li, Effect of humidity and thermal cycling on the catalyst layer structural changes in polymer electrolyte membrane fuel cells, Energy Convers. Manag 189 (2019) 24–32, https://doi.org/10.1016/j.enconman.2019.03.066.
[453] Z.F. Pan, R. Chen, L. An, Y.S. Li, Alkaline anion exchange membrane fuel cells for cogeneration of electricity and valuable chemicals, J. Power Sources 365 (2017) 430–445, https://doi.org/10.1016/j.jpowsour.2017.09.013.
[454] X. Peng, D. Kulkarni, Y. Huang, T.J. Omasta, B. Ng, Y. Zheng, L. Wang, J. M. LaManna, D.S. Hussey, J.R. Varcoe, I.V. Zenyuk, W.E. Mustain, Using operando techniques to understand and design high performance and stable alkaline membrane fuel cells, Nat. Commun. 11 (2020) 3561, https://doi.org/10.1038/s41467-020-17370-7.
[455] C. Simon, D. Kartouzian, D. Müller, F. Wilhelm, H.A. Gasteiger, Impact of microporous layer pore properties on liquid water transport in PEM Fuel Cells: carbon black type and perforation, J. Electrochem. Soc. 164 (2017) F1697–F1711, https://doi.org/10.1149/2.1321714jes.
[456] A.M. Kannan, V.P. Veedu, L. Munukutla, M.N. Ghasemi-Nejhad, Nanostructured gas diffusion and catalyst layers for proton exchange membrane fuel cells, Electrochem. Solid-State Lett. 10 (2007) B47, https://doi.org/10.1149/1.2422751.
[457] Y. Tabe, Y. Aoyama, K. Kadowaki, K. Suzuki, T. Chikahisa, Impact of micro-porous layer on liquid water distribution at the catalyst layer interface and cell performance in a polymer electrolyte membrane fuel cell, J. Power Sources 287 (2015) 422–430, https://doi.org/10.1016/j.jpowsour.2015.04.095.
[458] V.M. Truong, C.-L. Wang, M. Yang, H. Yang, Effect of tunable hydrophobic level in the gas diffusion substrate and microporous layer on anion exchange membrane fuel cells, J. Power Sources 402 (2018) 301–310, https://doi.org/10.1016/j.jpowsour.2018.09.053.
[459] X. Xie, J. Zhou, S. Wu, J.W. Park, K. Jiao, Experimental investigation on the performance and durability of hydrogen AEMFC with electrochemical impedance spectroscopy, Int. J. Energy Res 43 (2019) 8522–8535, https://doi.org/10.1002/er.4851.
[460] R.B. Kaspar, M.P. Letterio, J.A. Wittkopf, K. Gong, S. Gu, Y. Yan, Manipulating water in high-performance hydroxide exchange membrane fuel cells through asymmetric humidification and wetproofing, J. Electrochem. Soc. 162 (2015) F483–F488, https://doi.org/10.1149/2.0131506jes.
[461] B. Eriksson, H. Grimler, A. Carlson, H. Ekström, R. Wreland Lindström, G. Lindbergh, C. Lagergren, Quantifying water transport in anion exchange membrane fuel cells, Int. J. Hydrog. Energy 44 (2019) 4930–4939, https://doi.org/10.1016/j.ijhydene.2018.12.185.
[462] P. Veh, B. Britton, S. Holdcroft, R. Zengerle, S. Vierrath, M. Breitwieser, Improving the water management in anion-exchange membrane fuel cells via ultra-thin, directly deposited solid polymer electrolyte, RSC Adv. 10 (2020) 8645–8652, https://doi.org/10.1039/C9RA09628K.
[463] D.R. Dekel, I.G. Rasin, M. Page, S. Brandon, Steady state and transient simulation of anion exchange membrane fuel cells, J. Power Sources 375 (2018) 191–204, https://doi.org/10.1016/j.jpowsour.2017.07.012.
[464] C. Weinzierl, U. Krewer, Model-based analysis of water management in alkaline direct methanol fuel cells, J. Power Sources 268 (2014) 911–921, https://doi.org/10.1016/j.jpowsour.2014.06.070.
[465] Y.-J. SOHN, J.-I. CHOI, K. KIM, Numerical analysis on water transport in alkaline anion exchange membrane fuel cells, Electrochemistry 83 (2015) 80–83, https://doi.org/10.5796/electrochemistry.83.80.
[466] H.-S. Shiau, I.V. Zenyuk, A.Z. Weber, Water management in an alkaline-exchange-membrane fuel cell, ECS Trans. 69 (2015) 985–994, https://doi.org/10.1149/06917.0985ecst.
[467] T. Wang, L. Shi, J. Wang, Y. Zhao, B.P. Setzler, S. Rojas-Carbonell, Y. Yan, High-performance hydroxide exchange membrane fuel cells through optimization of relative humidity, backpressure and catalyst selection, J. Electrochem. Soc. 166 (2019) F3305–F3310, https://doi.org/10.1149/2.0361907jes.
[468] T.J. Omasta, X. Peng, H.A. Miller, F. Vizza, L. Wang, J.R. Varcoe, D.R. Dekel, W. E. Mustain, Beyond 1.0 W cm− 2 performance without platinum: the beginning of a new era in anion exchange membrane fuel cells, J. Electrochem. Soc. 165 (2018) J3039.
[469] S. Huo, H. Deng, Y. Chang, K. Jiao, Water management in alkaline anion exchange membrane fuel cell anode, Int. J. Hydrog. Energy 37 (2012) 18389–18402, https://doi.org/10.1016/j.ijhydene.2012.09.074.
[470] X. Gao, H. Yu, B. Qin, J. Jia, J. Hao, F. Xie, Z. Shao, Enhanced water transport in AEMs based on poly(styrene–ethylene–butylene–styrene) triblock copolymer for high fuel cell performance, Polym. Chem. 10 (2019) 1894–1903, https://doi.org/10.1039/C8PY01618F.
[471] K. Jiao, P. He, Q. Du, Y. Yin, Three-dimensional multiphase modeling of alkaline anion exchange membrane fuel cell, Int. J. Hydrog. Energy 39 (2014) 5981–5995, https://doi.org/10.1016/j.ijhydene.2014.01.180.
[472] G. Rambabu, N. Nagaraju, S.D. Bhat, Functionalized fullerene embedded in Nafion matrix: a modified composite membrane electrolyte for direct methanol

fuel cells, Chem. Eng. J. 306 (2016) 43–52, https://doi.org/10.1016/j.cej.2016.07.032.
[473] M.R. Gerhardt, L.M. Pant, A.Z. Weber, Along-the-channel impacts of water management and carbon-dioxide contamination in hydroxide-exchange-membrane fuel cells: a modeling study, J. Electrochem. Soc. 166 (2019) F3180–F3192, https://doi.org/10.1149/2.0171907jes.
[474] J. Mishler, Y. Wang, R. Mukundan, J. Spendelow, D.S. Hussey, D.L. Jacobson, R. L. Borup, Probing the water content in polymer electrolyte fuel cells using neutron radiography, Electrochim. Acta 75 (2012) 1–10, https://doi.org/10.1016/j.electacta.2012.04.040.
[475] H. Deng, D. Wang, X. Xie, Y. Zhou, Y. Yin, Q. Du, K. Jiao, Modeling of hydrogen alkaline membrane fuel cell with interfacial effect and water management optimization, Renew. Energy 91 (2016) 166–177, https://doi.org/10.1016/j.renene.2016.01.054.
[476] M. Iravaninia, S. Azizi, S. Rowshanzamir, A comprehensive study on the stability and ion transport in cross-linked anion exchange membranes based on polysulfone for solid alkaline fuel cells, Int. J. Hydrog. Energy 42 (2017) 17229–17241, https://doi.org/10.1016/j.ijhydene.2017.05.200.
[477] T. Yamanaka, T. Takeguchi, H. Takahashi, W. Ueda, Water transport during ion conduction in anion-exchange and cation-exchange membranes, J. Electrochem. Soc. 156 (2009) B831, https://doi.org/10.1149/1.3129618.
[478] K.H. Gopi, S.G. Peera, S.D. Bhat, P. Sridhar, S. Pitchumani, Preparation and characterization of quaternary ammonium functionalized poly(2,6-dimethyl-1,4-phenylene oxide) as anion exchange membrane for alkaline polymer electrolyte fuel cells, Int. J. Hydrog. Energy 39 (2014) 2659–2668, https://doi.org/10.1016/j.ijhydene.2013.12.009.
[479] H. Zarrin, J. Wu, M. Fowler, Z. Chen, High durable PEK-based anion exchange membrane for elevated temperature alkaline fuel cells, J. Memb. Sci. 394–395 (2012) 193–201, https://doi.org/10.1016/j.memsci.2011.12.041.
[480] J. Fan, A.G. Wright, B. Britton, T. Weissbach, T.J.G. Skalski, J. Ward, T. J. Peckham, S. Holdcroft, Cationic polyelectrolytes, stable in 10 M KOHaq at 100 °C, ACS Macro Lett. 6 (2017) 1089–1093, https://doi.org/10.1021/acsmacrolett.7b00679.
[481] S. Holdcroft, J. Fan, Sterically-encumbered ionenes as hydroxide ion-conducting polymer membranes, Curr. Opin. Electrochem 18 (2019) 99–105, https://doi.org/10.1016/j.coelec.2019.10.014.
[482] S. Gu, J. Wang, R.B. Kaspar, Q. Fang, B. Zhang, E. Bryan Coughlin, Y. Yan, Permethyl cobaltocenium (Cp*2Co+) as an ultra-stable cation for polymer hydroxide-exchange membranes, Sci. Rep. 5 (2015) 11668, https://doi.org/10.1038/srep11668.
[483] M.G. Marino, K.D. Kreuer, Alkaline stability of quaternary ammonium cations for alkaline fuel cell membranes and ionic liquids, ChemSusChem 8 (2015) 513–523, https://doi.org/10.1002/cssc.201403022.
[484] C.H. Choi, C. Baldizzone, J. Grote, A.K. Schuppert, F. Jaouen, K.J.J. Mayrhofer, Stability of Fe-N-C catalysts in acidic medium studied by operando spectroscopy, Angew. Chem. 127 (2015) 12944–12948.
[485] M. Ferrandon, X. Wang, A.J. Kropf, D.J. Myers, G. Wu, C.M. Johnston, P. Zelenay, Stability of iron species in heat-treated polyaniline–iron–carbon polymer electrolyte fuel cell cathode catalysts, Electrochim. Acta 110 (2013) 282–291, https://doi.org/10.1016/j.electacta.2013.03.183.
[486] Y. Zheng, G. Huang, L. Wang, J.R. Varcoe, P.A. Kohl, W.E. Mustain, Effect of reacting gas flowrates and hydration on the carbonation of anion exchange membrane fuel cells in the presence of CO_2, J. Power Sources 467 (2020), 228350, https://doi.org/10.1016/j.jpowsour.2020.228350.
[487] M.S. Thorum, J.M. Hankett, A.A. Gewirth, Poisoning the oxygen reduction reaction on carbon-supported Fe and Cu electrocatalysts: evidence for metal-centered activity, J. Phys. Chem. Lett. 2 (2011) 295–298, https://doi.org/10.1021/jz1016284.
[488] T. Reshetenko, A. Serov, K. Artyushkova, I. Matanovic, S. Stariha, P. Atanassov, Tolerance of non-platinum group metals cathodes proton exchange membrane fuel cells to air contaminants, J. Power Sources 324 (2016) 556–571, https://doi.org/10.1016/j.jpowsour.2016.05.090.
[489] J.L. Oberst, M.S. Thorum, A.A. Gewirth, Effect of pH and azide on the oxygen reduction reaction with a pyrolyzed Fe phthalocyanine catalyst, J. Phys. Chem. C. 116 (2012) 25257–25261, https://doi.org/10.1021/jp309707b.
[490] D. von Deak, D. Singh, J.C. King, U.S. Ozkan, Use of carbon monoxide and cyanide to probe the active sites on nitrogen-doped carbon catalysts for oxygen reduction, Appl. Catal. B Environ. 113–114 (2012) 126–133, https://doi.org/10.1016/j.apcatb.2011.11.029.
[491] Q. Zhang, K. Mamtani, D. Jain, U. Ozkan, A. Asthagiri, CO poisoning effects on FeNC and CNx ORR catalysts: a combined experimental–computational study, J. Phys. Chem. C. 120 (2016) 15173–15184, https://doi.org/10.1021/acs.jpcc.6b03933.
[492] H.M. Barkholtz, L. Chong, Z.B. Kaiser, T. Xu, D.-J. Liu, Highly active non-PGM catalysts prepared from metal organic frameworks, Catalysis 5 (2015) 955–965, https://doi.org/10.3390/catal5020955.
[493] B. You, N. Jiang, M. Sheng, W.S. Drisdell, J. Yano, Y. Sun, Bimetal–organic framework self-adjusted synthesis of support-free nonprecious electrocatalysts for efficient oxygen reduction, ACS Catal. 5 (2015) 7068–7076, https://doi.org/10.1021/acscatal.5b02325.
[494] A. Serov, M.J. Workman, K. Artyushkova, P. Atanassov, G. McCool, S. McKinney, H. Romero, B. Halevi, T. Stephenson, Highly stable precious metal-free cathode catalyst for fuel cell application, J. Power Sources 327 (2016) 557–564, https://doi.org/10.1016/j.jpowsour.2016.07.087.
[495] A. Serov, K. Artyushkova, P. Atanassov, Fe-N-C oxygen reduction fuel cell catalyst derived from carbendazim: synthesis, structure, and reactivity, Adv. Energy Mater. 4 (2014) 1301735, https://doi.org/10.1002/aenm.201301735.
[496] A. Serov, M.H. Robson, M. Smolnik, P. Atanassov, Templated bi-metallic non-PGM catalysts for oxygen reduction, Electrochim. Acta 80 (2012) 213–218, https://doi.org/10.1016/j.electacta.2012.07.008.